1

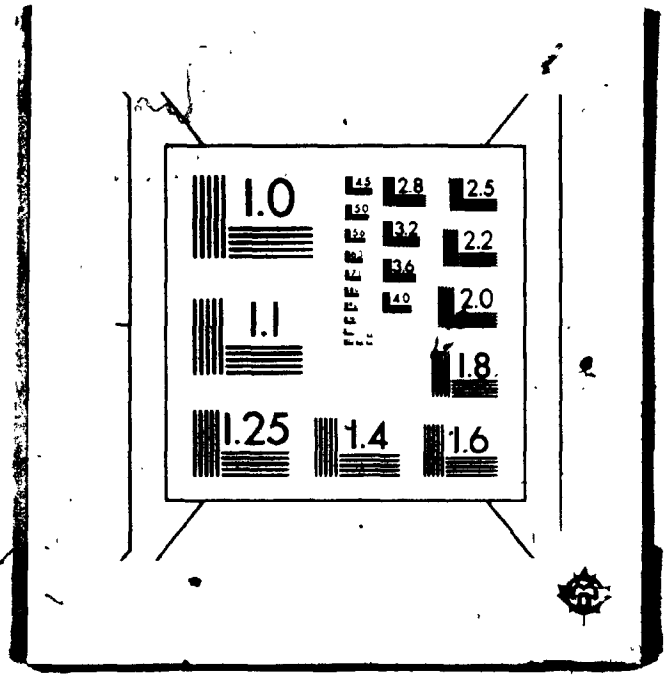

National Library of Canada | Bibliothèque nationale du Canada

CANADIAN THESES ON MICROFICHE | THÈSES CANADIENNES SUR MICROFICHE

44419

NAME OF AUTHOR/NOM DE L'AUTEUR JOHN DAVIDSON MILLER

TITLE OF THESIS/TITRE DE LA THÈSE AN EQUILIBRIUM SURFACE TEMPERATURE CLIMATE MODEL APPLIED TO FIRST YEAR SEA ICE GROWTH

UNIVERSITY/UNIVERSITÉ CARLETON UNIVERSITY

DEGREE FOR WHICH THESIS WAS PRESENTED/ GRADE POUR LEQUEL CETTE THÈSE FUT PRÉSENTÉE MASTERS (M.A.)

YEAR THIS DEGREE CONFERRED/ANNÉE D'OBTENTION DE CE DEGRÉ 1979

NAME OF SUPERVISOR/NOM DU DIRECTEUR DE THÈSE M.W. SMITH

DATED/DATÉ May 24/78 SIGNED/SIGNÉ John D. Miller

PERMANENT ADDRESS/RÉSIDENCE FIXE

3 SITE 5 Box 8
R.R. #1
Vernon, B.C.

NL-91 (3-74)

NOTICE

The quality of this microfiche is heavily dependent upon the quality of the original thesis submitted for microfilming. Every effort has been made to ensure the highest quality of reproduction possible.

If pages are missing, contact the university which granted the degree.

Some pages may have indistinct print especially if the original pages were typed with a poor typewriter ribbon or if the university sent us a poor photocopy.

Previously copyrighted materials (journal articles, published tests, etc.) are not filmed.

Reproduction in full or in part of this film is governed by the Canadian Copyright Act, R.S.C. 1970, c. C-30. Please read the authorization forms which accompany this thesis.

THIS DISSERTATION
HAS BEEN MICROFILMED
EXACTLY AS RECEIVED

AVIS

La qualité de cette microfiche dépend grandement de la qualité de la thèse soumise au microfilmage. Nous avons tout fait pour assurer une qualité supérieure de reproduction.

S'il manque des pages, veuillez communiquer avec l'université qui a conféré le grade.

La qualité d'impression de certaines pages peut laisser à désirer, surtout si les pages originales ont été dactylographiées à l'aide d'un ruban usé ou si l'université nous a fait parvenir une photocopie de mauvaise qualité.

Les documents qui font déjà l'objet d'un droit d'auteur (articles de revue, examens publiés, etc.) ne sont pas microfilmés.

La reproduction, même partielle, de ce microfilm est soumise à la Loi canadienne sur le droit d'auteur, SRC 1970, c. C-30. Veuillez prendre connaissance des formules d'autorisation qui accompagnent cette thèse.

LA THÈSE A ÉTÉ
MICROFILMÉE TELLE QUE
NOUS L'AVONS REÇUE

AN EQUILIBRIUM SURFACE TEMPERATURE CLIMATE MODEL APPLIED TO FIRST YEAR SEA ICE GROWTH

BY

John Davidson Miller

Submitted in Fulfillment of the
Requirements of Geography 45:599

Department of Geography
Carleton University
Ottawa, Canada

1979

The undersigned recommend to the Faculty of Graduate Studies acceptance of the thesis

"AN EQUILIBRIUM SURFACE TEMPERATURE CLIMATE MODEL APPLIED TO FIRST YEAR SEA ICE GROWTH"

submitted by John Davidson Miller, B.Sc., in partial fulfilment of the requirements for the degree of Master of Arts.

J. Kenneth Torrance
.....
Supervisor of Graduate Studies,
Geography Department

David B. Knight
.....
Chairman, Geography Department

Carleton University

May 24, 1979

ABSTRACT

The problem of sea ice growth is approached using an energy conservation methodology. A climate simulation is developed which utilizes information about the state of the atmosphere, snow/ice surface, snow/ice medium and underlying ocean and establishes an explicit relationship between the surface temperature and each component of the energy balance. In this manner sea ice growth is treated as a function of the dynamic interaction of atmosphere, ice and ocean.

The model furnishes daily estimates of the individual components of the radiation balance and the turbulent, conductive and melt induced energy fluxes. The surface temperature and temperature at the snow-ice interface are determined and the average ice salinity and ice thickness predicted. Thermal properties are internally modified as a response to changes in snow and ice properties. Also included is the transient occurrence and thermodynamic behaviour of a snowpack.

A comparison of sea ice growth observations at three Arctic locations with model predictions indicates a successful reproduction of real world conditions by the computer simulation.

ACKNOWLEDGEMENTS

I would like to acknowledge the assistance granted by both the faculty and staff of the Geography Department throughout my stay at Carleton. Requests of their abilities and knowledge were always met with prompt, professional and enthusiastic response.

Thanks are due to Stephanie Quennal who was responsible for typing the first draft of this thesis. Sheilah Marans did a superb job on the final draft as evidenced by this report.

The National Science and Engineering Research Council of Canada (formerly the National Research Council of Canada) provided financial support through a postgraduate scholarship. This support is gratefully acknowledged.

Mike Smith was an active, though sometimes absent, supervisor. Our wide ranging discussions together, his irreverent enthusiasm and even his squash backhand were all enjoyable and informative. His greatest ability as supervisor lay in the asking of very simple questions for they are the hardest to answer.

A special note of thanks goes to René Ramseier for providi ng an introduction to the problems associated with sea

ice, his advice and criticisms, his belief in my abilities and his help in expanding them.

Anne influenced this work by helping me to critically evaluate, both in the academic and personal sense, the purpose behind it, and thoughts within it and the road beyond it.

Finally, I would like to dedicate this effort to my parents, Katie and Dusty Miller. They are responsible for much of my learning, consisting mostly of that knowledge of the type that cannot be found in books.

I grow daily to honour
facts, more and more,
and theory less and less.

Thomas Carlyle
(1795 - 1881)

TABLE OF CONTENTS

LIST OF FIGURES

LIST OF TABLES

LIST OF SYMBOLS

a	constant
b	regression slope
c_p	specific heat
d	growth rate
e	vapour pressure
f	relative humidity
g	acceleration due to gravity
h	snow depth
	heat transfer coefficient
i	penetrating fraction for shortwave radiation
k	thermal conductivity
	von Karman's constant
m	amount of pure ice per unit mass
n	number of brine pockets per unit area
	number of observations
q	specific humidity
r	brine pocket radius
	correlation coefficient
s	standard deviation
t	time
	Student's t statistic
u	wind speed
u_*	friction velocity
y	predicted data point
z_o	aerodynamic roughness length
A	atmospheric turbidity coefficient
C	drag transfer coefficient
D	diffusion constant
	residual
F	mass or energy flux
H	ice thickness
I	solar constant
K	exchange coefficient (eddy diffusivity)
K↓	incoming shortwave radiation (0.15 - 4 microns)
K↑	outgoing shortwave radiation (0.15 - 4 microns)
L	latent heat
	Monin - Obukhov characteristic length
L↓	incoming longwave radiation (4-100 microns)
L↑	outgoing longwave radiation (4-100 microns)
P	atmospheric pressure
Q*	net radiation (0.15 - 100 microns)
R	universal gas constant
	integrated residual
S	salinity

T	temperature
V	brine pocket velocity
Z	distance
α	albedo
ε	emissivity
μ	solar declination
ν	volume fraction
ρ	density
σ	Stefan - Boltzmann constant
τ	atmospheric shearing stress (momentum flux)
ρ	density
ω	solar hour angle

Subscripts

a	air
b	brine
bi	bubbly ice
i	ice
o	ocean
s	snow
v	vapour
A	ablation
E	evaporation
EQ	equilibrium surface
H	sensible heat
I	conduction
M	momentum
S	salt

Superscripts

*	saturated condition

CHAPTER 1

THE NEED AND SUGGESTED APPROACH FOR THE DEVELOPMENT OF AN ICE GROWTH MODEL

1.1 Introduction

Simulating the energy balance over sea ice and sea ice growth is an interesting climatological study but it is more than this for it has applications in many other fields. A knowledge of the thickness, properties and coverage of first year ice is important in studies of climatic change, regional energy balances, ice dynamics, ice forecasting, mechanical properties, remote sensing response, northern oil and gas development (and the associated problem of oil spill containment), arctic transportation and others. The existence of a reliable model to predict sea ice growth as a climatological response will find wide ranging acceptance in the science and engineering fields.

Sea ice exhibits a strong influence on climate and climatic change due primarily to its very high albedo. Expansion of sea ice coverage in response to global cooling leads to a decrease in net radiation promoting further cooling and ice growth (Budyko, 1974). Proper understanding of the rate of this feedback mechanism is essential in determining the time scale of

climatic change (Kellogg, 1974).

Maykut (1978) has shown that for the present ice thickness distribution in the central Arctic, the total heat input to the atmospheric boundary layer from regions of young ice (<0.8 m) is equal to or greater than that from regions of open water or thick ice; these conclusions are based on young ice comprising only 10-15% of the total pack ice. Energy balance determination and modelling of climatic change should incorporate models of growth pertaining to young ice rather than those of pack ice because an increase in areal coverage by young ice will have a much greater impact on the regional energy balance than that previously envisaged using thick pack ice data.

The use of a thickness distribution, giving the areal coverage of ice of different thickness categories has been used in studies examining the large scale dynamic behaviour of the ice pack (Thorndike et al., 1975). Lead distribution, refreezing rates and subsequent ice thickening represent important considerations in an understanding of the problem.

Ice forecasting seeks to predict the start of ice formation, its rate of growth and changes in ice concentration. A rigorous method of growth estimation that responds to existing climatological conditions would replace the currently employed empirical formulas. Ice decay and concentration

changes during melt could benefit in much the same manner. In a later stage of development an ice climatological model may be linked with a theoretical model of the ocean to provide information on the time of formation of the initial ice cover in the fall.

The mechanical properties of sea ice (i.e tensile strength, flexural strength and modulus of elasticity) are highly dependent on the ice salinity characteristics (Weeks and Assur, 1967) which is itself a function of the growth history of the ice sheet. For example, rapid growth results in a high entrapment of brine in the skeletal layer which, when incorporated into the ice structure as brine pockets, reduces ice strength relative to a low salinity or freshwater ice. The change in the salinity distribution with time as a function of thermal and isostatic adjustments produces a continuous change in the mechanical properties. A knowledge of growth rate, thermal history and overall thickness of ice would be of great benefit in these studies.

The electromagnetic response of ice is also affected in the same manner. A distinction is made between first year ice and multiyear ice in microwave remote sensing applications where the thicker, lower salinity older ice has a lower brightness temperature (220°K) than the thinner, higher salinity young ice (245°K, Gloersen et al., 1975). This

distinction is further complicated due to the presence of a high salinity layer at the top of the snow free ice surface for then a new signature, similar to that for multiyear ice, develops. Brine expulsion directed towards the surface in first year ice is a possible source of these high salt concentrations; a knowledge of thermal history of the ice sheet is required to test the validity of this mechanism.

Oil spill containment in an arctic environment is sensitive to the season when the spill occurs and the nature of the ice coverage (Lewis, 1976; NORCOR, 1976). Oil on the surface is expected to retard growth in the fall, while enhancing decay in the spring. An estimate of the magnitude and timing of these changes can be obtained from a simulation model in advance of an actual spill. Oil beneath the ice becomes entrapped and incorporated directly into the ice structure altering the thermal properties of the ice medium and these changes and their impact should also be amenable to computer simulation.

Ship-based transport in the Arctic is dependent upon many of the processes discussed. Penetration through a region may be determined by the dynamic response of the ice, compression and expansion of the ice field expressing itself in the formation of leads and pressure ridges. In the melt period the concentration of ice in shipping lanes is related to the

thermodynamic processes governing the ice ablation and ocean dynamics. Icebreaker resistance can be related to ice strength just as the feasibility of surface transport across ice depends on its strength and thickness.

The applications of a comprehensive climatological model of ice growth are many and only some have been detailed (others may require more imagination, such as the need for an ice growth model as it concerns the laying of naval mine fields (see Gerson and Perchal, 1973)). The following section introduces the approach to the problem that was adopted while the remaining chapters detail some of the work undertaken to develop a computer simulation model relating ice growth to atmosphere-ice-ocean interaction and changes within the ice medium itself. Chapter 2 reviews previous research concerning the computer simulation of ice behaviour while Chapter 3 examines the processes of ice growth and their relation to the atmosphere and ocean. The conceptual development and implementation of an ice growth model are discussed in Chapter 4 and an assessment of the model predictions is presented in Chapter 5. Chapter 6 provides a summary of the work in association with a discussion of the limitations of the model.

1.2 The Simulation Approach

It was proposed that a one-dimensional climatological simulation model be developed to study the growth and decay of sea ice. An energy conservation methodology was adopted because it (i) allows the computation of the fluxes at the earth's surface from external parameters given by the state and processes in the atmospheric boundary layer and (ii) allows the study of the variation in fluxes in time and space dependent on all the parameters influencing the energy exchange (Krause, 1972). The latter provides an effective method of obtaining an improved insight into the problems under examination.

A simulation approach involves the designation of a system which comprises a set of dynamically related components. Because the real world system appears very complex it must be simplified conceptually and represented as a model which is regarded here as an artificial system that attempts to portray the characteristics of the real system. The model must be constructed in such a way that the interactions of its components and both its abstract and physical boundaries are clearly defined (Harbaugh and Bonham-Carter, 1970).

The goals of the simulation are an understanding of the phenomenon and a related predictive ability. Building the simulation model requires a clear understanding of the nature of our system. The active mechanisms and processes must be well defined before they can be reduced to sets of equations and logic statements. Functional relationships between the components must be specified and while these equations are not necessarily correct, they are explicit and unambiguous. The answers we obtain from our model will reflect the understanding we have of our system.

Validation of the simulation usually involves testing the model against a situation where the outcome is known. If the model adequately reproduces the observed behaviour then we may have some faith in its ability to provide a useful analog to the real system. It is proposed to test the simulation model using previously assembled ice thickness data and meteorological observations from several arctic locations.

After verification of the model it may be employed to explore the consequences of different sets of assumptions. An example of this is its use as a technique to assess the outcome of intentional or accidental changes in parameters such as the surface albedo. We may also make use of one of the major advantages of computer simulation, the compression of the time scale. Years of real time may be simulated in

minutes of computer time.

It is hoped that through the development of a computer simulation model of the growth and decay of sea ice we may satisfy both our goals of understanding and prediction.

CHAPTER 2

SURVEY OF PREVIOUS RESEARCH

2.1 Introduction

Investigations into sea ice growth may be divided amongst the empirical, analytical and numerical approaches. Empirical forms are restrictive in that an historical record of ice thickness and the variables employed is required. Most of the variables that affect ice growth are subsumed under one or two surrogate variables (e.g., degree days below -1.8°C). This effectively masks an understanding of process interaction resulting in a 'black box' solution. An empirical relation developed in this manner must also be considered as site specific further restricting the application of such investigations. A review of some of the empirical work on this topic may be found in Bilello (1961).

The first analytical approach to the problem of sea ice was that of Stefan (1891) who obtained a solution that was a simplified form of the von Neumann equation. Later studies have identified the form of the interaction between the four components (atmosphere-snow-ice-ocean) involved in the energy and mass balances but have failed to provide solutions that may be applied to produce realistic results due to the complexity of the problem. Doronin (1970) reviews much of the

literature concerning analytical approaches to sea ice growth.

The numerical approach is closely linked to analytical developments differing only in its method of arriving at a solution. Numerical techniques provide a method to obtain approximate solutions where conditions necessary for analytical solutions are too complex. This methodology is adopted as the numerical approach allows the most realistic representation of real world conditions in a mathematical model for which a solution may be generated. The following review deals only with studies adopting a numerical approach; the list is short due to the fact that an efficient numerical application to the problem has become available only with the advent and availability of high speed computers.

2.2 Review of the Literature

Maykut and Untersteiner (1969) present a one-dimensional thermodynamic model of sea ice. Energy and radiation fluxes (with the exception of outgoing longwave radiation), ocean heat flux, snow accumulation and density, surface albedo and ice salinity are treated as time dependent model inputs. These parameters allow the energy balance to be calculated as a function of an effective surface temperature. Coupling this temperature with the sea water temperature provides sufficient boundary conditions to compute the temperature distribution within the ice and evaluate mass changes (accretion or ablation) at the ice boundaries. The parabolic heat

conduction equation is solved using an explicit finite difference technique suggested by Sauliev (1957). The formulation is unconditionally stable removing restrictions on the time step and grid spacing but requires that the boundary temperature be specified at least one time step in advance.

Starting from an arbitrary initial condition the model was integrated numerically until annual equilibrium patterns of temperature and thickness were achieved. Steady state is defined in their model as the point where annual bottom accretion is within 1 mm of the surface ablation; equilibrium was achieved after 30-100 years integration. In all, twenty-eight simulations under a variety of postulated conditions were performed. The ice parameters employed were those of multiyear ice and the mean climatic inputs were determined from Fletcher's (1965) heat budget.

The authors recognize that the most serious limitation of the model lies in the simplified boundary conditions chosen. The energy fluxes we observe are dependent upon the nature of and conditions at the boundary surface. In nature, the turbulent fluxes show a marked dependence on surface conditions, a dependence the model fails to duplicate. The model has also never been evaluated in a real time situation, the comparisons are based on the equilibrium ice thicknesses generated after 30-100 years forcing under a 'constant'

climate. Computationally, the model is complex and costly to run.

Despite these limitations, the model represents a pioneering work in the modelling of ocean-ice-atmosphere interaction. The model is capable of predicting the steady state behaviour of sea ice under a variety of postulated climatic conditions and the simulations perfomed afford an insight into the complex relationship between ice thickness and both the dependent and independent energy fluxes. To date, it remains the most comprehensive treatment of ice thermal behaviour and as Semtner (1976) remarks in a discussion of his own work, "In the absence of observational data on the response of sea ice to changes in climatic forcing, their model has been used as the standard against which to test a simplified model." (p. 386)

Pease (1975) attempted to verify the hypothesis that the mean seasonal changes in ice extent in the Antarctic can be explained, in part, by the mean thermodynamic conditions in both the atmosphere and the ocean. A simulation was performed to evaluate equilibrium ice thicknesses and extent under mean climatic conditions. Although the surface energy balance components are treated in a crude manner (see Table 2.1), the energy exchanges between the ice and the ocean are well detailed. Three versions of the model are presented, each bringing an increasing sophistication to the mathematical treatment of the

TABLE 2.1

PARAMETERIZATION SUMMARY FOR PREVIOUS ICE MODELLING ATTEMPTS

AUTHOR	K↓	K↑	L↓	L↑	Q_H	Q_E	
Maykut and Untersteiner 1969	Input	$\alpha K\downarrow$ $\alpha = 0.64$ fixed	Input	ϵT_s^4 $\epsilon = 1.00$	Input	Input	$\frac{k_1(T_s}{Z}$ solut yield profi
Goddard 1974	$(1-C\alpha_c)IA^{\sec\Omega}\cos\Omega$ clear $\alpha_c = 1.00$ cloudy $\alpha_c = 0.77$ $A = 0.93$ $I = 1360\ W\cdot m^{-2}$	$\alpha K\downarrow$ $\alpha = 0.79$ fixed	$a_1\epsilon_2\sigma T_a^6$ $a_1 = 9.35 \times 10^{-6}$ (cgs) clear $\epsilon_2 = 1.14$ cloudy $\epsilon_2 = 1.00$	$(1-bc)\epsilon T_s^4$ clear $b = 0.75$ cloudy $b = 0.73$	$\frac{c_p k^2 (T_a-T_s) u\ 1.25(1-R_i)^2}{\ln(z/z_0)}$ $z_0 = 0.001$ cm	$\frac{L k^2 (q_a-q_s) u_a\ 1.25(1-R_i)^2}{\ln(z/z_0)}$ R.H. fixed at 1.00 q_s, q_a taken as saturation values	$\frac{k_1(T_z}{Z}$ linear prof
Pease 1975	$Q_{ro}(1-a_1C^3)$ $a_1 = 0.6$	$\alpha K\downarrow$ $\alpha = 0.80$ fixed	$\epsilon_s\epsilon_a\sigma T_a^4$ $\epsilon_a = a_2T_a^4(1-a_3C)+a_3C$ $a_2 = 9.2 \times 10^{-4}$ $a_3 = 0.96$	ϵT_s^4 $\epsilon = 0.97$	$a_4V(T_s-T_a)$ a_4 variable	$a_5(a_6e_s - e_a)$ a_5 variable $a_6 = 0.98$ e_s, e_a saturation values	$\frac{k_1(T_o}{H}$
Semtner 1976	Input	$\alpha K\downarrow$ $0.85 > \alpha_s > 0.64$ $\alpha = f$(time of year)	Input	$\sigma T_{s(t-1)}^4 + 4\sigma T_{s(t-1)}^3\Delta T$	Input	Input	$\frac{k_1(T_s}{H/2}$
Maykut 1978	Input	$\alpha K\downarrow$ $0.47 > \alpha_s > 0.27$ $\alpha = f$(ice thickness)	$\sigma T_a^4(a_1+a_2C^{a_3})$ $a_1 = 0.7855$ $a_2 = 0.000312$ $a_3 = 2.75$ $[L\downarrow] = KJ\cdot cm^{-2}\cdot day^{-1}$	ϵT_s^4 $\epsilon = 1.00$	$\rho c_p C_D u_a(T_a-T_s)$ $C_D = 0.003$ $\bar{u}_a = 5\ m\cdot s^{-1}$	$\rho L C_E u_a(q_a-q_s)$ $C_E = 0.003$ $\bar{u}_a = 5\ m\cdot s^{-1}$ R.H. fixed at 0.90 q_a, q_s saturation values	$\frac{k_1(T_o}{H}$

Compiled from sources indicated; see original papers for details of parameterization (e.g. units) and implementation; Subscript s - surface

TABLE 2.1

AMETERIZATION SUMMARY FOR PREVIOUS ICE MODELLING ATTEMPTS

	K↓	L↓	L↑	Q_H	Q_E	Q_I	Q_O
	$\alpha K\downarrow$ $\alpha = 0.64$ fixed	Input	ϵT_s^4 $\epsilon = 1.00$	Input	Input	$\frac{k_i(T_s-T_z)}{z}$ solution by f.d. to yield temperature profiles	Input
$\sec\Omega\cos\Omega$ $= 1.00$ $= 0.77$ $W\cdot m^{-2}$	$\alpha K\downarrow$ $\alpha = 0.79$ fixed	$a_1\epsilon_2\sigma T_a^6$ $a_1 = 9.35 \times 10^{-6}$ (cgs) clear $\epsilon_2 = 1.14$ cloudy $\epsilon_2 = 1.00$	$(1-bc)\epsilon T_s^4$ clear $b = 0.75$ cloudy $b = 0.73$	$\frac{c_p k^2 (T_a-T_s) u\ 1.25(1-R_i)^2}{\ln(z/z_o)}$ $z_o = 0.001$ cm	$\frac{L k^2 (q_a-q_s) u_a\ 1.25(1-R_i)^2}{\ln(z/z_o)}$ R.H. fixed at 1.00 q_s, q_a taken as saturation values	$\frac{k_i(T_z-T_s)}{z}$ linear temperature profile	none
$_1C^3)$	$\alpha K\downarrow$ $\alpha = 0.80$ fixed	$\epsilon_s\epsilon_a\sigma T_a^4$ $\epsilon_a = a_2T_a^4(1-a_3C)+a_3C$ $a_2 = 9.2 \times 10^{-4}$ $a_3 = 0.96$	ϵT_s^4 $\epsilon = 0.97$	$a_4V(T_s-T_a)$ a_4 variable	$a_5(a_6e_s - e_a)$ a_5 variable $a_6 = 0.98$ e_s, e_a saturation values	$\frac{k_i(T_o - T_s)}{H}$	$\frac{\rho_w c_w D(T_D - T_o)}{\tau}$ $\tau = 0.4$ m $D = 5 \times 10^{-5} m^2/s$
	$\alpha K\downarrow$ $0.85 > \alpha_s > 0.64$ $\alpha = f$(time of year)	Input	$\sigma T_{s(t-1)}^4 + 4\sigma T_{s(t-1)}^3 \Delta T$	Input	Input	$\frac{k_i(T_s - T_z)}{H/2}$	Input
	$\alpha K\downarrow$ $0.47 > \alpha_s > 0.27$ $\alpha = f$(ice thickness)	$\sigma T_a^4(a_1+a_2C^{a3})$ $a_1 = 0.7855$ $a_2 = 0.000312$ $a_3 = 2.75$ $[L\downarrow] = kJ\cdot cm^{-2}\cdot day^{-1}$	ϵT_s^4 $\epsilon = 1.00$	$\rho c_p C_D u_a(T_a-T_s)$ $C_D = 0.003$ $\bar{u}_a = 5 m\cdot s^{-1}$	$\rho L C_E u_a(q_a-q_s)$ $C_E = 0.003$ $\bar{u}_a = 5\cdot m\cdot s^{-1}$ R.H. fixed at 0.90 q_a, q_s saturation values	$\frac{k_i(T_o - T_s)}{H}$	none

dicated; see original papers for details of
nits) and implementation; Subscript s - surface

FIGURE 2.1

PARAMETERIZATION SUMMARY FOR PREVIOUS ICE MODELING ATTEMPTS

AUTHOR	SW PENETRATION	SNOW	SALINITY	k_i
Maykut and Untersteiner 1969	$a_1 K^*$ a_1 = 0.17 fixed	- yes - temp. profile by f.d. solution - $k_s = 0.0058\rho_s^2$ - linear decay in albedo with decreasing thickness	- steady state profile specified - S = f(depth) - variable with time as f(depth)	$k_o + \frac{a_z S}{T-273}$ $k_o = 4.86 \times 10^{-3}$ $a_z = 0.28$ (T in °C, c.g.s.)
Goddard 1974	none	- composite 15 cm snow and 15 cm ice considered. (data from Maykut and Untersteiner, 1969)	none	- see SNOW - fixed $k_i = 1.26 \times 10^{-3}$ (c.g.s.)
Pease 1975	$a_7 K^*$ a_7 = 0.20 fixed	- no snow allowed but albedo set at 0.90 to compensate	- average ice salinity fixed - no variability	- fixed - no values given
Semtner 1976	$a_1 K^*$ a_1 = 0.17 fixed to a limit of 30% of heat required to melt all ice	- yes - linear temp. profile imposed - allowed to ablate $k_s = 7.4 \times 10^{-4}$ (c.g.s.) $\rho_c = 0.165$ $\rho_s = 0.33$	- average salinity = f(ice thickness) - at a given thickness, salinity is considered constant throughout	- fixed $k_i = 4.86 \times 10^{-3}$ (c.g.s.)
Maykut 1978	$a_4 = K^*$ a_4 = 0.17	- yes - linear gradient k_s = 0.31 (M.K.S.)		$k_o + \frac{a_s S}{T-273}$ $k_o = 2.03$ $a_s = 0.117$ (T in °C, M.K.S)

Compiled from sources indicated. See original papers for details of parameterization (e.g. units) and implementation. Subscript s = surface.

ocean. The first model employs a stable water layer of fixed temperature, salinity and diffusivity. The second model has a deep water layer with the properties as previously described but a mixed layer, where heat and salt fluxes are allowed to vary in response to changes in the upper boundary, is introduced between the ice and the stable water layer. The third version features the deep water layer, the mixed layer and a surface layer of low salinity meltwater which is transient, disappearing by refreezing or mixing with the underlying layers.

A comparison of observed with predicted ice thickness and extent along a longitudinal transect in the Antarctic showed acceptable agreement with regard to phase (i.e., the time of occurrence of maximum and minimum thicknesses) but poor with respect to magnitude. The first model consistently underestimated ice growth while the second and third forms produced overestimates. The poor agreement obtained may be due to the fact that a snowpack was not considered in the model formulation leaving out the influence of this very effective thermal barrier. Although only fair results were obtained, it is a model worthy of attention because of its detailed treatment of ocean processes.

Semtner (1976) presents a model to be used to predict the thickness and extent of sea ice in climate simulations.

A basic one-dimensional diffusion process is taken to act in the ice with modifications due to the penetration of solar radiation, melting of internal brine pockets and accumulation of an insulating snow cover. The model is essentially that of Maykut and Untersteiner (1969) but a streamlined numerical method is employed.

An energy balance approach is used but the fluxes of latent heat, sensible heat, incoming solar radiation and incoming longwave radiation must be supplied as inputs. In evaluating the model a climatic forcing identical to that of Maykut and Untersteiner was employed and the results also compared with those of Maykut and Untersteiner.

Due to the large number of required inputs and the lack of comparison with independent data it is difficult to evaluate the effectiveness of the model. The most interesting feature is the computational method adopted for the ice phase which represents a cross between a costly fine grid finite difference. technique (Maykut and Untersteiner) and a bulk substrate model (this study).

Goddard (1974) employed a climate simulation model derived from Myrup (1969) in which information about the state of the atmosphere, the surface and the underlying medium is utilized in conjunction with an explicit relationship between the surface temperature and each component of the energy balance.

In this type of approach, often referred to as an 'equilibrium surface temperature model', the energy and radiation fluxes reflect and respond to the characteristics of the site surface. Taking available climatic data as input Goddard's model calculates the atmospheric stability and uses this to estimate the boundary layer shear stress and thence the sensible, latent and conductive heat fluxes in terms of the available energy (see Table 2.1).

The model was tested on arctic pack ice at 75°N latitude (AIDJEX test site) in early April. Good agreement was found between the hourly measured micrometeorological variables and those which were simulated. This agreement was taken as a demonstration of the geophysical soundness of the model and its self consistency. Goddard suggests that the model should be applied to the case of seasonal growth to determine its potential as a technique for assessing the consequences of changes in surface or climatic variables.

Maykut (1978) presents a model of energy exchange over young sea ice in the central Arctic. It is a systematic investigation of variations in the surface energy balance related to ice thickness and is accomplished by combining a simple sea ice model with climatological data on incoming radiation and air temperature to calculate how the fluxes of sensible heat, latent heat and emitted longwave radiation over

sea ice depend on season, ice thickness and snow cover.

The paper investigates the impact of areas of young ice and open water on the large scale heat and mass balance at the surface of the polar oceans. By calculating the energy balance for different ice thicknesses under the same climate conditions and then weighting these results by the areal extent of each thickness group, a realistic estimate of the regional energy balance was produced.

An energy conservation approach based on an equilibrium surface temperature is adopted and the specification of component terms is similar to that presented in this paper (see Table 2.1). The temperature inputs are specified from the equilibrium climate determined over pack ice using Maykut and Untersteiner's model; daily values throughout the year were obtained by interpolation of a smoothing polynomial fitted to the monthly averages. The results obtained reflect the response to a slowly varying 'average' climate. Maykut's work differs fundamentally from the present study in that ice growth is not considered, the ice thickness is a fixed constant which is specified as an input.

The work of Maykut and Untersteiner, Pease, Semtner and Maykut have demonstrated the usefulness of the energy balance approach in the study of sea ice growth. These models suffer in that there is an insufficient comparison with field obser-

vations, a reflection more of the lack of data rather than the inadequacy of the models. Goddard's work provides field confirmation of the ability of this approach to provide realistic estimates of the components of the energy balance when applied to sea ice. The work presented here advances from its predecessors by employing an equilibrium surface temperature energy balance model which includes ice growth and compares the results obtained (with respect to magnitude and time) with field observations from several locations throughout the Canadian Arctic.

It was only after the completion of this paper that the work of Lally (1973) and Conway (1976) on ice modelling was brought to the author's attention. No investigation has been made of the relative merits or applicability of their approaches.

CHAPTER 3

ICE GROWTH AND ITS RELATION TO THE ATMOSPHERE AND OCEAN

3.1 Physical Processes of Ice Growth

3.1.1 Ice Growth and Brine Entrapment

As the air temperature drops in the fall, heat is extracted from the sea until the freezing point is reached at the sea surface. The temperature of the freezing point is determined by the water salinity; sea water with 35 $^{o}/oo$ salinity freezes at -1.8^{o}C. In calm waters with a low temperature gradient, ice begins to form in localized regions where stable crystallization nuclei occur. The ice particles are disc shaped and grow outwards along the surface in interlocking hexagonal patterns. This rapid lateral growth forms a skim cover in which most of the ice crystals have a preferred vertical c-axis orientation because the ice crystals tend to float with their longer planes parallel to the water surface. If a strong temperature gradient is forcing the growth under calm conditions then either a random orientation of the c-axis or a vertical preferred orientation superimposed on a random orientation may result. Under conditions where the surface is agitated nucleation from frazil results in tabular, equiaxed

crystals with a random crystallographic orientation (Michel & Ramseier, 1969). This initial skim is known as primary ice.

After the establishment of a stable ice cover growth of secondary ice occurs in the vertical dimension. A crystallographic orientation transition zone occurs in the next 5-20 cm if we are dealing with a primary ice cover that has a random or random with preferred vertical orientation. Growth competition between crystals of different orientation occurs at the ice-water interface. Those crystals with horizontal c-axes grow downward more rapidly than the adjacent crystals because heat is transferred most effectively along an ice crystal's basal plane (perpendicular to the c-axis). While the mechanisms suggested to explain the development of a dominant crystal orientation are not fully satisfactory (Weeks & Assur, 1968), it is observed that beneath the transition zone the ice is mainly composed of long columnar ice crystals with their c-axes essentially horizontal. Figure 3.1 shows the characteristics of the crystal structure within young sea ice.

The ice propagates downward into the sea water as an irregular, dendritic surface. A series of plates of pure ice protrude into the underlying water, separated by layers of brine, forming the skeletal layer. Within the skeletal layer the plate to plate spacing is a function of the growth conditions but the thickness of the layer is a relatively constant

FIGURE 3.1 CRYSTAL STRUCTURE OF SEA ICE

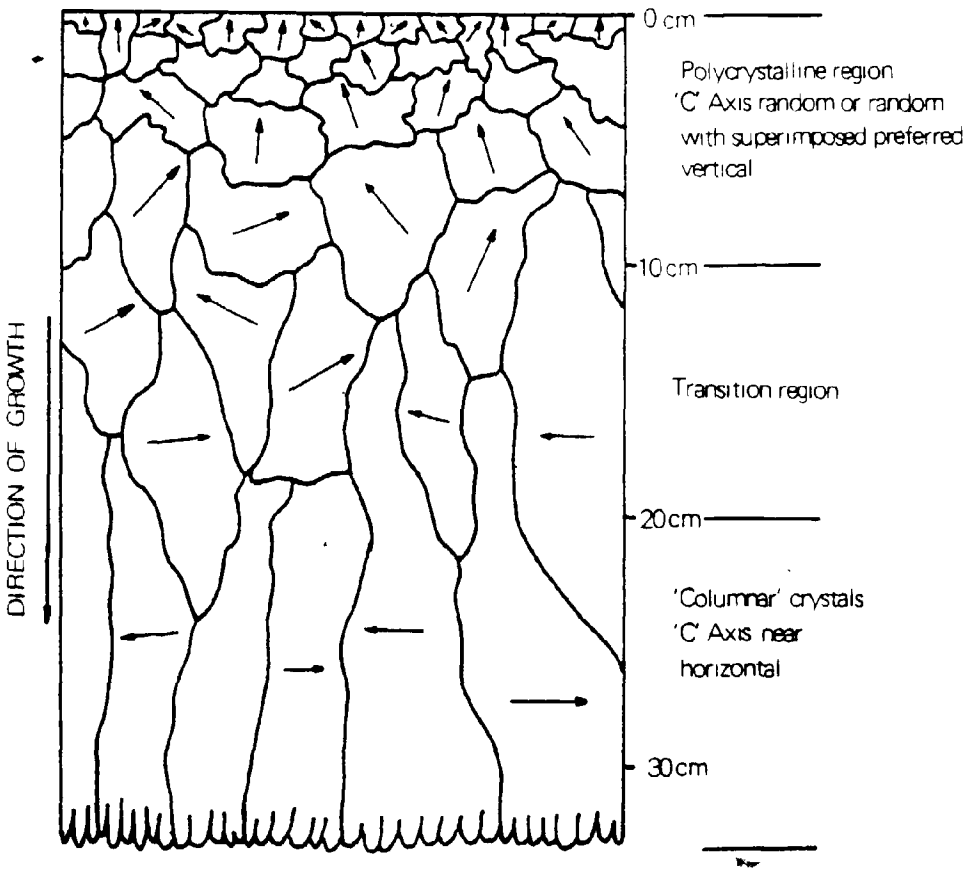

Source: Adapted from Milne (1976)

2-3 cm. The skeletal layer lacks appreciable strength as there is no lateral connection between plates. Bridging occurs laterally between the plates producing a series of elongated brine pockets in which brine is physically entrapped within the ice.

The process of bridging and incorporation of brine into the ice structure is poorly understood although Lake and Lewis (1970) provide a plausible hypothesis for brine pocket development. A typical brine tube in the skeletal layer is 2-3 cm long with a cylindrical shape closed at the upper end by a slightly bulbous cap. Ice forms within the tube on the cylindrical walls at the end cap. This ice growth is limited by the rapid increase in salinity as the salt is rejected back into the interstitial brine. The result is that the growth of ice within the tube is retarded with respect to the general interface and the tube elongates. Assuming the isotherms to be parallel to the ice-water interface, a temperature gradient will be established in the brine with the growth of the ice. Downward growth of the ice induces a density and density gradient increase in the brine immediately adjacent to the end cap. Convection occurs when the density gradient in the cap is about one order of magnitude greater than that existing in the main cylindrical portion of the tube. The cold dense brine within the tube is exchanged for the less

saline warmer water beneath creating a local deformation of the isotherms in the water body and promoting further growth.

Theoretical and experimental investigations of convection in a tube closed at one end show that under boundary conditions similar to those occurring in the sea ice case, a stagnant region will exist at the closed end of the tube. Rapid radial ice growth ('necking' or 'bridging') occurs a few millimetres below the bulbous end cap which is thought to define the stable region. This results in the sealing off of the upper portion of the tube creating a brine inclusion. The growth of the neck provides a source of salt to sustain convection and on sealing the tube reverts to its original length, thereby maintaining a constant thickness of the skeletal layer. General ice growth at the interface then proceeds until a density gradient sufficient to induce convection is established and necking is once again initiated. A schematic of the process is given in figure 3.2.

3.1.2 Brine Drainage

Salt is continually ejected from a growing ice sheet due to rejection during crystal growth as described above and by drainage of the dense brine from the interior of the ice sheet. The latter depends on the characteristic crystallographic features of the ice called brine drainage channels which Lewis

FIGURE 3.2 BRINE POCKET INCLUSION PROCESS

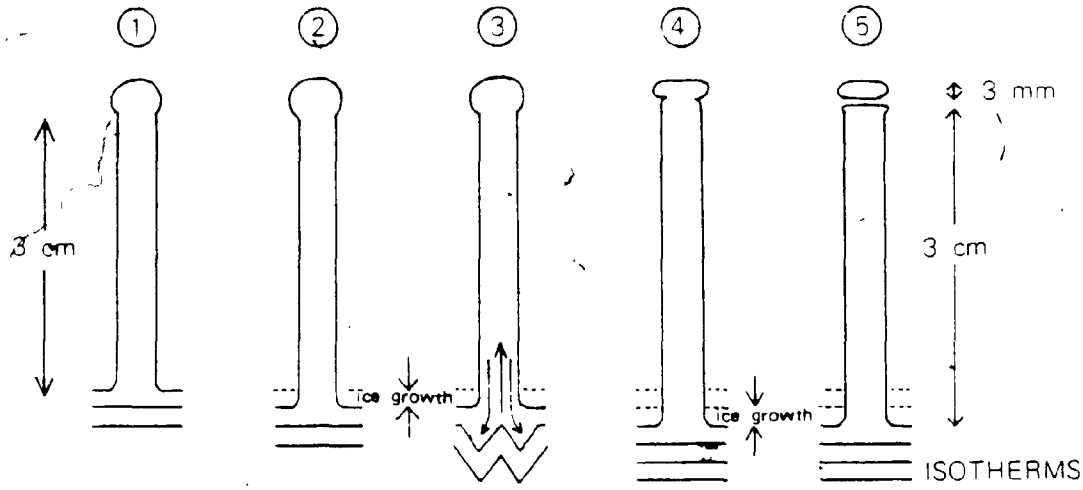

1. Initial tube.
2. Interface ice growth at base while growth inside tube is restricted due to the high salinity of the interstial brine. A density gradient develops between the end cap and the main body of the tube.
3. Convective overturning of the brine occurs when the density gradient in the cap is approximately an order of magnitude greater than the density gradient in the main body of the tube.
4. The overturning of (3) brings cold brine to the interface deforming the isotherms, resulting in more ice growth at the interface. A stagnant region at the closed end of the tube develops and bridging commences
5. The brine inclusion after bridging is completed.

(1976) likens to a river network extending upwards from the ice-water interface to the top of the secondary ice layer near the surface. These brine channels in thick ice are separated by 15-20 cm in the horizontal plane (Lake and Lewis, 1970) and have a diameter of approximately 1 cm at the terminus. Figure 3.3 illustrates the relation between crystal zonation, brine channels and the skeletal layer in a growing ice sheet. Niedrauer (1977) summarizes the results of a laboratory study of brine channel features and processes. Solute rejection during crystal growth has been treated analogously to impurity rejection during metal solidification. Qualitatively, the metallurgical equations agree with observations that the amount of salt rejected back into the sea-water increases as the growth velocity decreases but the numerical values should not be employed due to differences in the nature of the systems (see Lake (1969) and Kvajic, Pounder & Brajovic (1971) for examples).

The position of the brine pockets in relation to the upper and lower ice surfaces is changed as the ice cover thickens. The inclusion is progressively cooled which initiates partial freezing within the pocket, increasing the brine salinity, in order that the trapped brine remain in equilibrium with the temperature of the surrounding ice (e.g., it concentrates to remain on the eutectic). This process reduces the brine

FIGURE 3.3 STRUCTURES IN FIRST YEAR SEA ICE

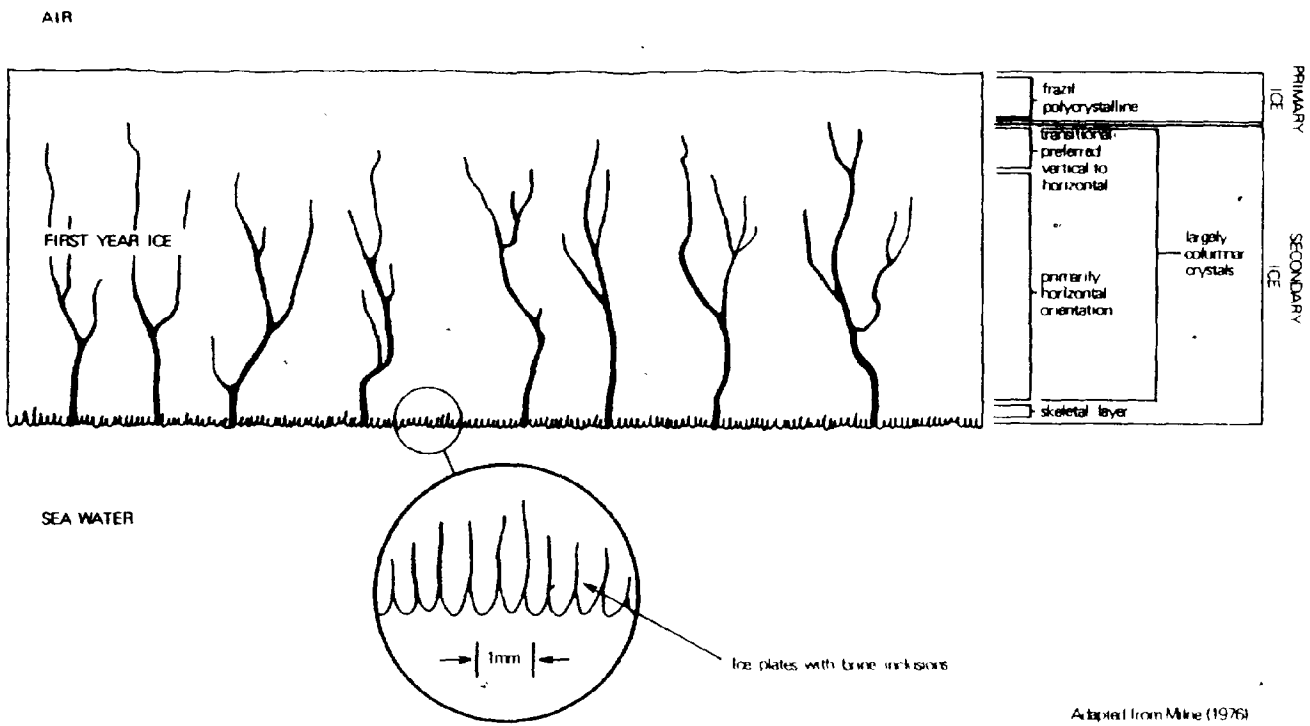

Adapted from Milne (1976)

(on a unit volume basis) but leaves the overall salinity unchanged in the absence of brine drainage. (This simplified description is valid only when crystallization of the entrapped brine does not occur. Below -8°C $Na_2SO_4 \cdot 10H_2O$ begins to crystallize from the brine followed by $NaCl \cdot 2H_2O$ at -23°C, which leads to a reduction in the brine concentration. The sequence of crystallization of salts may be found in Assur's (1958) phase diagram [illegible] ice.) Over time, desalination mechanisms act to redistribute and reduce the overall salt content.

Young first year ice has initially a C-shaped salinity profile indicating high salt contents at the surface and in the basal skeletal layer. In second year ice the salinity has decreased substantially in the upper layers and a peak occurs deeper within the ice mass. After several years the salinity profile is such that the surface layers are essentially salt free, the salinity increases with depth, and the average salinity of the ice is very much reduced. Representative profiles are shown in figure 3.4. Four major mechanisms have been suggested to account for the migration of the brine within the ice sheet. These are hydrostatic flushing, brine pocket diffusion, brine expulsion and gravity drainage.

FIGURE 34
SALINITY AS A FUNCTION OF DEPTH BELOW
THE SURFACE OF ICE

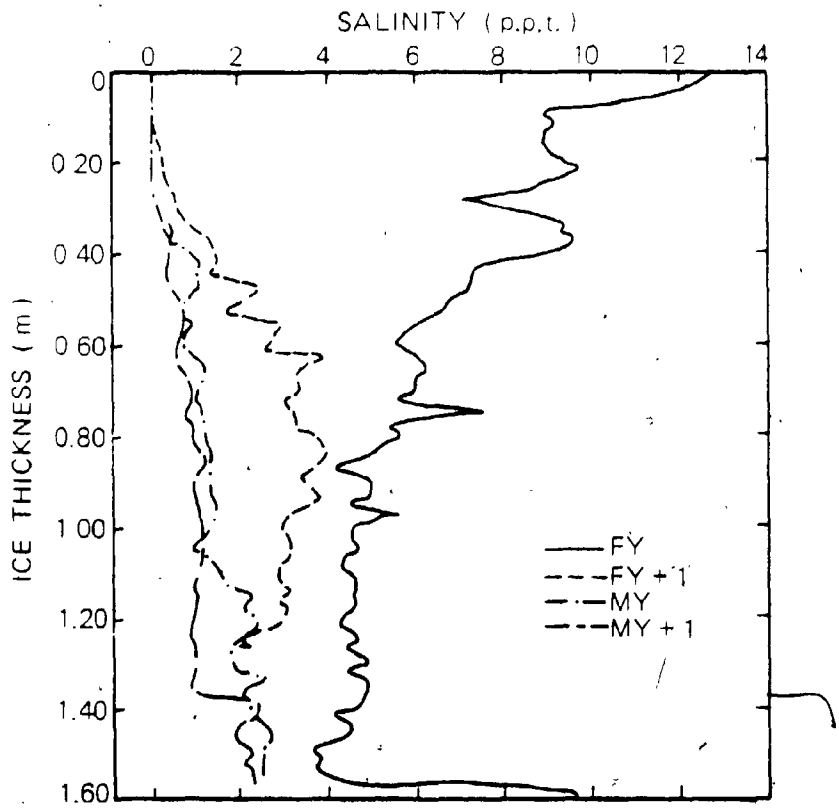

Salinity as a function of depth below surface of ice observed in (a) first yeat ice (FY); (b) first year plus 1 year (FY + 1); (c) multiyear ice (MY); and (d) multiyear plus 1 year (MY + 1). Only for FY and FY + 1 has the total thickness been shown whereas the other curves would extend to greater depths.

Source: Campbell et al. (1978)

Flushing occurs when meltwater is ponded on the surface of the ice creating a hydrostatic head which drives the low salinity meltwater through the permeable portions of the ice. Flushing is thought to be responsible for the rapid desalination of the upper ice levels observed during the melt period of the first year ice and in determining the upper profile in the multiyear ice. Due to its occurrence only during periods of extended melt it has no effect on salinity redistribution during the growth period of first year ice.

Brine pocket diffusion relates the brine migration as a diffusion process to the ice temperature gradient. Within a brine inclusion a temperature gradient exists between the cold upper portion and the warmer lower layers. As the brine density is temperature dependent this creates a concentration gradient which requires salt diffusion from the colder to the warmer end to minimize the gradient and drive the system towards equilibrium. This results in a brine concentration at the lower end that is greater than that imposed by the temperature field and melting is initiated to dilute the brine. At the upper end the brine is now less dense and freezing occurs to concentrate the solution. Repetition of this process produces a continuous migration of the inclusion towards a warmer temperature which is generally the ice-water interface. The process was studied by Hoekstra et al (1965)

who employed the diffusion equation

$$V = \frac{D}{S_b} \left(\frac{dS_b}{dT}\right)_T \frac{dT}{dZ} \tag{3.1}$$

where V = brine pocket velocity

T = temperature (^{o}K)

S_b = brine concentration

D = diffusion constant

Z = distance

$\frac{dS_b}{dT}$ = slope of liquidis curve

$\frac{dT}{dZ}$ = temperature gradient.

In a comparison of observed and predicted brine velocities the theoretical velocities were consistently higher. Experimentally observed velocities were in the range of 85 microns/hour (2 mm/day) under a temperature gradient of 3°C/cm and 30 microns/hour (0.7 mm/day) at 1°C/cm. Harrison (1965) employed a temperature gradient of 15°C/cm and obtained velocities in the millimetre per hour range. His observations also indicate that as the droplets approached the ice-water interface they accelerated steadily, increased in diameter and then punctured the interface and merged with the water leaving only clear ice behind. Employing temperature values typical of a natural sea ice cover, Lake and Lewis (1970) estimate a velocity of 0.07 mm/day. These results suggest that for gradients typically encountered in normal sea ice, brine drainage due to temperature induced diffusion is negligible.

Tsurikov (1967) attributes changes in salinity of ice to the movement of brine pockets under the influence of the temperature gradient in ice as a result of ice thawing at the warmer end of the pockets and the freezing of brine at the colder ends; a process he regards as distinct from ion diffusion phenomena as studied by Hoekstra et al (1965). The governing differential equation intended for the calculation of the variation in salinity of the individual layers of ice is given by

$$\frac{dS}{dt} = \frac{-a}{nr^2 L_f \Delta T_f} (S) \frac{\partial S}{\partial Z} \frac{\partial T}{\partial Z} \tag{3.2}$$

where n = number of brine pockets per unit area
r = radius of brine pocket
L_f = heat of phase transition
ΔT_f = change in freezing point of brine as a result of phase transition
a = temperature dependent constant.

This relationship does not appear to provide sufficient explanation of salinity redistribution in sea ice; further comments on its application may be found in Appendix A.

Brine expulsion is another suggested desalination agent. A specific ice depth undergoes continual cooling due to the movement of the ice-water interface as an ice sheet ages. Freezing will occur at the brine cavity edges to increase the brine concentration and maintain phase equilibrium. High internal pressures are produced due to the 10 per cent volume

increase associated with the ice growth. Nakaya (1956) observed that the mounting pressure in the liquid caused the ice to fail along the crystallographic basal plane allowing some liquid to escape and migrate toward the warm end of his samples. Within an ice cover, expulsion near the surface may drive the salt to the air-ice or snow interface which would provide a source for the brine found on the ice surface or absorbed in the overlying snowpack. The expulsion along the basal plane toward the warm ice-ocean interface drives the brine down and ultimately out of the ice sheet. The occurrence of cracking along the crystal boundaries (lines of natural weakness) may lead to the development of a primary drainage channel. This may then act as a focus towards which other cracks would tend to propagate leading to the development of a dendritic channel as has been observed in real ice (Lake and Lewis, 1970) and laboratory ice (Eide and Martin, 1975). Untersteiner (1968) examined the potential of the mechanism using what he considered a highly schematized model requiring later investigation by experiments and concluded it to be a valid process to account for the development of a salinity profile of multiyear ice. Cox and Weeks (1975) dismiss his results as irrelevant because continuity during warmer periods when a net increase in salt may result was neglected and their belief that brine expulsion should be evaluated on the basis of comparisons between sequential salinity profiles

from first year ice. They formulated a one-dimensional brine expulsion model by performing energy and mass balances over a control ice volume. This produces a thermal energy equation and two continuity equations involving three unknowns which may be solved employing numerical techniques. By comparison of their model with experimentally obtained sequential ice salinity profiles they were able to estimate the percentage of salinity change which could be attributed to brine expulsion (assuming the model to be correct). The results indicate that brine expulsion played a small role in overall desalination but in periods of rapid ice growth (ice thickness <25 cm) the change in salinity due to expulsion was significant.

Gravity drainage includes all processes by which brine under the influence of gravity drains out of an ice sheet. Kingery and Goodnow (1962) concluded from their experimental results that gravity drainage was the primary mechanism by which salt was eliminated from new ice. Untersteiner (1968) argued that the mechanism is probably effective only in young sea ice and is unlikely to occur in thick floating multiyear ice. Cox and Weeks (1975) also designate gravity drainage as the dominant desalination mechanism in young sea ice based on their experimental results. The rate of gravity drainage was highest in the lower, warmer part of the ice which they attribute to a higher ice permeability associated with the high

brine volumes at these levels. Gravity drainage should increase, at a given permeability, as the temperature gradient increases because of the dependency of the brine density on temperature; a result qualitatively observed in their experiments. Due to this dependency one would expect the rate of gravity drainage to decrease as an ice sheet thickens. Also tending to decrease the rate of gravity drainage is the fact that as the salt drains from the ice, its permeability decreases due to the presence of smaller volumes of brine.

To develop a theoretical model of gravity drainage information is required concerning the permeability of ice. This requires an understanding of the ice microstructure of which our present comprehension is poor. At present no model has been proposed that would allow quantitative estimation of the salt fluxes due to gravity drainage.

A knowledge of brine entrapment and migration is of concern in modelling the thermodynamic response of ice in that internal energy transfers and significant changes in the ice thermal properties may result. The original intent of this paper was to examine and quantify the interrelationships between salinity redistribution and thermal behaviour using an approach similar to that employed in studies of coupled heat and moisture flows in frozen soils. Due to the complex and irregular behaviour of brine within an ice sheet this goal

was not achieved. A simplified form of brine content - thermal property interaction was employed, details of which may be found in Chapter 4. A summary of some of the work performed on the brine redistribution aspect is presented in Appendix A.

3.2 Ocean-Ice-Atmosphere Interaction

3.2.1 The Atmosphere

In the atmosphere at heights in excess of 1000 m horizontal air motions proceed in a largely geostrophic manner, these motions are unretarded by friction and are usually smooth and free from turbulence. Below 1000 m we enter the planetary boundary layer where turbulence and other effects of frictional drag exerted by the earth's surface are seen. Between a level of approximately 50 m and the surface the speed of the wind reduces rapidly towards zero. This zone is known as the surface boundary layer. Wind characteristics are determined largely by the physical nature of the underlying surface and the form of the vertical temperature gradient. The distinction between the surface boundary layer and the outer or Eckman layer of the planetary boundary layer may be made on the basis of the surface friction Rossby number. The Eckman layer between 1000 m and 50 m is a transition zone between the smooth geostrophic flow in the free atmosphere and the turbulent flow near the ground. Immediately

FIGURE 3.5 TURBULENT STRUCTURE OF THE ATMOSPHERE

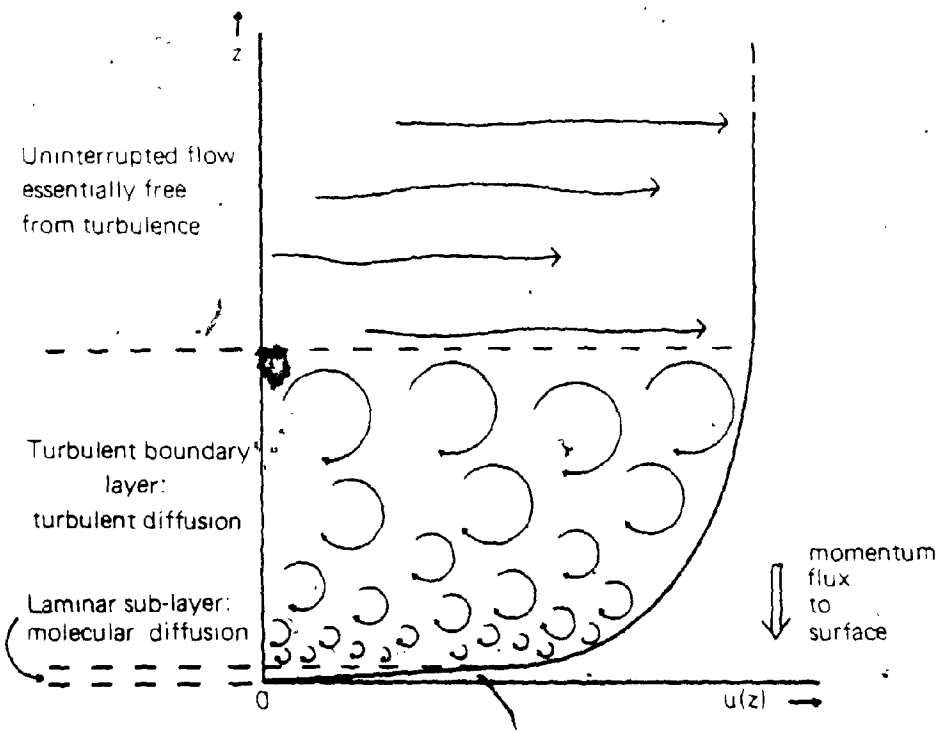

Source: McIntosh and Thom (1972)

adjacent to the lower boundary is the laminar sublayer in which the fluid flow is laminar and diffusive motions are entirely molecular in origin, character and scale.

Fluid moving over a level surface exerts a horizontal force on the surface in the direction of motion of the fluid. This force is a drag force and is usually expressed per unit area of surface and termed shearing stress. The shearing stress exerted on a surface by fluid flow is generated within the boundary layer and transmitted downwards to the surface in the form of a momentum flux (see figure 3.5). (Note that the dimensions of shearing stress can be expressed as a force per unit area or momentum per unit area per unit time.) This downward flux of streamwise momentum arises from the sheared nature of the flow within the boundary layer and derives from the interaction between this shear and vertical random motions within the air.

Assuming the shear stress to be constant within the region of measurement it can be shown that

$$\frac{\partial u}{\partial Z} = \frac{1}{kZ}\sqrt{\frac{\tau}{\rho_a}} \qquad (3.3)$$

where $\frac{\partial u}{\partial Z}$ = gradient of wind velocity with height

τ = shearing stress due to momentum transfer

ρ_a = density of air

Z = height from surface

k = von Karman's constant

Integration of this equation for a neutral atmosphere leads to the familiar logarithmic wind profile equation

$$u(Z) = \frac{1}{k} \sqrt{\frac{\tau}{\rho_a}} \ln \left(\frac{Z}{Z_o}\right) \tag{3.4}$$

where Z_o = surface roughness length.

Relating the momentum flux (τ) to the wind gradient (equation (3.3)) and defining an exchange coefficient for momentum, K_M, we arrive at

$$\tau = \rho K_M \, (\partial u/\partial Z) \tag{3.5}$$

With equation (3.4) we can solve for K_M

$$K_M = k u_* Z \tag{3.6.a}$$

$$= \frac{k^2 u(Z) Z}{\ln(Z/Z_o)} \tag{3.6.b}$$

where u_* = friction velocity $= \sqrt{\tau/\rho}$

For neutral conditions the momentum transfer coefficient increases in proportion to the height in the surface layer at a given height is proportional to the wind speed. With a knowledge of the local wind profile we may calculate the momentum transfer coefficient and the shear stress.

The transfers of sensible heat and latent heat may be described by similar gradient equations. These are given by equations 3.7 and 3.8 respectively.

$$F_H = \rho_a c_p K_H \frac{\partial T}{\partial Z} \tag{3.7}$$

$$F_E = \rho_a L_v K_E \frac{\partial q}{\partial Z} \tag{3.8}$$

where c_p = specific heat of air at constant pressure

L_v = latent heat of vapourization

$\frac{\partial T}{\partial Z}$ = gradient of temperature with height

$\frac{\partial q}{\partial Z}$ = gradient of specific humidity with height.

Similarity theory allows the assumption that the transfer coefficients for sensible heat (K_H) and water vapour (K_E) are equal to that for momentum transfer. This applies only to a narrow stability range centred on neutral (although there is evidence that $K_H > K_M$ under neutral conditions (Businger et al., 1971)). Stability refers to the state of the atmosphere with respect to vertical motions. Under stable conditions the vertical displacement of fluid particles is suppressed whereas enhancement occurs in the unstable case. Corrections can be made to the values of the transfer coefficients obtained under non-neutral conditions by the use of functional relations involving the Richardson number (a measure of stability expressing the ratio of buoyancy to shear effects) or through the concept of a characteristic Obukhov length where buoyant energy production equals shear production (Paulson, 1970).

An alternative approach is that of the drag coefficient. In this the observed shear stress is represented by

$$\tau = \frac{1}{2}\rho C_M (u(Z))^2 \tag{3.9}$$

where C_M = drag coefficient (dimensionless) for momentum transfer.

The drag coefficient is a measure of the observed shear stress relative to the theoretical maximum that could occur if a body was immersed into a fluid at right angles to the fluid flow. This maximum is given by

$$\tau_{max} = \frac{1}{2}\rho u^2 \tag{3.10}$$

which occurs if a fluid particle is brought to rest against the surface (the initial momentum per unit volume of fluid is ρu and the mean velocity of the fluid during deceleration is u/2, therefore the rate at which momentum is lost from the fluid is $(\rho u) \cdot (u/2) = 1/2\ \rho u^2$).

Therefore

$$C_M = \frac{\tau}{\tau_{max}} = \frac{\tau}{\frac{1}{2}\rho (u(Z))^2} \tag{3.11}$$

In comparison with the transfer coefficient theory, equivalent relations imply that

$$C_M = \frac{k^2 (u(Z))}{\{\ln(Z/Z_o)\}^2} = \frac{u_*^2}{u(Z)} \tag{3.12}$$

and

$$K_M = kZu\ (C_M/2) \tag{3.13}$$

The drag coefficient will be a function of height until the top of the planetary boundary layer is reached, at this point the winds are geostrophic, constant with height and we may define the geostrophic drag coefficient. In practice the drag coefficient is specified for a certain level where the wind speed is measured, 10 m. usually being the accepted level.

Sensible heat flux and evaporative heat flux may be deduced from the following relationships

$$F_H = \rho c_p u C_H (T_{Z_2} - T_{Z_1}) \tag{3.14}$$

$$F_E = \rho L_v u C_E (q_{Z_1} - q_{Z_1}) \tag{3.15}$$

where C_H = drag coefficient associated with the transfer of sensible heat

C_E = drag coefficient associated with the transfer of evaporative heat

3.2.2 Snow-Ice Medium

This section examines the thermal transfers within a natural snow and ice system. The steady state energy flux within a solid medium is given by the Fourier relation

$$F_I = k \frac{dT}{dZ} \tag{3.16}$$

where k = thermal conductivity

$\frac{dT}{dZ}$ = temperature gradient.

If the thermal conductivity is fixed then a constant temperature gradient is necessary to maintain steady state conditions. A temperature profile under these conditions is linear. When internal heating or cooling is occurring then the profile exhibits curvature and a steady state energy flux cannot be maintained. The temperature field of the medium then changes according to the parabolic heat conduction equation

$$\frac{\partial T}{\partial t} = \frac{k}{\rho c_p} \frac{\partial^2 T}{\partial Z^2} \tag{3.17}$$

With the specification of the temperature field that satisfies (3.17) the energy flux at any level may then be calculated. In most natural systems the solution of (3.17) is non-trivial. In sea ice the existence of brine pockets renders the thermal properties non-uniform, complicates the nature of the phase change mechanism and gives rise to internal heating through the absorption of penetrating solar radiation. For the case of a perennial sea ice cover Maykut and Untersteiner (1969) solved (3.17) using an explicit finite difference technique.

It has been observed in young sea ice (Billelo, 1978) and in arctic snow covers (Holtzmark, 1955) that temperature

profiles remain nearly linear. First year sea ice temperature measurements made on Eclipse Sound N.W.T. (Polar Continental Shelf Project, 1979) confirm Bilello's observations for young ice. Examination of ice temperature data during the later stages of growth show that linear profiles are also present in 2 m. ice. Using slowly varying incident energy fluxes, realistic salinity profiles and the model of Maykut and Untersteiner (1969), Maykut (1978) found that temperature profiles in rapidly growing thin ice remained nearly linear. Curvature was noted only in the case of strong internal heating or abrupt changes in climatic forcing. He argues that the Fourier steady state heat transfer relation (equation 3.16) may be used in modelling the behaviour of young ice because the thermal reaction time of ice is small in comparison with the time needed to change its thickness significantly and that the thermal conductivity is sensitive to salinity only at temperatures near the freezing point. Bilello (1978), Lewis (1967), Pounder (1965), and Schwerdtfeger (1964) have examined the question of thermal lag and the determination of the velocity of propagation of thermal effects. Bilello (1978) recorded that the time lag, as defined by the peak high and low temperatures, for a combined snow depth of 10 cm and ice thickness of 50 cm was roughly 1-2 days. This lag is associated with energy storage and release associated with the heat capacity of the ice medium. The instantaneous

adjustment of the ice to the new thermal regime, as specified by the use of the steady state relation, will cause ice growth to occur at a faster rate than if heat effects had been included.

3.2.3 Ocean-Ice Interface

The ocean beneath an ice surface behaves in the same manner as the earth's planetary boundary layer, only at different scales (see Table 3.1). Predictions of Reynold's stress and mean flow in the ocean beneath an ice cover by a model of a neutrally buoyant, horizontally homogeneous atmosphere are in close agreement with observations (McPhee and Smith, 1975).

The acceptance of the neutral stability has further imlications in modelling energy transfers at the sea ice boundary and so it is necessary to examine this further. In the atmosphere the force which causes warm parcels of air to rise is known as the buoyancy or Archimedian force. A parcel immersed in the air 'fluid' is subjected to an upward directed buoyancy equal to the weight of the amount of fluid that the parcel displaces. The parcel will then rise, sink or remain at the same level depending on whether this force is greater than, less than or equal to the downward force on the body due to the acceleration of gravity. These buoyancy differences may be related to temperature gradients indicating that changes in

TABLE 3.1

BOUNDARY LAYER SCALES: ATMOSPHERE AND OCEAN

	Atmosphere	Ocean
Friction velocity	30 $cm \cdot s^{-1}$	1 $cm \cdot s^{-1}$
Surface layer depth	30 m	1 m
Planetary boundary layer depth	1000 m	35 m

atmospheric stability are induced by daily heating and cooling.

There exists an analogy between the diurnal fluctuations of temperature found in the atmosphere and the annual freezing and melting of pack ice. As water freezes at the interface the brine that is excluded tends to sink because of its greater salinity just as air heated at the surface tends to rise due to its lower density. Introduction of a characteristic length L_o for the ocean allows a comparison to be made of stability in the ocean to that in the atmosphere. The ratio $-Z/L_o$ characterizes the contribution of buoyancy to the energy balance and L_o serves as a measure of the scale at which the buoyant production of turbulent energy becomes important relative to shear production (McPhee and Smith, 1975).

The turbulent density flux (F_S) in the surface layer of water is equivalent to the rate at which mass is excluded from freezing water and is proportional to the growth rate.

$$F_S = \frac{\rho_i \Delta S d}{1000} \tag{3.18}$$

where F_S = salt flux

ΔS = salinity difference between ice and water (p.p.t.)

d = growth rate

The Obukhov-like scaling length, L_o is defined as

$$L_o = \frac{\rho u_*^3}{g k F_S} \tag{3.19}$$

where g = acceleration due to gravity

With (3.18) and (3.19) we may solve for the growth rate required to produce significant instability (as defined by $Z/L_o = -1$; a $|Z/L_o| = 1$ implies that buoyancy is as important as shear at length scales comparable to the entire boundary layer depth - a negative value implies a net downward flux resulting from the conversion of potential energy to turbulent kinetic energy).

$$d = \frac{1000\rho_o u_*^3}{gk\rho_i \Delta S L_o} \tag{3.20}$$

Setting $u^* = 1$ cm/s, $\rho_i = 0.92$ g·cm^{-3}, $\rho_o = 1.0$ g·cm^{-3}, $k = 0.40$, $g = 980$ cm/s, $L_o = 30$m and $S = 15\%$ (McPhee and Smith, 1975) one arrives at a growth velocity of 6.17×10^{-5} cm/s or 5.3 cm/day. This indicates that in a moderate shear environment even weak instability requires rapid freezing. These freezing rates would be reached only under conditions of initial ice formation. These calculations are similar to the results of Weber's (1977) theoretical investigation of the transient state of ice formation and associated change in sea water salinity due to salt rejection. He concludes that growth rates required to generate salinity induced instability are of the order of 1 cm/hour (24 cm/day) which affirms McPhee and Smith's suggestion that the occurrence of unstable conditions resulting from brine expulsion relatively rare.

Melting at the ice-water interface is analogous to a radiation inversion in the atmosphere and melt rates of the

same magnitude as for freezing would be required. Using these arguments it is possible to rule out instability due to freezing or melt induced stability as likely conditions and allow us to treat the boundary layer as neutrally stable.

Having identified the water beneath the ice surface to be neutral we may use this information in discussing the existence of a mixed layer beneath the ice cover. The term mixed layer refers to a zone in which hydrographically significant variations are absent. This implies that variations in salinity and temperature do not occur rendering the layer isohaline and isothermal. Beneath multiyear pack ice in the Beaufort Sea McPhee (1975) observed this layer to be 35-40 m in depth (Figures 3.6(a) and 3.6(b)). Lewis and Walker (1970) observed a 25 m depth for the mixed layer at Cambridge Bay while 11 m was observed on Greely Fjord by Lake and Lewis (1971). In Eclipse Sound a seasonal variation from 35 m in January to about 50 m in May was observed (Barber, 1977).

It has also been observed that the temperature of the layer immediately below the ice is at the freezing point, as determined by its salinity. Figures 3.6(a) and 3.6(b) show this for the AIDJEX site where the 29.7$^{o}/oo$ salinity

FIGURE 3.6(a)
TEMPERATURE AND SALINITY PROFILES
BENEATH BEAUFORT SEA ICE (9 APRIL 1972)

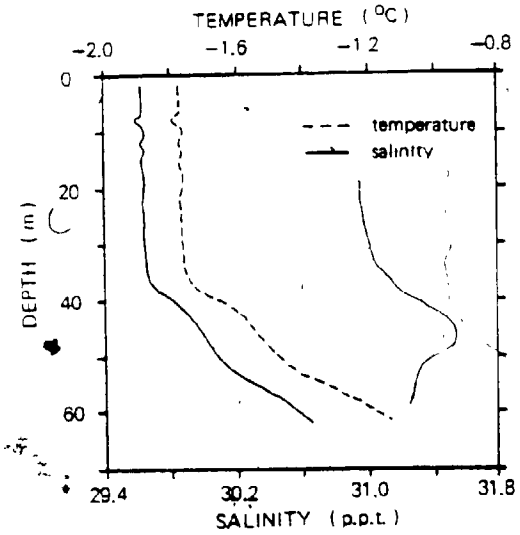

FIGURE 3.6(b)
TEMPERATURE AND SALINITY PROFILES
BENEATH BEAUFORT SEA ICE (11 APRIL 1972)

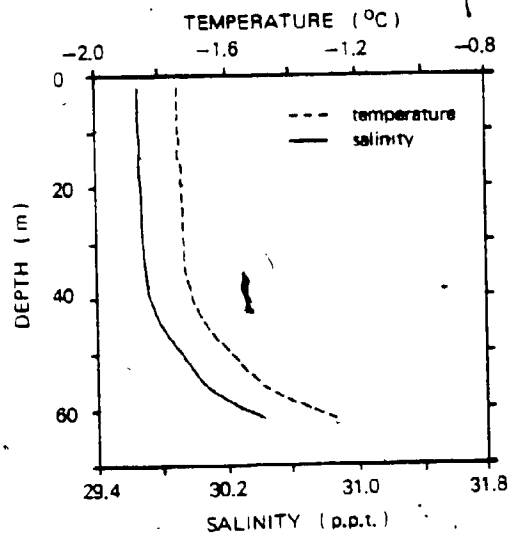

Source: McPhee (1975)

has a calculated freezing point of -1.62° (as given by Doherty and Kester's (1974) relation), and a measured freezing point of the same value. While the measurements for these and other cases may be suspect because of the transient introduction of the sensor, a very detailed study by Lake and Lewis (1971) again confirm the observations. Beneath first year ice on D'Iberville Fjord permanently installed sensors allowed the determination of salinity and temperature with no disruption of the layer. Some results comparing the observed temperature and the freezing point calculated from salinity information for the 2 m immediately below the ice are shown in Table 3.2 and Figure 3.7. These show that an isohaline, isothermal layer exists beneath growing first year sea ice and that the temperature of this layer is at the freezing point as determined by the water salinity.

The question arises as to whether or not the ocean supplies a heat flux to the base of the ice which would act to moderate the growth of the ice. For the case of a bulk fluid with uniform velocity past the lower ice boundary the heat flux may be calculated from

$$F_o = h\,(T_f - T_i) \tag{3.21}$$

where h = heat transfer coefficient
T_f = bulk fluid temperature
T_i = ice boundary temperature

TABLE 3.2

CONDITIONS BELOW THE SEA ICE - D'IBERVILLE FIORD
APRIL 7, 1970

Depth (cm)	Salinity, $^0/_{00}$ ±.01	Density, gm/cc ±.00001	T Freezing, Calc. from Salinity, °C ±.001	Mean Temp., °C ±.005	No. of Samples	Standard Deviation	Range, °C
0	25.59	1.020 58	-1.378	-1.387	12	.005	.017
10	25.60	1.020 59	-1.379	-1.388	33	.002	.008
20	25.60	1.020 59	-1.378	-1.388	33	.003	.010
30	25.59	1.020 58	-1.378	-1.386	42	.002	.009
40	25.60	1.020 59	-1.378	-1.386	22	.001	.006
50	25.60	1.020 59	-1.379	-1.390	12	.004	.013
60	25.60	1.020 59	-1.378	-1.387	12	.002	.005
70	25.61	1.020 60	-1.379	-1.385	13	.001	.005
80	25.60	1.020 59	-1.379	-1.386	12	.004	.013
90	25.60	1.020 59	-1.379	-1.386	13	.002	.008
100	25.60	1.020 59	-1.379	-1.384	14	.001	.005
150	25.78	1.021 54	-1.442	-1.063	13	.003	.009
200	27.71	1.022 29	-1.493	-0.920	14	.004	.009

FIGURE 3.7

WATER STRUCTURE IN THE FIRST TWO METRES BENEATH SEA ICE

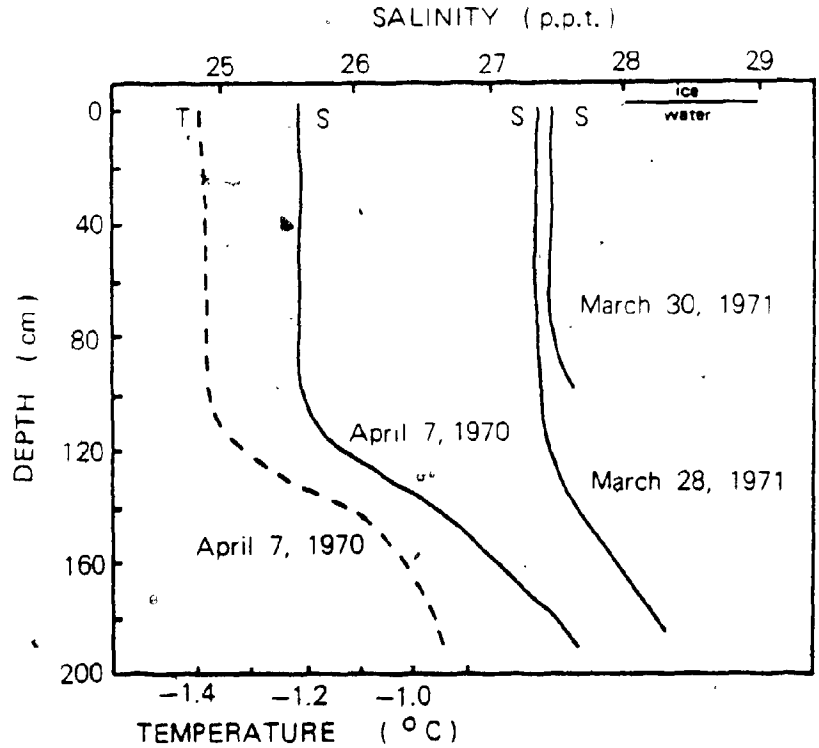

Source: Lake and Lewis (1971)

If we assume the water beneath the ice is isothermal and isohaline and at the ice freezing point then $T_f = T_i$ and there should be no heat flux from the fluid to the ice. Under these conditions an oceanic heat flux does not exist.

The effect of an influx of heat from the water to the ice will increase with increasing ice thickness (and therefore age) (Doronin, 1970). A situation may arise when the oceanic heat flux term equals that required by conduction in the ice phase. There would therefore be no ice accretion at the interface. If the flux were to exceed that required by conduction in the ice phase then the extra energy supplied by the ocean would be used to melt the ice at the interface. This, in addition to the question of spatial variability of ice thickness, may account for recorded decreases in ice thickness during periods when growth should be occurring. During the decay period the existence of low salinity melt water beneath the ice sheet results in a complex double diffuse layer (Martin, 1973). Heat energy is lost by the meltwater layer to both the overlying sea ice and the high salinity water beneath.

In discussing the relative importance of the conductive heat flux in multiyear pack ice and the turbulent heat flux in the ocean Maykut and Untersteiner (1969) note that the magnitude of the two fluxes is similar with one or the other

dominating during different seasons. They also note that it is not possible to calculate the magnitude of the ocean heat flux without the inclusion of a theoretical model of the ocean. In dealing with the growth of young sea ice the dominant energy term is the conductive heat flux.

CHAPTER 4

MODEL DEVELOPMENT AND IMPLEMENTATION

4.1 Conceptual Development

The model is based on the physical principle of the conservation of energy which results in an energy conservation equation. Such an approach is sometimes also known as an 'energy balance' of a surface.

The surface thermal regime is an expression of the ice or snow microclimate which results from the thermal, radiative and aerodynamic properties of the site. The interaction of these factors determines the magnitude and the direction of the components which constitute the surface energy balance.

The energy conservation equation (ignoring signs) has the form

$$Q^* = F_H + F_E + F_I \tag{4.1}$$

where Q^* = net radiation flux

F_H = sensible heat flux in the atmosphere

F_E = evaporative heat flux in the atmosphere

F_I = conductive heat flux in the ice

The equality may be rewritten so as to underline the central idea of energy conservation by noting that the components of

surface energy transfer must have a zero sum

$$Q^* - (F_H + F_E + F_I) = 0 \tag{4.2}$$

To simulate ice growth we require some manner in which to specify the component fluxes. To fix them in advance is an arbitrary and constraining method that ignores the surface-microclimate interaction. It is the interaction of regional climatic variables with a site's properties that produce a unique microclimate.

The simulation model attempts to combine the synoptic scale climate variables with the site characteristics to evaluate the energy balance. It is possible to do this by noting that each component of the energy balance can be expressed as a function of the surface temperature.

The net radiation flux may be expressed as the sum of four radiation terms.

$$Q^* = K\downarrow - K\uparrow + L\downarrow - L\uparrow \tag{4.3}$$

where $K\downarrow$ = incoming shortwave radiation
$K\uparrow$ = outgoing shortwave radiation
$L\downarrow$ = incoming longwave radiation
$L\uparrow$ = outgoing longwave radiation

$K\downarrow$ is the incoming shortwave or solar radiation while $K\uparrow$ is that portion of the shortwave radiation which is reflected by the surface. $L\downarrow$ is the incoming longwave radiation due

to emission by atmospheric components (water vapour, cloud banks) and $L\uparrow$ is the longwave radiation emitted by the surface itself. In the model the incoming shortwave radiation is required as a specified input. The outgoing radiation is expressed as

$$K\uparrow = \alpha K\downarrow \tag{4.4}$$

where α = surface albedo

This holds true for the case of a snow covered ice surface where penetration of the shortwave radiation into the snow layer does not occur to any significant degree. (O'Neil and Gray, 1971) When the ice surface is snow free this is not the case and equation (4.4) must be modified. The problem in modelling this in a physically realistic sense are discussed by Maykut and Untersteiner (1969) and their approach is adopted here. A predetermined percentage of the net shortwave radiation was assigned to penetration of the ice and the remaining portion used to determine the surface energy balance. This percentage is fixed during the snow free period. The net shortwave is calculated as

$$K^* = (1-\alpha)(1-i)K\downarrow \tag{4.5}$$

where i = penetrating fraction

which gives outgoing shortwave as

$$K\uparrow = (i+\alpha-\alpha i)K\downarrow \tag{4.6}$$

Incoming longwave radiation is estimated using an empirical relation developed by Idso and Jackson (1969).

$$L\downarrow = \varepsilon\sigma T_a^4 (1-0.261 \exp(-7.77\times10^{-4}(T_a-273)^2)) \qquad (4.7)$$

where ε = surface emissivity

σ = Stefan-Boltzman constant = $5.57 \times 10^{-8} \frac{W}{m^2 {}^oK^4}$

T_a = air temperature (screen ht) [^oK]

The outgoing radiation is given by the simple Stefan-Boltzman relation

$$L\uparrow = \varepsilon\sigma T_{EQ}^4 \qquad (4.8)$$

where T_{EQ} = surface temperature [^oK]

With equations (4.3) through (4.8) and the incoming shortwave radiation we may specify all the radiation fluxes.

We require similar quantitative expressions for the remaining terms of energy conservation equation. Adopting the drag coefficient approach to turbulent transfer relations (Businger, 1973) the sensible heat flux may be written as

$$F_H = \rho_a c_p u c_H (T_a - T_{EQ}) \qquad (4.9)$$

Similarly, the expression for evaporative heat flux becomes

$$F_E = \rho_a L_v u c_E (q_a - q_{EQ}) \qquad (4.10)$$

Conduction in the ice is treated using the simple Fourier steady state relation. Under snowfree conditions this becomes

$$F_I = \frac{k_i (T_o - T_{EQ})}{H} \qquad (4.11)$$

where k_i = thermal conductivity of ice
H = ice thickness
T_o = ocean temperature

With the addition of snow, a two-layer slab model is used and through simultaneous solution of the two flux equations, one in the snow and the other in the ice, equation (4.12) results

$$F_I = \left\{ \frac{k_i k_s}{k_s H + k_i h} \right\} (T_o - T_{EQ}) \tag{4.12}$$

where h = snow thickness
k_s = snow thermal conductivity

Equations (4.4) through (4.12) provide a means for evaluating the various components of the radiation and energy balance given certain inputs. The intention is that given inputs of air temperature and incident shortwave radiation we may generate a unique surface temperature that satisfies the energy conservation equation and predicts the values of the component radiation and energy fluxes.

The evaporative heat flux equation is notable in that it does not explicitly contain the surface temperature. It would also be valuable if we could treat the specific humidity at screen height as a calculable parameter rather than a required input. Due to the cool arctic temperatures only low values of q are required for saturation to occur and for much of the year conditions of high relative humidity

prevail. The relative humidity was selected as a specified input. This in conjunction with the air temperature allows the determination of the specific humidity. We may write q as a function of the partial pressure of water vapour (or vapour pressure, e).

$$q = \frac{0.622e}{P-e} \tag{4.13}$$

where P = total atmospheric pressure (mb)

As P>>e, this may be reduced to

$$q = 0.622 \frac{e}{P} \tag{4.14}$$

Since the saturation vapour pressure e* depends only on temperature it follows that q is a function of temperature and pressure.

In order to determine the dependence of saturation vapour pressure on temperature the Clausius-Clapeyron equation is used (Fleagle and Businger, 1963), which under normal atmospheric conditions, in combination with the equation of state for water vapour yields

$$\frac{de^*}{e} = \frac{L}{R_v} \frac{dT}{T^2} \tag{4.15}$$

where e^* = the saturation water vapour pressure

R_v = specific gas constant for water vapour

This may be integrated if we allow L to be a constant, resulting in

$$\ln(e_1^*) = \frac{L}{R_v}\left(\frac{1}{T_2} - \frac{1}{T_1}\right) + \ln(e_2^*) \tag{4.16}$$

Setting $L = 2.500 \times 10^3 J \cdot g^{-1}$, $R_v = 0.4617 J \cdot g^{-1}\ {}^oK^{-1}$ and noting that $e^* = 6.11$ mb and $T_a = 273^oK$ we find

$$e^* = \exp\left\{21.644 - \frac{5414.7}{T_a}\right\} \tag{4.17}$$

At the surface it was assumed that the air was saturated. Air in this equilibrium state has a vapour pressure e_i^* which is known as the saturation vapour pressure over a plane ice surface. The saturation vapour pressure over ice is different from the saturation vapour pressure over water and at all temperatures $e_w^* > e_i^*$ because water evaporates more easily than ice. The magnitude of $e_w - e_i$ reaches a peak value of about 0.26 mb near -12^oC (Wallace and Hobbs, 1977). Equation (4.16) also describes the variation in the saturation vapour pressure over ice where the substitution of $L = 2.834 \times 10^3 J \cdot g^{-1}$, $R_v = 0.417 J \cdot g^{-1}\ {}^oK^{-1}$ and $e_i^* = 6.11$ mb at 273^oK yields

$$e^* = \exp\left\{24.294 - \frac{6138}{T_{EQ}}\right\} \tag{4.18}$$

Equations (4.17) and (4.18) were used to determine saturation vapour pressures at air and surface level respectively. With these relations we may specify the specific humidities as

$$q_a = \frac{0.622f}{P} \exp\left\{21.644 - \frac{5414.7}{T_a}\right\} \tag{4.19}$$

$$q_{EQ} = \frac{0.622}{P} \exp\left\{24.294 - \frac{6138}{T_{EQ}}\right\} \tag{4.20}$$

where f = the relative humidity

In this manner the evaporative heat flux may be related to the air temperature (input) and surface temperature. The energy conservation equation (4.2) may be rewritten in expanded form (adopting the convention that an energy flux gain by the surface has a positive sign).

$$(1-\alpha)(1-i)K\downarrow + \varepsilon\sigma T_a^4(1-0.261 \exp(-7.77\times10^4(T_a-273)^2))$$
$$-\sigma T_a^4 + \rho_a c_p u C_H (T_a - T_{EQ})$$
$$+\rho_a L_v u C_E \left\{\frac{0.622}{P}\left(f \exp\left(21.644-\frac{5414.5}{T_a}\right)-\exp\left(24.294-\frac{6138}{T_{EQ}}\right)\right)\right\}$$
$$+\frac{k_i k_s}{k_s H + k_i h}(T_o - T_{EQ}) = 0 \qquad (4.21)$$

A unique value of T_{EQ} will satisfy equation (4.21) and by back substitution provide an estimate of each energy flux component.

The equation is solved using a simple, iterative residual search algorithm. An upper and lower bound (20°C and -50°C) are prescribed for the solution temperature and the initial trial temperature is taken as the mean of these bounds. The upper and lower bounds are reset during the iterative sequence depending on the sign of the residual; a positive residual indicates a solution temperature that is too warm while the opposite is true for a negative residual. The iteration sequence is stopped when the absolute value of the residual

is less than 0.5 $W \cdot m^{-2}$. The solution appears unconditionally stable and allows any non-linear relations in T_{EQ} to be used which enables change in the flux estimating equations to be made without rewriting the algorithm. The provision also exists for new interface energy sources or sinks to be added.

Ice growth is calculated after the component energy fluxes have been evaluated. The energy conducted through the ice to the surface requires a source which is assumed to be the latent heat energy associated with the ice formation. Equating these quantities yields

$$F_I = \rho_i L_{f_i} \frac{dH}{dt} \tag{4.22}$$

where ρ_i = ice density

L_{f_i} = latent heat of fusion of ice during formation

$\frac{dH}{dt}$ = rate of change of ice thickness with time

from which the ice growth for a finite time period may be calculated

$$\Delta H = \frac{F_I \, \Delta t}{\rho_i L_{f_i}} \tag{4.23}$$

where ΔH = ice growth

Δt = time period

The new ice thickness after growth then becomes $H + \Delta H$. (Equation (4.21) also allows the determination of the growth

velocity which is valuable for entrapment studies.)

Under non-melt conditions the equilibrium surface temperature was chosen by satisfying the relation

$$Q^* + F_H + F_E + F_I = 0 \tag{4.2}$$

When melt occurs another energy source must be included and the equation becomes

$$Q^* + F_H + F_E + F_I + F_A = 0 \tag{4.24}$$

where F_A = energy flux due to ablation

To implement melt conditions a special segment of the program is called if the solution of equation (4.2) yields a surface temperature in excess of 273°K (0°C). Such a solution is unrealistic as the snow surface must remain at or below 273°K (0°C). (During melt the snowpack is assumed to be isothermal at 0°C, a condition reported frequently in the literature (Weller and Holmgren, 1974).) The equilibrium surface temperature is set at 273°K (0°C) and the sensible and evaporative fluxes evaluated. To satisfy the energy conservation equation the 'missing' energy is supplied by melt of the snowpack. The energy flux due to melt is given by

$$F_{A_s} = \rho_s L_{f_s} \frac{dh}{dt} \tag{4.25}$$

where ρ_s = snow density

L_{f_s} = latent heat of fusion for snow

$\frac{dh}{dt}$ = rate of change of snow depth with time

By taking the residual obtained when T is set to 273°K (0°C) to be F_{A_S} we may calculate the depth of snow melted. For a finite time increment Δt

$$\Delta h = \frac{F_{A_S} \Delta t}{\rho_s L_{f_s}} \tag{4.26}$$

where Δh = depth of snow melted.

The snow depth is assigned its new value $h-\Delta h$ (note that F_{A_S} has a positive sign indicating energy supplied to the surface) and the next simulation step is entered.

The same strategy is employed to melt ice after the ablation of the snow pack. The flux due to ice melt is given by

$$F_{A_i} = \rho_i L_{f_i} \frac{dH}{dt} \tag{4.27}$$

where ρ_i = ice density

L_{f_i} = latent heat of fusion for ice

$\frac{dH}{dt}$ = rate of change of ice thickness with time

and the change in ice thickness by

$$\Delta H = \frac{F_{A_i} \Delta t}{\rho_i L_{f_i}} \tag{4.28}$$

4.2 Parameterization of Variables

4.2.1 Introduction

The remainder of this chapter deals with the internal model parameterization of the variables described in the previous section. Their discussion is presented in terms of their occurrence in the radiative, conductive or turbulent exchange processes. The radiative exchange section examines the albedo, emissivity and penetrating fraction for short-wave radiation. Conductive exchange deals with thermal conductivity, latent heat of fusion for freezing and melting, ocean temperature and ice density and salinity. Turbulent exchange includes the specification of the density and specific heat capacity of air, the latent heat of vapourization and the drag coefficients.

4.2.2 Radiative Exchange Properties

4.2.2.1 Albedo

The albedo of a snow surface is highly variable dependent upon its age and history. Table 4.1 lists some albedo values recorded for different snow surfaces. Theoretical attempts at modelling the relationship between shortwave radiation penetration and reflection and a snowpack have been made by Giddings and LaChappelle (1961), Barkstrom (1972)

TABLE 4.1

ALBEDO OF SNOW AND ICE SURFACES

Structure	Water content and colour	Albedo		
		avg.	max.	min.
Fresh fallen snow	dry bright-white clean	88	98	72
Freshly fallen snow	wet bright-white	80	85	80
Freshly drifted snow	dry clean loosely packed	85	96	70
Freshly drifted snow	moist grey-white	77	81	59
Snow, fallen or drifted 2-5 days ago	dry clean	80	86	75
Snow, fallen or drifted 2-5 days ago	moist grey-white	75	80	56
Dense snow	dry clean	77	80	66
Dense snow	wet grey-white	70	75	61
Snow and ice	dry grey-white	65	70	58
Melting ice	wet grey	60	70	40
Melting ice	moist dirty grey	55	65	36
Snow, saturated with water (snow during intense thawing)	light green	35	--	28
Melt puddles in first period of thawing	light blue water	27	36	24
Melt puddles, 30-100 cm deep	green water	20	26	13
Melt puddles, 30-100 cm deep	blue water	22	28	18
Melt puddles covered with ice	smooth grey-green ice	25	30	18
Melt puddles covered with ice	smooth ice, covered with icy white hoar frost	33	37	21

Source: Vowinckel and Orvig (1970)

and Barkstrom and Querfield (1975) but for application these theories require empirical coefficients which are uniquely dependent on the particular snowpack under consideration. They also predict that snow albedo is independent of the albedo of the underlying surface when its depth is greater than 2-4 cm which is confirmed by the measurements of O'Neill and Gray (1972).

Surface albedo is affected by the position of the sun with an increase in albedo associated with decreasing solar elevation. The variation may be difficult to detect in a systematic fashion due to the inherent design and response characteristics of the pyranometers employed. Under some conditions albedos in excess of 100% may be recorded (Brown, 1969) revealing the practical problems encountered. Langleben (1968) found that the solar elevation-albedo variation to be less than 0.025 (absolute units) and was unable to discern if this was a real effect. The albedo is also affected by the surface roughness elements of the snow itself. Under diffuse illumination multiple scattering of light between the cloud base and snow surface may raise the snow albedo. Weller (1968) found the albedo to be 11% higher under overcast skies relative to the clear sky case in Antarctica while Hanson (1960) reported a 7% increase. Langleben (1966)

was unable to detect any such difference on first year sea ice in Greely Fjord near Ellesmere Island.

The specification of snow albedo can be a complex problem. Qualitatively, it is high after deposition and decreases as the snow undergoes metamorphosis. Mellor (1974) cites observations that the albedo is inversely related to grain size which is in qualitative agreement with Bohren and Barkstrom's (1974) prediction that the albedo will be inversely proportional to the square root of the grain size. In the model an albedo of 0.75 is chosen as a representative value for snow during the non-melt period and reduced to 0.45 when melting begins.

The albedo of sea ice, like that of snow, is also highly variable. In a discussion of its characteristics it is convenient to separate the growth period from that of decay.

Little is known of the variation in albedo of sea ice during the initial stages of growth. Weller (1972) obtained albedo data from a refreezing lead experiment for a 5-100 cm range in ice thickness. A polynomial regression fitted to the data allows the estimation of albedo (α) in the model as a function of ice depth under snowfree conditions.

$$\alpha_i = 0.2467 + 0.7049(H) - 0.8608(H)^2 + 0.3812(H)^3 \qquad (4.29)$$
$$0.05\text{m} < H < 1.00 \text{ m}$$

where α_i = ice albedo
H = ice thickness (m)

The data points and regression line are shown in Figure 4.1. The plot indicates that with increasing thickness the albedo increases and approaches a constant value of 0.47. For thicknesses less than 0.05 m the following relation is used

$$\alpha_i = 0.04(H) + 0.07 \qquad H < 0.05 \text{ m} \tag{4.30}$$

This sets a lower limit for the albedo at 7%, chosen as a representative figure for calm seas.

During the winter incoming solar radiation levels are low and the error associated with the chosen albedo value is probably minor in terms of the radiation balance. During summer, high insolation values are recorded and a difference in albedo of 10-20% represents a significant energy contribution. It is problematic that a great uncertainty exists in the albedo value to be assigned to the ice during this period. The research to date suggests a bimodal distribution of albedo measurements with modal values near 0.65 and 0.45. The lower values increase the rate and magnitude of ablation substantially relative to the higher albedo (see Maykut and Untersteiner (1969) cases #5 and #6 for an illustration of these effects). For the decay season an albedo value of 0.45 was used. It is difficult to determine the real influence of changing the albedo during decay because ice measurements at the recording stations ceased too early to allow a meaningful

FIGURE 4.1 ICE ALBEDO VERSUS THICKNESS

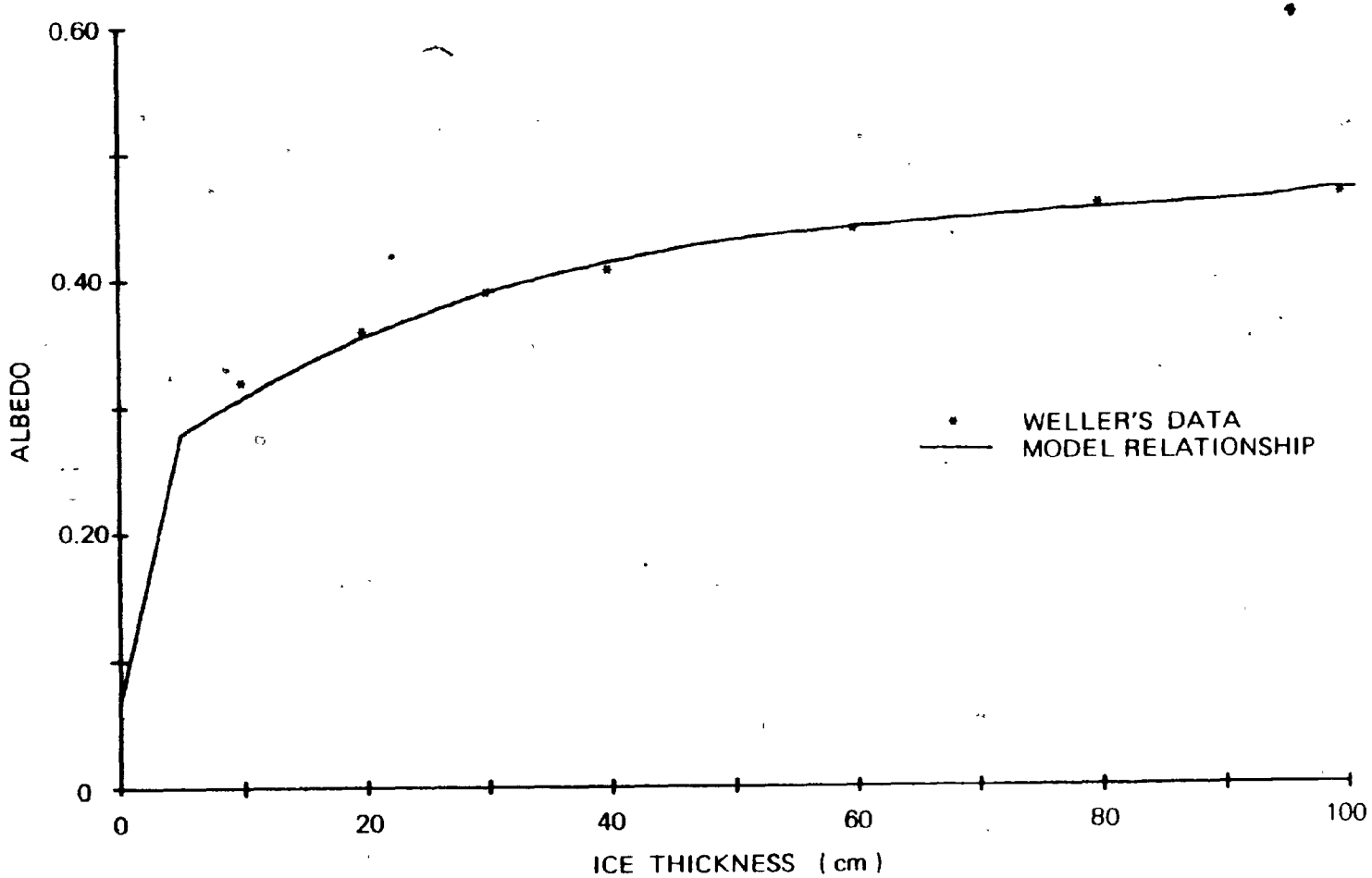

Source Weller (1972)

comparison between modelling and observed results.

4.2.2.2 Emissivity

Ice is an effective longwave radiation emitter with 0.97 being the generally accepted emissivity value (Dorsey, 1968; Mellor, 1977). Measurements of snow emissivity show a wider range (0.82 - 0.995, Sellers, 1965) with the lower emissivity linked to decreasing grain size and temperature (Mellor, 1977). An emissivity of 0.97 is also employed for snow in the model.

4.2.2.3 Penetrating Fraction of Incoming Shortwave Radiation

Only an estimate of the magnitude of this term (i) can be made. It is chosen as 0.17 for ice on the basis of the work of Maykut and Untersteiner (1969) and as 0.00 for snow. The influence exerted by this term is restricted to the initial snowfree growth period and summer ablation of the ice surface.

4.2.3 Conductive Exchange Properties

4.2.3.1 Thermal Conductivity

Schwerdtfeger (1963) derives a theoretical expression, based on Assur's (1958) model of sea ice, to evaluate the conductivity of sea ice over the temperature range 0 to -8°C. The ice is treated as a system of parallel connected

conductors where plates of pure ice are separated by thin brine films. If the heat flow is parallel to the brine cells then the pure ice will transfer most of the heat due to its higher thermal conductivity and the reduction in system thermal conductivity will be roughly proportional to the fraction of the cross sectional area occupied by the brine. Schwerdtfeger also includes the effects of air bubbles in the system by employing Maxwell's measure of resistivity. The thermal conductivity for bubbly ice (k_{bi}) is

$$k_{bi} = \frac{2k_i + k_a - 2\nu_a(k_i - k_a)k_i}{2k_i + k_a + \nu_a(k_i - k_a)} \tag{4.31}$$

where k_i = thermal conductivity of pure ice

k_a = thermal conductivity of pure air

ν_a = volume fraction of air bubbles

Since $k_i >> k_a$, equation (4.31) becomes

$$k_{bi} \doteq \frac{2k_i\ (1-\nu_a)}{(2 + \nu_a)} \tag{4.32}$$

For saline ice Schwerdtfeger arrives at the relation

$$k_{si} = k_{bi} - (k_{bi} - k_b)\left\{ \frac{s_i \rho_s}{-0.0182\rho_w(T_i - 273)} \right\} \tag{4.33}$$

where k_b = thermal conductivity of brine

Schwerdtfeger treated k_i as constant although it possesses a temperature dependence as given in Pounder (1965). Lewis

(1967) found that when the proper allowance for the temperature variation is made, Schwertfeger's formula provided values in good agreement with experimental results.

Below -8.2°C the precipitation of solid hydrates complicates the theoretical conductivity derivation. For low ice salinities (<10‰) Schwerdtfeger believes that discontinuities in the conductivity - temperature function where salts begin to precipitate are unlikely to occur. At -40°C most salts in the ice have been precipitated and the thermal conductivity of sea ice should be equivalent to that of freshwater ice of the same density. A reasonable procedure is to accept a continuous asymptotic approach to the thermal conductivity of pure ice at -40°C beyond -8°C.

Returning to equation (4.33) and regrouping the terms in a slightly different manner we obtain

$$k_{si} = k_{bi} + \left\{\frac{(k_b - k_{bi})\rho_i}{-0.0182\rho_w}\right\} \left\{\frac{S}{T-273}\right\} \tag{4.34}$$

This may be compared with an expression obtained by Untersteiner (1961) to express the variation in thermal conductivity of sea ice as a function of salinity and temperature

$$k_{si} = k_i + a \left(\frac{S}{T-273}\right) \tag{4.35}$$

This is the formula that is employed in the model with k_i = 2.03 $W \cdot m^{-1} \cdot {}^{o}K^{-1}$ and a = 0.117 $W \cdot m^2 \cdot kg^{-1}$. One further condition

was added in that when $T > 272^{o}K$ the thermal conductivity is fixed at $1.32\ W \cdot m^{-1} \cdot {}^{o}K^{-1}$ because a singularity occurs as T approaches $273^{o}K$. Equation (4.35) is presented in diagramatic form for various salinities and temperatures in Figure 4.2.

Snow acts as an effective insulator due to its low thermal conductivity. Its presence early in the growth season or in sufficient depths can reduce ice growth substantially. Evaluating the thermal conductivity of snow is difficult because snow undergoes a continuous change of state due to metamorphism. In new snow rapid changes in conductivity are the result of rounding of the snow grains during sublimation. In old coarse grained snow there is only slight alteration of the structure and the conductivity remains constant. Yen (1969) reviews the experimental expressions for snow thermal conductivity in which the investigators correlated their results with snow density. Considerable differences exist between the expressions and are ascribed to contrasting methodologies and conditions where the effect of vapour diffusion are dissimilar. In the model Van Dusen's (1927) equation is used.

$$k_s = 2.053 \times 10^{-3} + 4.2166 \times 10^{-4} (\rho_s) - 1.0909 \times 10^{-8} (\rho_s)^2 + 2.1838 \times 10^{-9} (\rho_s)^3 \quad (4.36)$$

where ρ_s = snow density $[kg \cdot m^{-3}]$

FIGURE 4.2
ICE THERMAL CONDUCTIVITY AS A FUNCTION OF TEMPERATURE AND SALINITY

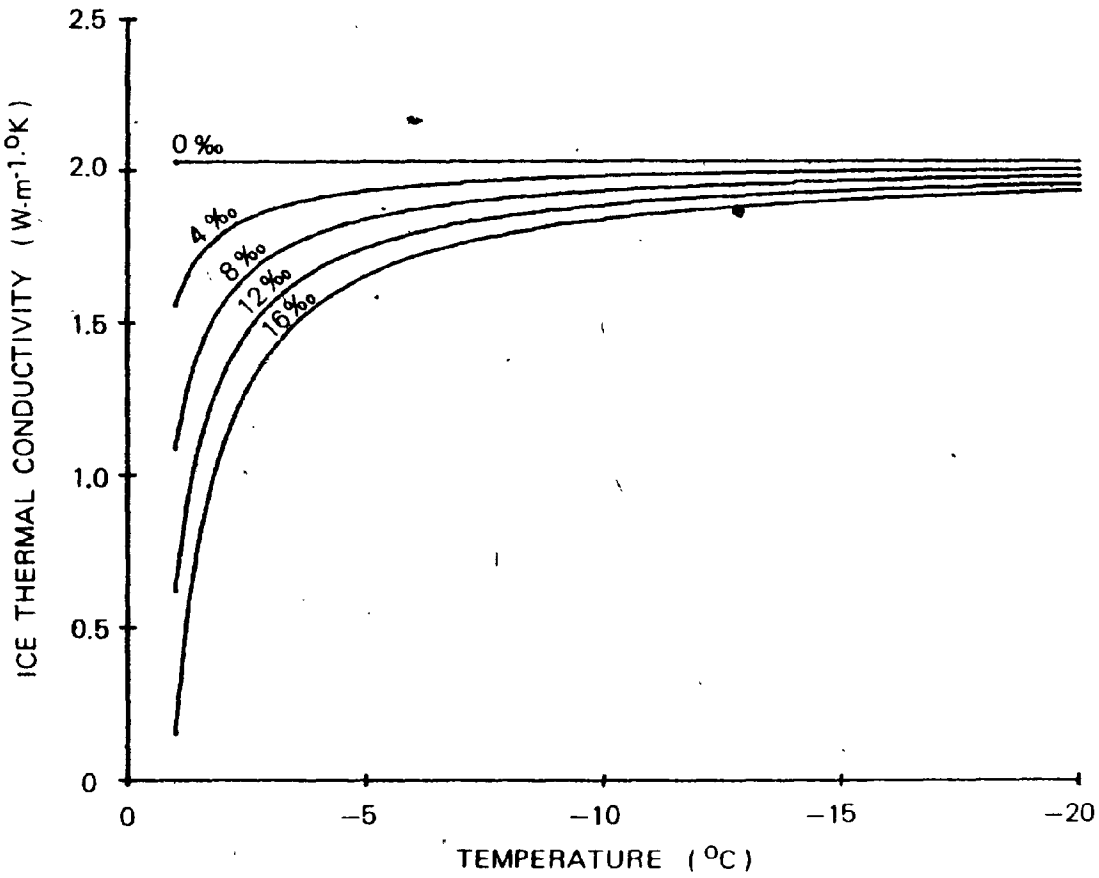

Ice growth in both the real and computer environments is sensitive to the snow and its thermal properties. To illustrate the effect Lake and Walker (1966) attribute a 50 cm difference in seasonal ice growth between Slidre Fjord and D'Iberville Fjord under similar climatological conditions to the existence of the snow thickness difference of only 5 cm.

4.2.3.2 Latent Heat of Fusion

Sea water of a given salinity (S_o) freezes at a unique temperature. When the sea water is cooled to this temperature and freezing occurs a certain amount of pure ice will be formed with some brine trapped within. The amount of pure ice present in a unit mass (m_i) is

$$m_i = 1 - \left(\frac{S_i}{1000}\right) - \left(\frac{S_i}{S_b}\right) \tag{4.37}$$

where S_i = salinity of sea ice

S_b = salt content of the entrapped brine

The latent heat of formation, L_{f_i}, (the quantity of heat released in freezing) is given by the mass of ice times the latent heat of fusion for pure ice.

$$L_{f_i} = \left(1 - \left(\frac{S_i}{1000}\right) - \left(\frac{S_i}{S_b}\right) \right) L \tag{4.38}$$

where L = latent heat fusion of pure ice

$= 3.33 \times 10^5 \ J \cdot kg^{-1}$

In applying equation (4.38) it is assumed that the salinity of the entrapped brine equals that of the sea water from which the ice is growing. The fractional salt content of the brine may then be given as

$$S_b = \frac{\left(\frac{S_o}{1000}\right)}{\left(\frac{1 - S_o}{1000}\right)} \tag{4.39}$$

Substitution of (4.39) into (4.38) yields

$$L_{f_i} = \left\{ 1 - \left(\frac{S_i}{1000}\right) - \frac{S_i}{S_o}\left(1 - \frac{S_o}{1000}\right) \right\} \tag{4.40}$$

This equation was first given by Malmgren (1927). Pounder (1965) notes that the assumption that the salinity of the entrapped brine is the same as that of the underlying sea-water is incorrect as salt rejection occurs at the growing ice interface. This results in the rejection of salts from the ice into the brine, which is found between the ice crystal platelets. This brine will then have a salt content higher than that of the underlying sea water. Anderson (1966) also examined the latent heat problem for sea ice and found many of the simplifications, such as neglecting the heats of solution and precipitation of salts in brine at low temperatures and neglecting the selective salt precipitation or dissolution of the remaining brine during freezing, and assumptions, as in the adequacy of the specific heats assumed

2

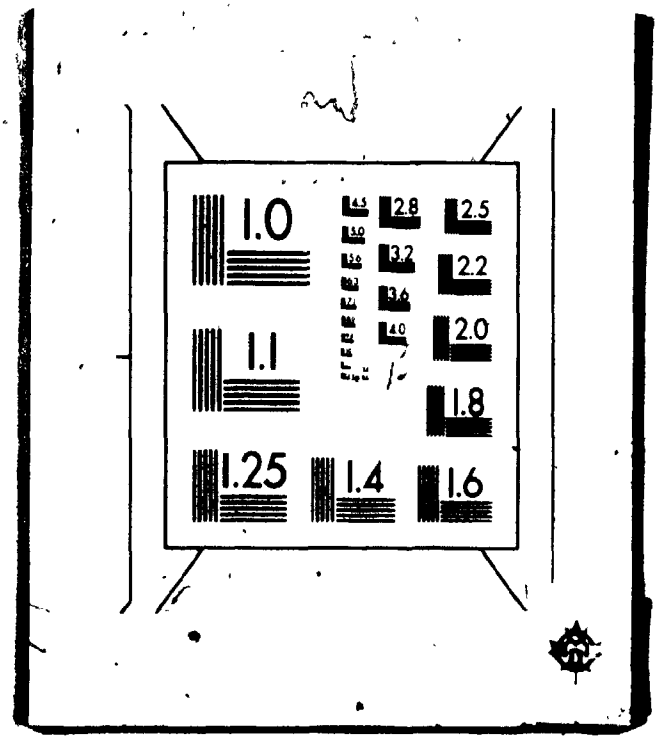

for the ice and occluded brine, to be questionable. The use of equilibrium thermodynamic relationships in a non-equilibrium system is also subject to debate. Anderson suggests that until the true values are established, published values of the latent heat of fusion should be used with discretion. Lewis (1967) dramatically states the need for an experimental determination of the latent heat of formation. In view of the uncertainty in the determination of the latent heat of formation a fixed value of 2.72×10^5 $J \cdot kg^{-1}$ was chosen for use in this model.

The determination of the latent heat of fusion associated with melting is an even more complex problem than that encountered for freezing. Depending on the age and temperature of the ice variable quantities of brine are present in the ice and as such has no definite melting point. Schwertfeger (1963) concludes that a true latent heat, which implies an absorption of heat at a constant temperature, does not exist during the melting of sea ice. An alternative approach has been to calculate the total heat required to raise the temperature of the ice and brine and melt the pure ice component. Anderson (1966) has again detailed some of the problems associated with this procedure, such as the specification of the final melting temperature. The model employs a real latent heat term with an assigned value of 3.344×10^5 J/kg.

This is characteristic of pure ice and is the same value designated for snow.

4.2.3.3 Ocean Temperature

The ocean temperature is evaluated from a knowledge of the ocean salinity. The water is assumed to be at its salinity-determined freezing point which is evaluated using Doherty and Kester's (1974) relationship

$$T_o = 273. - 0.0137 - 5.199 \times 10^{-2}(S) - 7.225 \times 10^{-5}(S)^3$$

$$[S] = 0/00 \qquad (4.41)$$

4.2.3.4 Ice Density

A fixed ice density of 920 kg/m^3 is assumed in the model. This value is close to that of 915 kg/m^3 suggested by Schwerdtfeger (1963) and the measurements of Campbell et al (1978) of 900 kg/m^3 to 920 kg/m^3 for first year ice.

4.2.3.5 Ice Salinity

Due to the complex nature of ice salinity determination (Appendix 1) an empirical approach was adopted. Cox and Weeks (1974) observed that salinity observations of sea ice of varying thicknesses and ages collected at various arctic and subarctic locations revealed a strong correlation between the average salinity of the ice, $\overline{S}_i$, and the ice thickness, H. For salinity samples collected during the

growth season the relationship could be represented by two linear equations.

$$\bar{S}_i = 14.24 - 19.39\ (H) \qquad (H \leq 0.4m) \qquad (4.42)$$

$$\bar{S}_i = 7.88 - 1.59\ (H) \qquad (H > 0.4m) \qquad (4.43)$$

Data from Eclipse Sound, N.W.T., obtained during the 1976-1977 and 1977-1978 growth seasons (P.C.S.P.) are shown in Figure 4.3 with equations (4.43) and (4.44). These data confirm the applicability of (4.43) and (4.44) which are used in the model to determine the average ice salinity during the growth period.

Cox and Weeks (1974) also present an equation to estimate the salinity during the melt period but the values were too large in comparison to the other data and lacked continuity in the change from growth to melt conditions (i.e. a large jump, either an increase or decrease, occurs at the onset of melt). Salinity values and continuity are obtained in the model by noting the salinity at the end of the growth period and then decreasing its value in a linear fashion with thickness subject to the end point restriction that $\bar{S}_i = 0.5\ ^0/00$ when $H = 0.10$ m.

4.2.4 Turbulent Exchange Properties

4.2.4.1 Drag Coefficients

Values for the stress related drag coefficients for snow and ice surfaces appear in Table 4.2. The transition

FIGURE 4.3 AVERAGE ICE SALINITY VERSUS THICKNESS

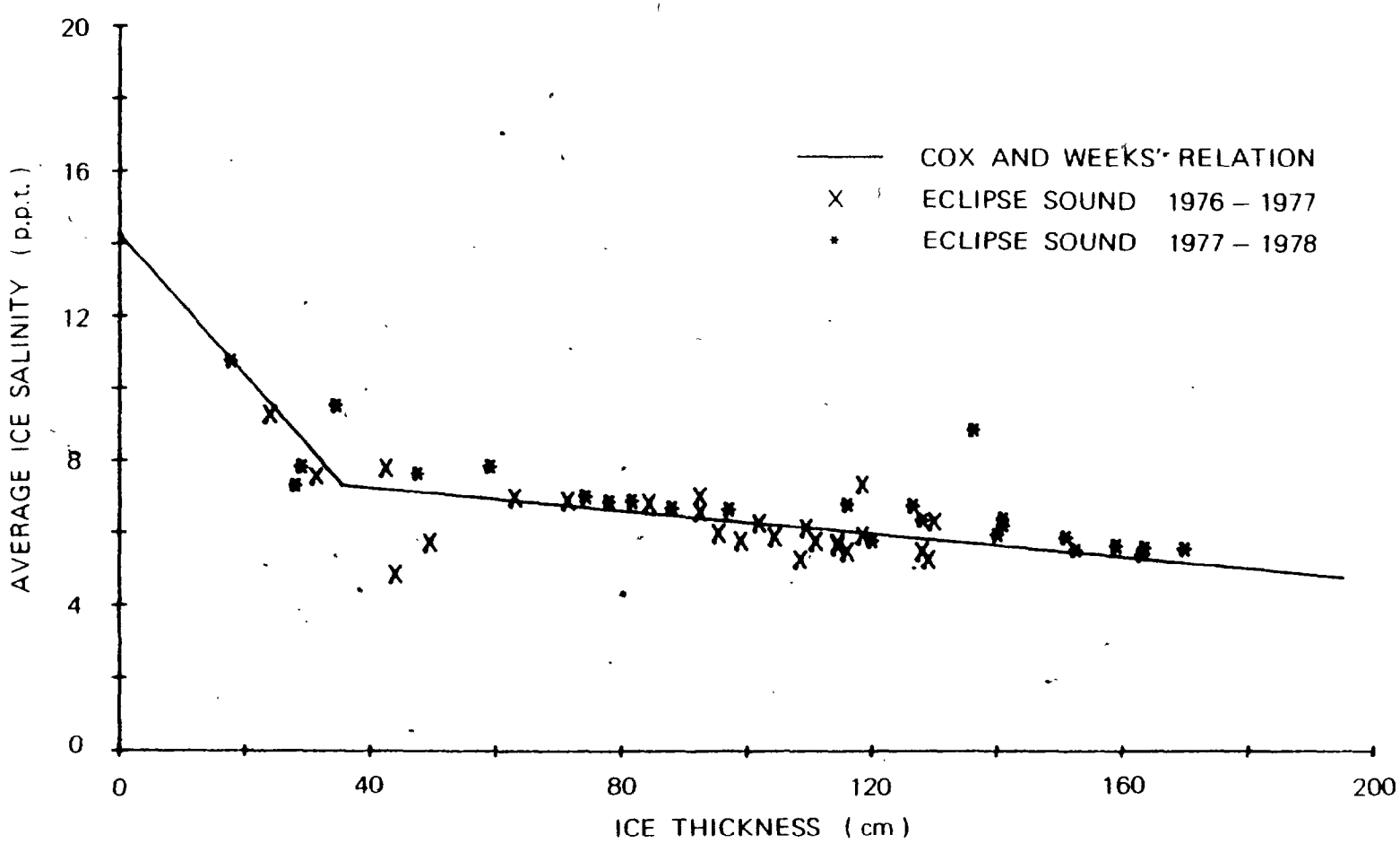

TABLE 4.2

MOMENTUM DRAG COEFFICIENTS FOR SNOW AND ICE

Investigator	Surface/Location	$C_D \times 10^3$
Suzuki (1967)*	smooth ice covered by snow	1.1
Leavitt et al (1977)	AIDJEX site 1975/1976	1.20±0.26
Smith (1972)[1]	Gulf of St. Lawrence	1.3
Untersteiner and Badgley (1965)	polar pack ice	1.42
Langleben and Pounder (1972)	AIDJEX 1972	1.58±0.19
Langleben (1972)	polar pack ice - smooth	1.66±0.08
Banke et al (1976)	Robeson Channel 1974 - wet slushy snow, (numerous meltwater ponds)	1.68
Langleben (1972)	polar pack ice - smooth	1.69±0.05
Siefert and Langleben (1972)	Gulf of St. Lawrence - 20-30 cm thickness	1.7
Langleben and Pounder (1972)	AIDJEX 1972	1.74±0.25
Banke and Smith (1973)	AIDJEX 1972	1.8 ±0.2
Deacon (1953)*	snow surface on natural prairie	1.9
Banke and Smith (1973)	AIDJEX 1972	1.9 ±0.2
Banke and Smith (1973)	Robeson Channel 1972 - wet slushy snow	2.1 ±0.3
Siefert and Langleben (1972)	Gulf of St. Lawrence - 20-30 cm thickness	2.2
Sverdrup (1936)*	firnlike snow surface	2.3
Thorpe et al (1973)	AIDJEX 1972 - 2 m ice	2.3
Thorpe et al (1973)	Robeson Channel 1972 - slushy wet ice (some melt ponds)	2.3
Langleben (1972)	rough rafted ice surface	2.46±0.04
Smith et al (1970)	Gulf of St. Lawrence 1967 - small pan floes	2.6
Banke and Smith (1973)	moderately rough ice	2.6

Source: *Siefert and Langleben (1972), [1]Banke and Smith (1973)

from smooth snow-covered ice to rough ice may be characterized by a range of values such that $0.001 \leq C_M \leq 0.0026$. The total drag component is expressable as the sum of the form drag component and the skin friction component. Banke and Smith (1973) determine a limit for C_M of 1.2×10^{-3} for a completely flat snow surface. The increase in the total drag coefficient beyond this value represents the increasing contribution of form drag induced by surface roughness elements. The value of the total drag coefficient has been correlated with both the slope and root mean square elevation of the ice surface (Banke and Smith, 1973) but was found to be independent of the wind speed.

Similarity theory has often been invoked to produce the equality that

$$C_M = C_H = C_E \tag{4.44}$$

This allows the determination of C_H and C_E from wind stress measurements. Little published material is available concerning the direct evaluation of these coefficients over snow and ice surfaces. Thorpe et al (1973) employed eddy correlation techniques to obtain values of $C_M = 2.33 \times 10^{-3}$, $C_H = (1.2 \pm 0.7) \times 10^{-3}$ and $C_E = (0.55 \pm 0.23) \times 10^{-3}$ for the AIDJEX test site. These results were obtained under near neutral conditions where similarity theory predicts the drag coefficients for momentum, moisture and sensible heat

transfer to be equal. At Robeson Channel near Ellesmere Island values of $C_M = 2.3 \times 10^{-3}$ and $C_H = 0.97 \times 10^{-3}$ were recorded. In July 1974 Banke et al (1976) returned to Robeson Channel to record the drag coefficients using microbead thermistors and a thrust anemometer. The momentum drag coefficient was $C_M = (1.68 \pm 0.42) \times 10^{-3}$ while the drag coefficient for sensible heat transfer was found to be $C_H = 1.20 \times 10^{-3}$.

Constant but unequal drag coefficients are assigned in the model for sensible and evaporative heat transfer. Treating them as constants is not an unreasonable restriction as Banke et al (1976) found that variations in the surface texture from late winter through spring and early summer did not introduce a systematic difference in the neutral drag coefficients. Under stable conditions they also suggest their data can be represented by a low and constant drag coefficient. C_H is assigned the value 1.1×10^{-3} while $C_E = 0.6 \times 10^{-3}$. These values are in better agreement with existing observations than the values of 3×10^{-3} given for C_H and C_E by Maykut (1978) and Semtner (1976) in their models.

4.2.4.2 <u>Air Density</u>

The density of the air is fixed at 1.32 kg/m^3 which is the value at a temperature of -10°C (List, 1949).

4.2.4.3 Specific Heat Capacity

A value of 1010 $J \cdot kg^{-1}$ is used in the model for the specific heat capacity of air (Montieth, 1973).

4.2.4.4 Latent Heat of Vapourization

The latent heat of vapourization is fixed at 2.533 x 10^6 J/kg corresponding to a temperature of -15°C. The variation in this term is less than 3% over the 0 to -40°C temperature interval (List, 1949).

4.3 Computer Implementation

The model as conceived in 4.1 and structured in 4.2 was programmed for the computer in the FORTRAN language and given the name ICE. A program listing for ICE is given in Appendix B.

Initial inputs consist of the station name, date of the start of the simulation, mean station pressure (mb), mean wind speed ($m \cdot s^{-1}$), snow density ($kg \cdot m^{-3}$), ocean salinity (parts per thousand), initial ice thickness (cm) and snow depth (cm). During the simulation three inputs are required for each day; these are the mean daily temperature (°C), incoming daily shortwave radiation ($W \cdot m^{-2}$) and change in snow depth (cm). The last term is allowed to be negative accounting for changes in thickness due to the drifting effect of wind. A sample data set is reproduced with the model in Appendix C.

The daily output generated by the model includes the outgoing shortwave radiation, incoming longwave radiation, outgoing longwave radiation and the energy fluxes associated with sensible heat transfer, evaporative heat transfer, conductive heat transfer and that due to the melt of snow and ice. The equilibrium surface temperature, air temperature, temperature at the snow-ice interface, ice salinity, snow depth, ice growth and ice thickness are also provided. At the completion of the period the ice thickness-time record for the station is reproduced to facilitate comparison with the model (this information must of course be supplied as input data and has no bearing on the working of the model).

The main structural features of the program are as follows:

(1) Input of the site location and starting data, ocean salinity, the initial ice and snow thicknesses, the mean wind speed and atmospheric pressure and the snow density.

(2) Daily inputs of air temperature, incoming shortwave radiation and snowfall are used in conjunction with the data from (1) and the internal model specifications as described in 4.2 to constrain the surface energy balance.

(3) The components of the energy balance equation are specified as explicit functions of the surface temperature

and an iterative search employed to seek a solution.

(4) The temperature satisfying the energy conservation equation is known as the equilibrium surface temperature. It is then used to evaluate the flux components of the energy balance.

(5) These fluxes are then used in conjunction with the snow and ice thermal properties to assess the resulting daily ice growth, snow melt or ice ablation.

The computing was carried out on the Carleton University Xerox Sigma 9 computer. Compilation of the source program requires approximately 0.4 minutes of C.P.U. time. Execution of 200 and 300 day simulations use 0.2 and 0.3 minutes of C.P.U. time respectively. As an approximation

$$\text{C.P.U. Time} = n/100 \text{ minutes} \tag{4.45}$$

where n = number of days simulated.

CHAPTER 5

ASSESSMENT OF MODEL PREDICTIONS

5.1 Data Sources and Site Locations

Three sites were chosen at which to evaluate the effectiveness of the computer model in predicting ice thicknesses. These sites are Eureka, N.W.T. (80° 00N, 85° 86W) located alongside Slidre Fjord on Ellesmere Island, Resolute, N.W.T. (74° 43N, 94° 59°W) on Cornwallis Island and Frobisher Bay (63° 45N, 68° 33W) at the mouth of Koojessee Inlet on Baffin Island (see figure 5.1). These sites were chosen in the hope that they would provide a significantly varied range of environments to test the ability and independence of the computer model. Table 5.1 presents the 30 year normals of temperature, precipitation, snow fall and wind speed for each of the sites.

Meteorological observations at each site are made by the Atmospheric Environment Service (A.E.S.) which makes the data available in published summaries. Temperature, wind speed and pressure data may be found in the A.E.S. "Monthly Record of Meteorological Observations in Canada", radiation data in the A.E.S. "Monthly Radiation Summary", and snow and ice

FIGURE 5.1
SITE LOCATIONS

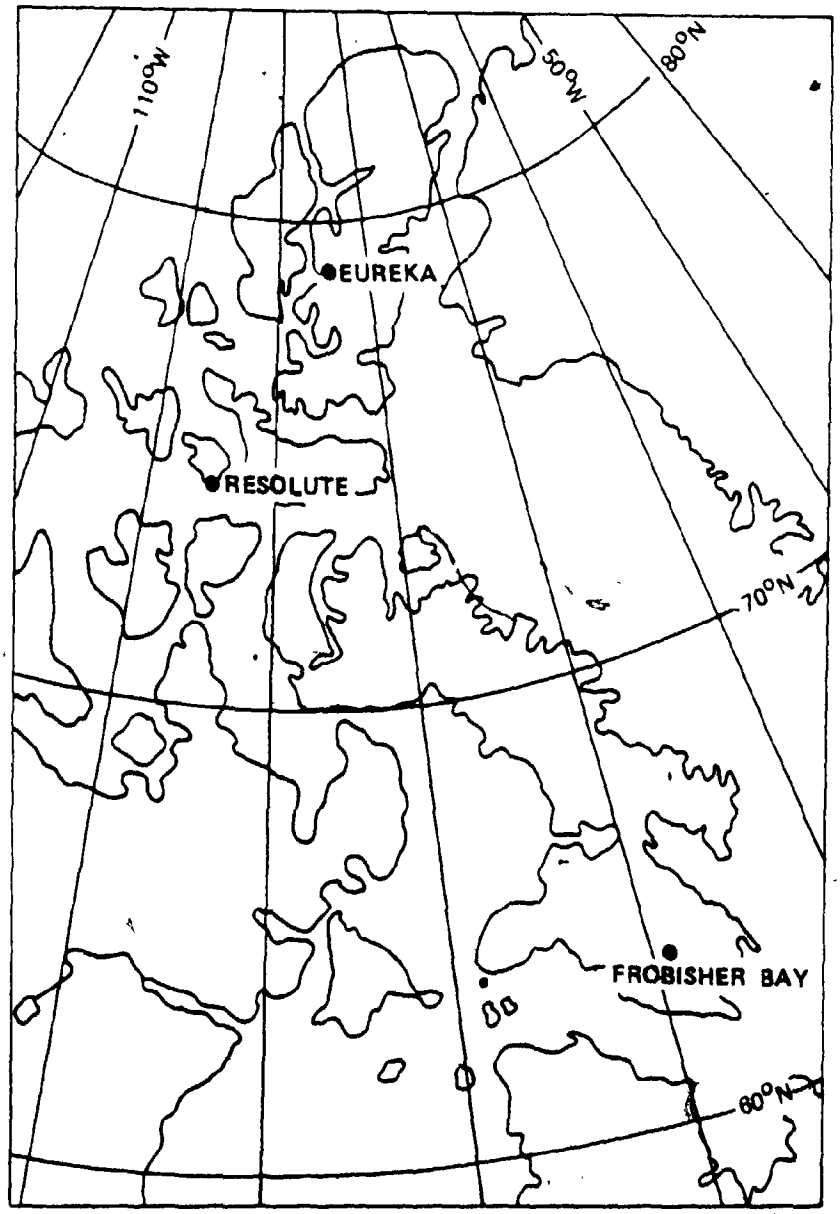

TABLE 5.1

CLIMATOLOGICAL NORMALS
EUREKA, RESOLUTE AND FROBISHER BAY, N.W.T.

EUREKA													
MONTH	J	F	M	A	M	J	J	A	S	O	N	D	YEAR
TEMPERATURE (°C)	-36.6	-37.7	-36.7	-27.6	-10.0	2.3	5.5	3.6	- 7.7	-21.8	-30.7	-34.8	-19.3
PRECIPITATION (cm)	0.28	0.23	0.15	0.20	0.28	0.38	1.30	0.91	1.02	0.61	0.28	0.20	5.84
SNOWFALL (cm)	3.3	2.5	1.8	2.0	3.0	1.8	0.5	1.5	10.4	6.4	3.0	2.0	38.4
WIND SPEED (m/s)	2.9	2.6	2.4	2.7	3.7	4.7	4.9	4.0	3.2	2.7	2.4	2.4	3.2

RESOLUTE													
MONTH	J	F	M	A	M	J	J	A	S	O	N	D	YEAR
TEMPERATURE (°C)	-32.6	-33.5	-31.3	-23.1	-10.7	- 0.3	4.3	2.7	- 4.9	-14.7	-24.2	-28.8	-16.4
PRECIPITATION (cm)	0.28	0.33	0.30	0.58	0.86	1.24	2.64	3.05	1.78	1.52	0.56	0.48	13.62
SNOWFALL (cm)	2.8	3.3	3.3	5.8	8.9	6.6	3.0	4.8	14.2	15.5	5.6	4.8	78.7
WIND SPEED (m/s)	6.0	6.3	6.0	5.5	6.0	6.2	5.6	6.3	7.1	7.0	5.9	5.8	6.1

FROBISHER BAY													
MONTH	J	F	M	A	M	J	J	A	S	O	N	D	YEAR
TEMPERATURE (°C)	-26.2	-25.2	-22.3	-14.0	- 3.3	3.5	7.9	6.9	2.4	- 4.7	-12.4	-20.3	- 8.9
PRECIPITATION (cm)	2.44	2.79	2.06	2.24	2.29	3.78	5.31	5.79	4.34	4.17	3.68	2.62	41.50
SNOWFALL (cm)	25.7	29.0	21.6	23.6	21.6	8.4	0.3	0.3	14.5	36.1	37.8	28.2	246.9
WIND SPEED (m/s)	4.3	4.3	3.9	4.7	5.5	4.8	3.7	3.8	5.0	5.6	5.1	4.6	4.6

thickness data in the annually published "Ice Thickness Data for Canadian Selected Stations".

The climatological data is collected at location of the airport of each settlement. The ice measurement sites are described by the A.E.S. in the following manner: Eureka - 100 yards due south on Slidre Fjord, Resolute - Resolute Bay, 100 yards south-south-east of Tidal Shack, and Frobisher Bay - Koojessee Inlet, 200 yards from M.O.T. causeway.

5.2 Data Analysis

5.2.1 Introduction

A sample output for the model has been provided as Appendix D. The remaining outputs have not been included due to space limitations but will remain on file with the Department of Geography, Carleton University, and will be available through the Supervisor of Graduate Study. For each site and year the results have been summarized graphically in the following set: ice thickness (observed and predicted) versus time (figures 5.2(a) - 5.2(i)), observed ice thickness versus predicted ice thickness (figures 5.3(a)-5.3(i)), shortwave radiation (incoming and outgoing) versus time (figures 5.4(a)-5.4(i)), longwave radiation (incoming and outgoing) versus time (figures 5.5(a)-5.5(i)), energy fluxes (sensible, evaporative, conductive and ablative) versus time (figures 5.6(a)-5.6(i)), temperatures (air, surface and snow-ice interface)

versus time (figures 5.7(a)-5.7(i)) and ice salinity versus time (figures 5.8(a)-5.8(i)).

5.2.2 Ice Growth and Decay

Figures 5.2(a) through 5.2(i) are plots of ice thickness versus time for the three growth seasons 1973-74, 1974-75, and 1975-76 at each of the sites. The model predictions are shown as the continuous trace while the observed ice thickness data are represented by the discrete points. This presentation allows a visual comparison of the modelled and observed growth. Figures 5.3(a) through 5.3(i) present a direct comparison between the observed and predicted ice thicknesses. The diagonal line in each figure is the 1:1 line representing the situation of perfect agreement between the two data sets.

A series of statistical tests were performed on each of the observed-predicted data sets. As a first step a correlation coefficient (r) was computed to measure the strength of the mutual dependence of the two variables. Table 5.2 summarizes these results showing a range in r from 0.962 to 0.993, all the values are significantly different at the 0.001 level from the no correlation case (r=0) as determined by a Student's t-test. The high correlation coefficients indicate that very good agreement is obtained between the model predicted ice growth and the observed ice growth. The coefficient of determination ranges from 0.925 to 0.986 indicating that ice

TABLE 5.2

STATISTICAL DATA SUMMARY FOR
ICE THICKNESS COMPARISONS

Site	Year	r[1]	b[1]	N
Eureka	1973-74	0.987	0.95	39
Eureka	1974-75	0.993	0.94	30
Eureka	1975-76	0.992	1.02	37
Frobisher Bay	1973-74	0.991	1.05	26
Frobisher Bay	1974-75	0.992	1.02	27
Frobisher Bay	1975-76	0.990	1.01	28
Resolute	1973-74	0.968	0.96	35
Resolute	1974-75	0.962	0.90	31
Resolute	1975-76	0.984	1.07	31

r = correlation coefficient
b = least squares estimate of slope
N = number of observations

[1] all values significantly different from 0 at the 0.001 level

thickness deviations not accounted for in the modelling rep-represent only 1% - 7% of the total variance.

The 1:1 lines in Figures 5.3(a)-5.3(i) provide a visual estimate of the relation of one variable to the other. Points lying above the line indicate overprediction by the model while underprediction results in points plotting below the line. By computing a regression slope we can provide a statistically based estimate of this dependence between the two variables. Perfect agreement between variables results in a slope with a value of 1.0 and an intercept of 0.0. Overprediction will yield slope values greater than 1.0 and underprediction slopes less than 1.0. When it is known in advance that y_i vanishes when $x_i = 0$ ($x_i = 0 = y_i$) then the appropriate regression line is one that passes through the origin (Seber, 1977). In this case the intercept of a normal regression line vanishes and the line is described by

$$y_i = bx_i \tag{5.1}$$

where y_i = predicted value

x_i = observed value

b = regression slope

The least squares estimate of the slope is given by

$$b = \frac{\sum_{i=1}^{n} x_i y_i}{\sum_{i=1}^{n} x_i^2} \tag{5.2}$$

and the unbiased estimate of variance s^2 is

$$s^2 = \frac{1}{n-1} \left\{ \sum_{i=1}^{n} y_i^2 - b^2 \sum_{i=1}^{n} x_i^2 \right\} \tag{5.3}$$

Confidence limits on the slope are given by

$$b \pm (t_{n-1}^{\alpha/2}) \ (s) \ \left(\sum_{i=1}^{n} x_i^2 \right)^{-1/2} \tag{5.4}$$

The regression slopes determined in this manner may be found in Table 5.2 and illustrate a range of 0.90 - 1.07 with a mean of 0.98. All are significantly different from a slope of zero at the 0.001 level. The lower slope value shows that overall a least squares estimate of 10% underprediction of ice thickness occurred while a least squares estimate of 7% overprediction existed overall for the upper slope value. All other values fell within these limits.

Lewis (1967) noted that variations in thickness of up to 15% were a permanent feature of the ice cover on Cambridge Bay. As the climatic conditions were essentially similar, the variations were tentatively ascribed to variations in snow cover. Accepting the 15% figure as representative for other similar ice covers we can suggest that a rough criteria for the range in slope value should be

$$b = 1. \pm 0.075$$

$$0.925 < b < 1.075 \tag{5.5}$$

All the slopes, with the exception of Resolute 1974-1975,

satisfy the relation defined by (5.5) It is also possible to test whether a regression slope is significantly different from any specified theoretical slope (Sokal and Rohlf, 1969). The t-statistic for this comparison is

$$t_{\alpha/2,n-1} = \frac{b - \beta}{S_b} \tag{5.6}$$

where β = theoretical slope

S_b = variance of regression slope

$$= \frac{S^2}{\sum_{i=1}^{n} x_i^2}$$

In doing this test it is found that all the slopes are not significantly different (at the 5% level) from the limits specified by (5.5). Under these conditions it appears that overall the model ice thickness estimates are compatable with observed ice thicknesses and their naturally occurring variation.

Lewis (1967) also details some of the problems estimating and comparing ice growth by means of conventional ice drilling techniques. When sequential measurements are made from one location all results other than the first are liable to error due to the perturbations in heat flow resulting from the initial drilling. If different locations are used then any rate of growth from zero up to a given maximum may be found. Leahey (1966) notes three other sources of error in observed ice thickness data; (i) error made by the operator in taking

the measurement; (ii) sudden growth of snow ice; and (iii) rafting occurring in the vicinity of the measured ice. Assuming a certain degree of competence the error due to the operator should be at a minimum and contained within the resolution of the measurement, although this may not be true when a new and unskilled operator is responsible for the measurement. Snow ice is caused by the freezing of slush on the ice surface. The slush is produced by flooding the snow which may be due to tidal effects or the depression of an ice surface beneath the hydrostatic level by a load (such as the weight of the snow, see Shulyakovski (1969)). Rafting is most commonly observed during autumn freezeup or spring thaw. It is the sliding of one ice sheet under another due to the pressure induced by ocean currents or wind.

These agents increase the variation in thickness for a growing ice sheet and reduce the confidence that can be placed in a single observation of ice thickness. In his analysis of ice thickness data Leahey (1966) rejected values that were "clearly non-representative" (p.7). This state was determined qualitatively and consisted of removing any terms that deviated from a smoothed growth curve. For example, in the sequence 9-25-<u>20</u>-36-46-52-60-<u>78</u>-65 the value of 20 would be rejected for being too low while 78 would be considered too high. The same sort of variation is evident in the data for each of the stations examined (see especially that for Resolute 1973-

74, figure 5.2(g). It is evident by studying these figures that a better agreement between predicted and observed values could be obtained by the selective editing of the ice thickness observations. This is not a recommended course of action as it introduces a bias and reduces the independence of the data. A more acceptable technique would consist of smoothing the data (as by the use of a triangular filter) to reduce such high frequency, high amplitude noise. This should have the effect of reducing the deviations between the model and the observed data. Filtering was not conducted on the ice thickness observations employed here because an acceptable level of agreement is achieved without the necessity of this action.

The model operates in a continuous sense and simulates the changeover from ice growth to ice ablation in response to the forcing climate. Ablation of the ice surface begins only after the melting of the snowpack has been accomplished. Although the rate of snowpack melt is dependent on snow density and the meteorologic conditions, rates of 0-7 cm per day were predicted by the model. This is followed by a very rapid decay of the ice as can be seen in figures 5.2(a), 5.2(d), 5.2(e), and 5.2(f), where ablation rates of the order of 5-10 cm per day were simulated. It is very difficult to evaluate the ability of the model during this phase. Radiation penetrating into the ice cover heats the brine within the brine pockets

leading to internal melting and enlargement. The enlargement and subsequent drainage of these pockets produce a decrease in the strength of an ice cover. This rapid decay renders the ice unsafe for travel so that observations of ice thickness may no longer be collected. Due to this there are few or no measurements during this period with which to compare the model predictions. Of the three sites chosen, Frobisher Bay has the best record during the melt period. Examination of figures 5.1(d), 5.1(e), and 5.1(f) shows that a decrease in ice thickness at a rate comparable to that predicted is observed. Good agreement with respect to both the magnitude and timing of melt occurs. Further comparisons can be made from comments concerning break-up contained within the A.E.S. Ice Summary. At Frobisher Bay in 1973-74 break-up occurred at "the end of June" (p.7); on June 30, 1974 the model predicts 11 cm of ice with complete disintegration (in a thermodynamic sense) occurring one day later, on July 1, 1974. In the 1974-75 season break-up is given as June 27, 1975; the model thickness on this day was 29 cm and the ice cover disappeared 2 days later, on June 29, 1975.

5.2.3 Energy Flux Behaviour

5.2.3.1 Conductive Flux

The conductive heat flux is initially very high for thin ice conditions and decreases over time as the ice thickens and becomes snow covered. The term supplies energy derived

from the energy of phase change associated with ice formation at the ice-water interface, to the surface during the growth period. When the ice thickness is approaching its maximum or an extensive snowcover exists, the value of this flux is quite small ($<10W/m^2$). During the melt season the flux is reversed and represents a loss of heat from the surface, the surface being warmer than the base of the ice sheet (0^oC versus -1.8^oC). The magnitude of the flux during this period is very small and plays only a minor role in the energy exchange.

5.2.3.2 Sensible Heat Flux

Throughout much of the winter the sign of the sensible heat flux is negative indicating energy is being transferred from the surface to the atmosphere. This is in contrast to the inversion conditions which may persist over perennial sea ice and ground surfaces throughout much of the polar night. The difference is a result of the much lower conductive heat flux in the latter case. Initially, the magnitude of the sensible heat flux may be less than that of the conductive heat flux but becomes comparable in size as the ice thickens. After the spring temperature change to above freezing air temperatures the sign of the sensible heat transfer term is always positive as heat is transferred from the atmosphere to the ice surface which remains at 0^oC. The term increases in magnitude substantially and dominates over the conductive and evaporative energy transfers.

5.2.3.3 Evaporative Heat Flux

The evaporative heat flux during the winter period is very low due to the reduced capacity of the air to hold water at these temperatures. Throughout most of the growth period the magnitude of this flux is 1-2 orders of magnitude lower than the sensible and conductive heat fluxes. It is not until after the commencement of melt and the associated higher temperatures increase the water bearing capacity of the air that it attains an appreciable magnitude. In this period it exceeds the conductive heat flux and approaches the value of the sensible heat flux. During melt the simplifying assumptions made in the model concerning the nature of the evaporative process begin to break down. Measurements of evaporative heat flux over an ice surface at this time may yield a negative flux due to evaporation while the model will predict a positive flux indicating condensation onto the ice surface. The discrepancy occurs because the model assumes an ice surface at $0^{o}C$ whereas ponded melt water with a surface temperature in excess of $0^{o}C$ with a vapour pressure sufficient to drive the evaporative transfer in the opposite direction (surface to atmosphere) may occur.

5.2.3.4 Ablative Heat Flux

The ablative flux is introduced to satisfy the energy conservation equation when an equilibrium surface temperature is generated that exceeds $0^{o}C$. It is initially supplied by

the melting of any snowcover and then by the ablation of the ice. The ablative flux and sensible heat flux are the dominant non-radiative energy terms during the decay period. The magnitude of the ablative flux increases as the air temperature and incoming shortwave radiation increase.

5.2.4 Energy Flux Assessment

The components of the radiative and energy balances are provided by the computer model on a daily basis. The relative magnitudes and directions at any particular date are determined by the interplay of atmospheric, surface and ocean processes. Figures 5.4(a)-(i), 5.5(a)-(i), and 5.6(a)-(i) show the variation in these components over the ice. It is difficult to evaluate the capability of the model to simulate the energy and radiative fluxes in the absence of independent observational data. An indirect assessment is possible by the comparison of model results with previous work.

Maykut (1978) studied the energy exchange over young sea ice in the central Arctic using a similar modelling technique. He calculated the heat balance over ice thicknesses of 0.05 m - 0.80 m for the period September through June. A comparison between the two models was made using the climatological inputs specified in his Table One (p. 3649). His results and those generated by this model are shown in Table 5.3. Very good agreement was obtained between the two models with

TABLE 5.3

COMPARISON OF ENERGY FLUX PREDICTIONS OF PRESENT MODEL WITH THOSE OF MAYKUT (1978)

Month	F_{H_1} ($W \cdot m^{-2}$)	F_{H_2} ($W \cdot m^{-2}$)	F_{E_1} ($W \cdot m^{-2}$)	F_{E_2} ($W \cdot m^{-2}$)	F_{I_1} ($W \cdot m^{-2}$)	F_{I_2} ($W \cdot m^{-2}$)	K↓ ($W \cdot m^{-2}$)	Ta (°C)
			H=0.05 m					
OCT	-136	-142	-41	-50	238	218	26.7	-15.0
NOV	-266	-261	-45	-49	390	380	0	-25.3
DEC	-322	-311	-44	-47	446	445	0	-29.5
JAN	-326	-312	-44	-46	450	449	0	-29.8
FEB	-349	-334	-43	-45	473	472	0	-31.5
MAR	-375	-362	-43	-44	495	494	7.8	-33.4
APR	-324	-313	-49	-51	401	401	92.2	-28.5
MAY	-180	-179	-57	-62	183	176	232.2	-15.8
	r = 1.00		r = 0.89		r = 0.999			
			H=0.10 m					
OCT	- 89	-101	-23	-34	166	153	26.7	-15.0
NOV	-187	-186	-25	-30	275	271	0	-25.3
DEC	-230	-222	-24	-27	317	318	0	-29.5
JAN	-233	-222	-23	-26	320	321	0	-29.8
FEB	-251	-238	-23	-25	336	338	0	-31.5
MAR	-272	-262	-22	-24	353	355	7.8	-33.4
APR	-242	-232	-28	-31	284	288	92.2	-28.5
MAY	-143	-143	-41	-47	129	127	232.2	-15.8
	r = 0.999		r = 0.918		r = 0.999			
			H=0.2 m					
OCT	- 48	- 64	-10	-22	105	97	26.7	-15.0
NOV	-114	-115	-11	-16	176	172	0	-25.3
DEC	-145	-137	-10	-14	203	204	0	-29.5
JAN	-146	-136	-10	-14	205	207	0	-29.8
FEB	-159	-147	-10	-13	216	218	0	-31.5
MAR	-175	-165	-10	-12	227	228	7.8	-33.4
APR	-164	-154	-14	-17	183	184	92.2	-28.5
MAY	-108	-109	-28	-34	83	80	232.2	-15.8
	r = 0.998		r = .903		r = 0.999			

*1 = this paper
2 = Maykut (1978)

Table 5.3 continued

Month	F_{H_1} ($W \cdot m^{-2}$)	F_{H_2} ($W \cdot m^{-2}$)	F_{E_1} ($W \cdot m^{-2}$)	F_{E_2} ($W \cdot m^{-2}$)	F_{I_1} ($W \cdot m^{-2}$)	F_{I_2} ($W \cdot m^{-2}$)	K↓ ($W \cdot m^{-2}$)	Ta (°C)
			H=0.40 m					
OCT	- 17	- 36	- 2	-14	61	56	26.7	-15.0
NOV	- 58	- 62	- 3	- 9	103	102	0	-25.3
DEC	- 79	- 72	- 3	- 6	119	119	0	-29.5
JAN	- 80	- 70	- 3	- 6	120	121	0	-29.8
FEB	- 88	- 77	- 3	- 6	127	128	0	-31.5
MAR	-100	- 91	- 3	- 5	134	134	7.8	-33.4
APR	-103	- 93	- 6	-10	108	108	92.2	-28.5
MAY	- 79	- 82	-18	-26	50	49	232.2	-15.8
	r = 0.974		r = 0.884		r = 0.999			
			H=0.8 m					
OCT	3	- 18	3	- 9	33	31	26.7	-15.0
NOV	- 22	- 27	1	- 4	56	55	0	-25.3
DEC	- 36	- 30	1	- 3	65	66	0	-29.5
JAN	- 36	- 27	1	- 2	66	66	0	-29.8
FEB	- 42	- 31	0	- 2	69	70	0	-31.5
MAR	- 50	- 42	0	- 2	73	75	7.8	-33.4
APR	- 63	- 53	- 2	- 5	59	59	92.2	-28.5
MAY	- 59	- 61	-12	-19	27	27	232.2	-15.8
	r = 0.878		r = 0.818		r = 0.999			

	OCT	NOV	DEC	JAN	FEB	MAR	APR	MAY
$L\downarrow_1$	189	171	165	164	162	159	166	186
$L\downarrow_2$	245	199	176	172	166	165	174	215
$\Delta L\downarrow$	-56	-20	-11	- 8	- 4	- 6	- 8	-29

some divergence of results, attributable to different values of incoming longwave radiation, occurring in the warmer months. The values of incoming longwave radiation are generated internally in this model and are lower than the input values employed by Maykut. This difference between the models is also shown in Table 5.3.

Goddard (1974) applied a similar type of climate simulation model to Arctic pack ice and compared his model predictions against net radiation and energy flux measurements made over the ice surface. A simulation was conducted to compare Goddard's results with the output of this model. Temperature, net radiation, sensible heat flux and evaporative heat flux values were obtained from his Figure Two. Wind at 10 m (u_{10} = 5.7 m·s^{1}) was calculated using u_2 = 5.0 m·s^{1} and Z_o = 0.001 cm assuming a neutral condition. 15 cm of snow were applied to the ice whose thickness was taken as 1.0 m (Banke and Smith, 1973). No measurements of incoming shortwave radiation were available but these were estimated using Goddard's equation (3) in which the average intensity of the solar radiation is estimated by

$$K\downarrow = IA^{\sec(\Omega)} \cos(\Omega) \qquad (5.7)$$

where I = solar constant

A = atmospheric turbidity coefficient

Ω = zenith angle

The zenith angle is determined from

$$\cos(\Omega) = \sin(\phi)\sin(\mu)+\cos(\phi)\cos(\mu)\cos(\omega) \tag{5.8}$$

where ϕ = latitude

μ = declination of the sun

ω = hour angle

Values of $I=1360\ W/m^2$, $A=0.93$, $\phi=75^{\circ}N$ and $\mu=4.67^{\circ}$ were employed for April 1, 1972, a day on which clear sky conditions prevailed. The model was run using these inputs and the comparison with Goddard's results for net radiation, sensible heat flux and evaporative heat flux are tabulated in Table 5.4.

The agreement is very good as indicated by the strength of the correlation coefficients. (Q^*, $r=0.99$: Q_H, $r=0.99$: Q_E, $r=0.99$). It is unfortunate that the data provided in the original report was not sufficient to allow a direct comparison between this model and field observations. However, by using his Table Three in which correlation coefficients for his measured and simulated values are presented, we see that good agreement was obtained for the net radiation ($r = 0.99$), sensible heat flux ($r = 0.94$) and evaporative heat flux ($r = 0.97$). As the agreement between Goddard's results and this model is good we may infer that a similar high degree of correlation exists between this model and field observations.

TABLE 5.4

COMPARISONS OF ENERGY FLUX PREDICTIONS OF PRESENT MODEL WITH THOSE OF GODDARD (1974)

TIME (local)	Q_1^* ($W \cdot m^{-2}$)	Q_2^* ($W \cdot m^{-2}$)	F_{H_1} ($W \cdot m^{-2}$)	F_{H_2} ($W \cdot m^{-2}$)	F_{E_1} ($W \cdot m^{-2}$)	F_{E_2} ($W \cdot m^{-2}$)
0700	-13	- 7	- 3	-13	0	1
0800	2	7	-17	-23	- 1	0
0900	16	19	-29	-33	- 2	- 2
1000	26	29	-38	-40	- 3	- 2
1100	33	37	-44	-45	- 3	- 3
1200	36	39	-45	-46	- 4	- 3
1300	33	37	-44	-43	- 3	- 3
1400	26	31	-38	-38	- 3	- 2
1500	16	21	-29	-30	- 2	- 2
1600	2	10	-17	-19	- 1	0
1700	-13	3	- 3	- 9	0	1
	r = 0.985		r = 0.992		r = 0.951	

1 - this paper
2 - Goddard (1974)

all r-values significant at the 0.01 level.
simulation for AIDJEX test site, April 1, 1972

Thorpe et al (1973) made eddy correlation measurements of evaporation and sensible heat flux over sea ice at the AIDJEX test site (75°N, 150°W) in April 1972. Values of sensible heat flux show a range from -34 W/m^2 through 23 W/m^2 dependent upon local climatological conditions. The ice was 2 m thick with a 10-15 cm snow cover, temperatures ranged through -28°C to -16°C and wind speeds varied from 2.6 m/s to 9.9 m/s. Although it is not possible to simulate these conditions directly we can compare the results with some obtained under similar conditions. Frobisher Bay (75°N) was characterized by a 1.7 m ice depth and 8-13 cm snowpack. For April 1-8 temperatures ranged from -27.8^{o}C to -16.1^{o}C and the sensible heat flux predicted fell within the range -23W/m^2 to 3W/m^2. Similar conditions prevailed for April 14-20 where temperatures in the range -25.6^{o}C to -13.9^{o}C produced predicted sensible heat fluxes of -26W/m^2 to -2W/m^2. The period April 9-13 was warmer (-11.7^{o}C to -6.1^{o}C) and generated sensible heat fluxes from -2W/m^2 to 21W/m^2. Although no direct comparisons may be made between the data sets we may infer that the fluxes produced by the model are not contradictory with respect to the magnitude of observed fluxes.

FIGURE 5.2(a) ICE THICKNESS VERSUS TIME
EUREKA 1973 - 1974

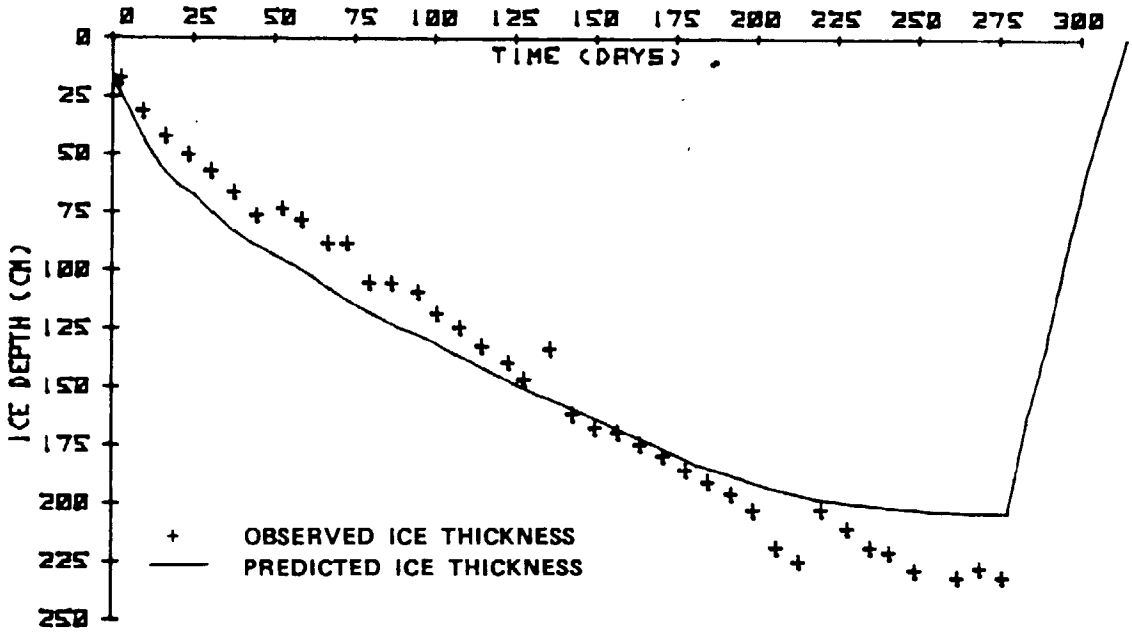

FIGURE 5.3(a) OBSERVED VERSUS PREDICTED ICE THICKNESS
EUREKA 1973 - 1974

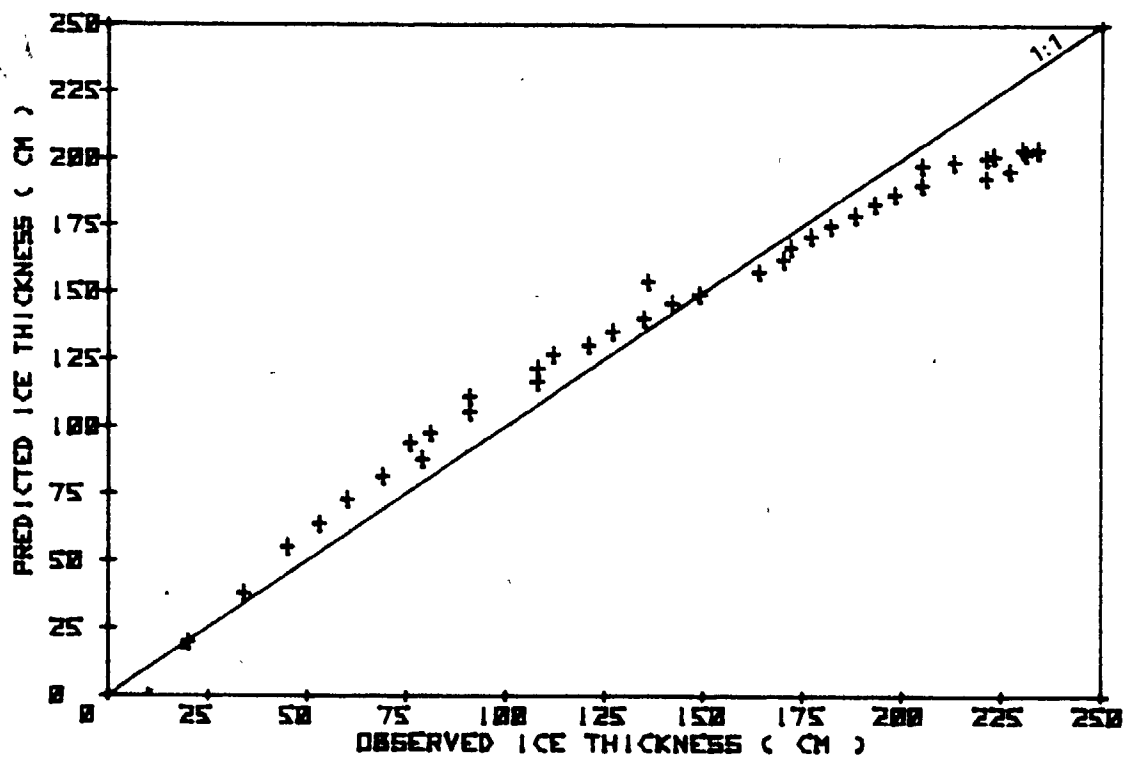

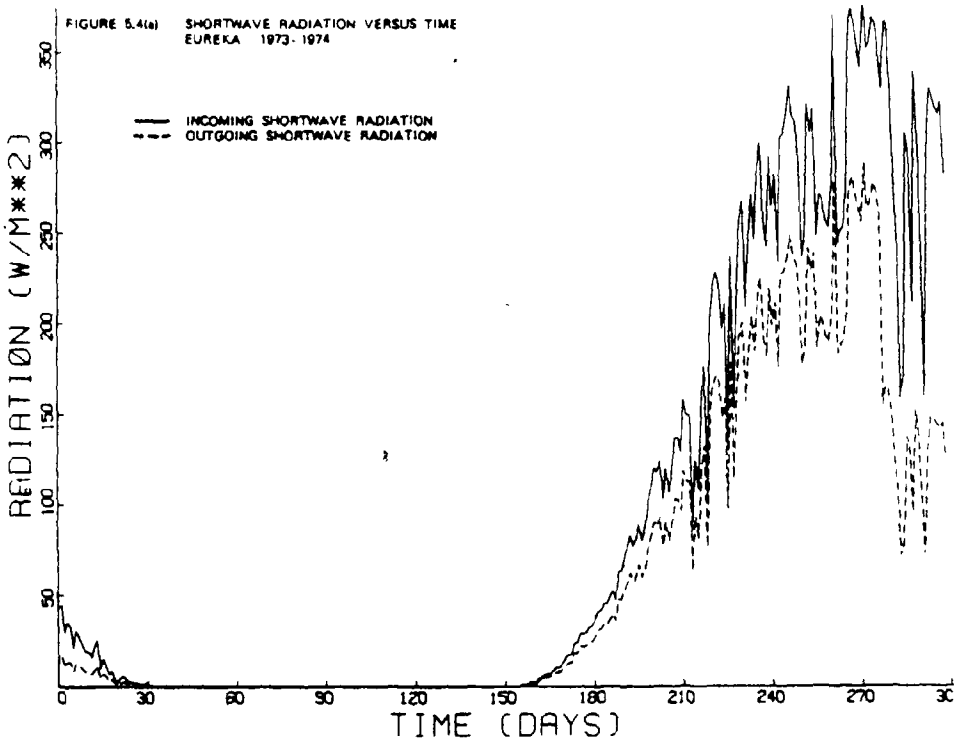
FIGURE 5.4(a) SHORTWAVE RADIATION VERSUS TIME
EUREKA 1973-1974
INCOMING SHORTWAVE RADIATION
OUTGOING SHORTWAVE RADIATION
RADIATION (W/M**2)
50
100
150
200
250
300
350
0
30
60
90
120
150
180
210
240
270
TIME (DAYS)

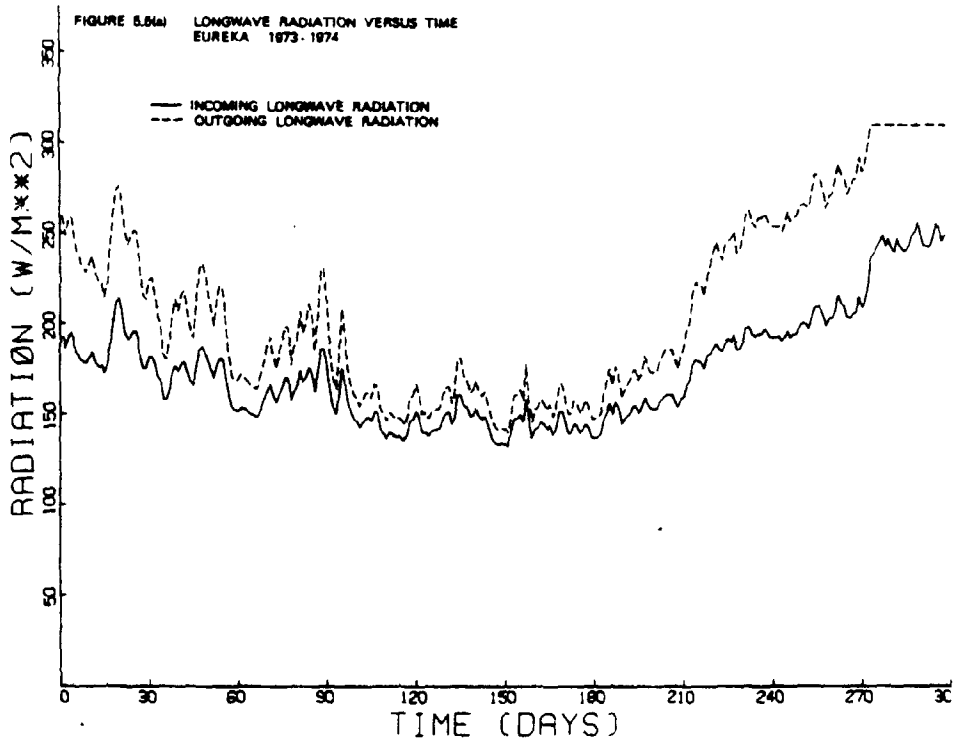
FIGURE 5.5(a) LONGWAVE RADIATION VERSUS TIME
EUREKA 1973-1974
INCOMING LONGWAVE RADIATION
OUTGOING LONGWAVE RADIATION
RADIATION (W/M**2)
50
100
150
200
250
300
350
0
30
60
90
120
150
180
210
240
270
TIME (DAYS)

FIGURE 5.6(a) ENERGY FLUXES VERSUS TIME
EUREKA 1973 1974

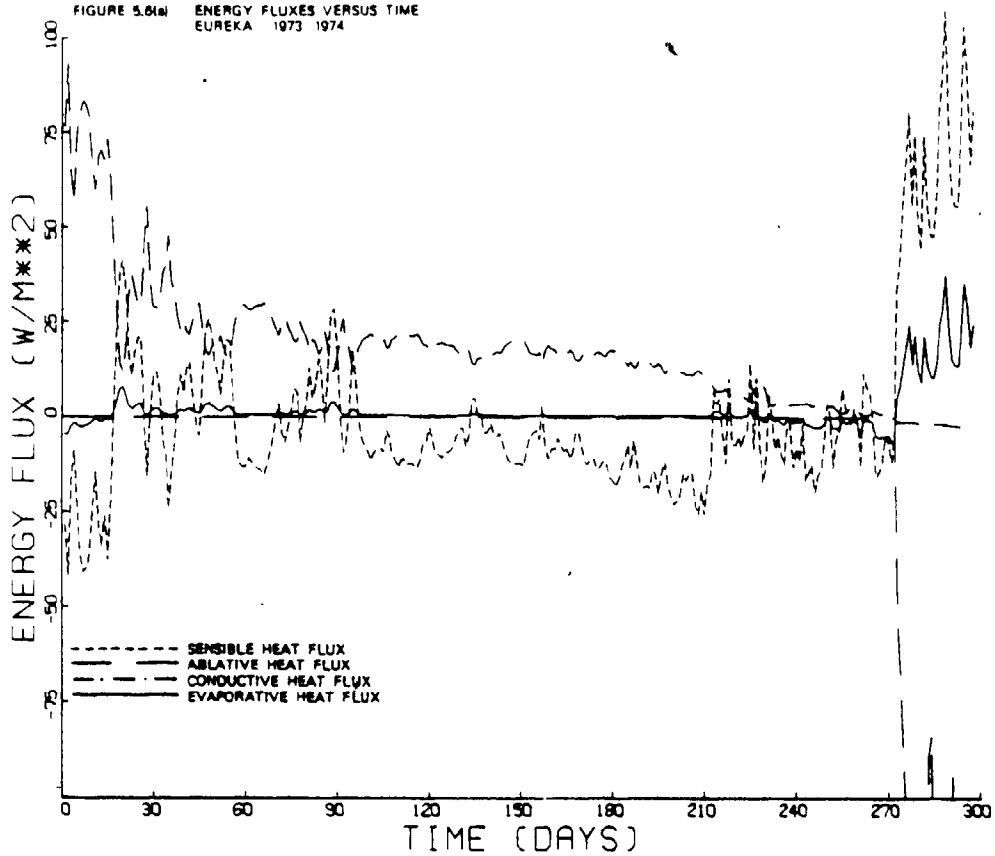

FIGURE 5.7(a) TEMPERATURES VERSUS TIME
EUREKA 1973 - 1974

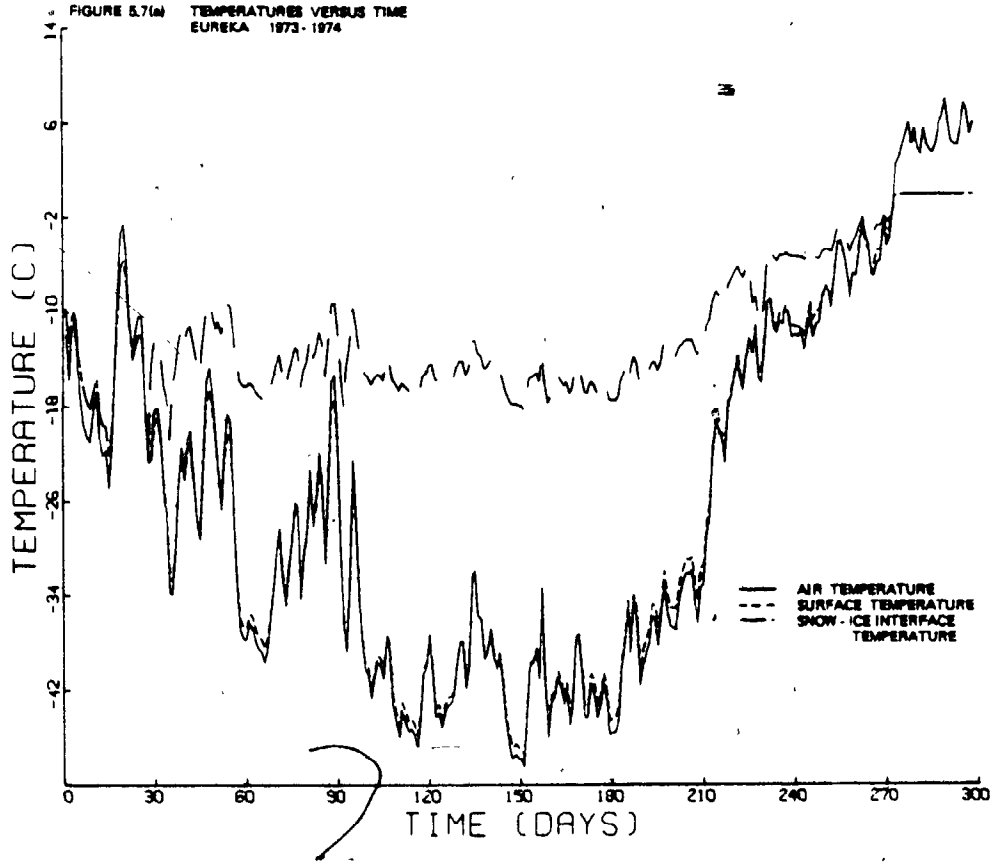

FIGURE 5.8(a) ICE SALINITY VERSUS TIME
EUREKA 1973 - 1974

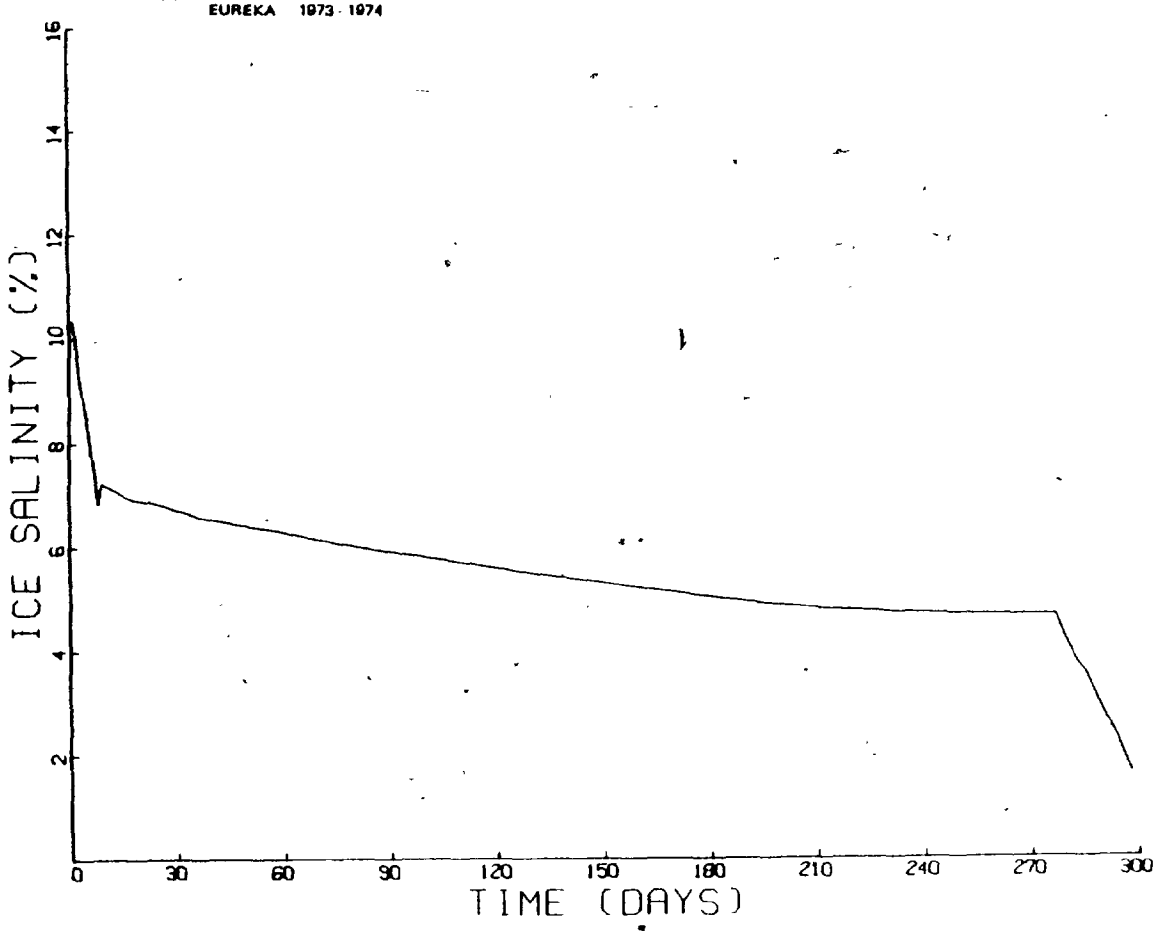

FIGURE 5.2(b) ICE THICKNESS VERSUS TIME
EUREKA 1974 - 1975

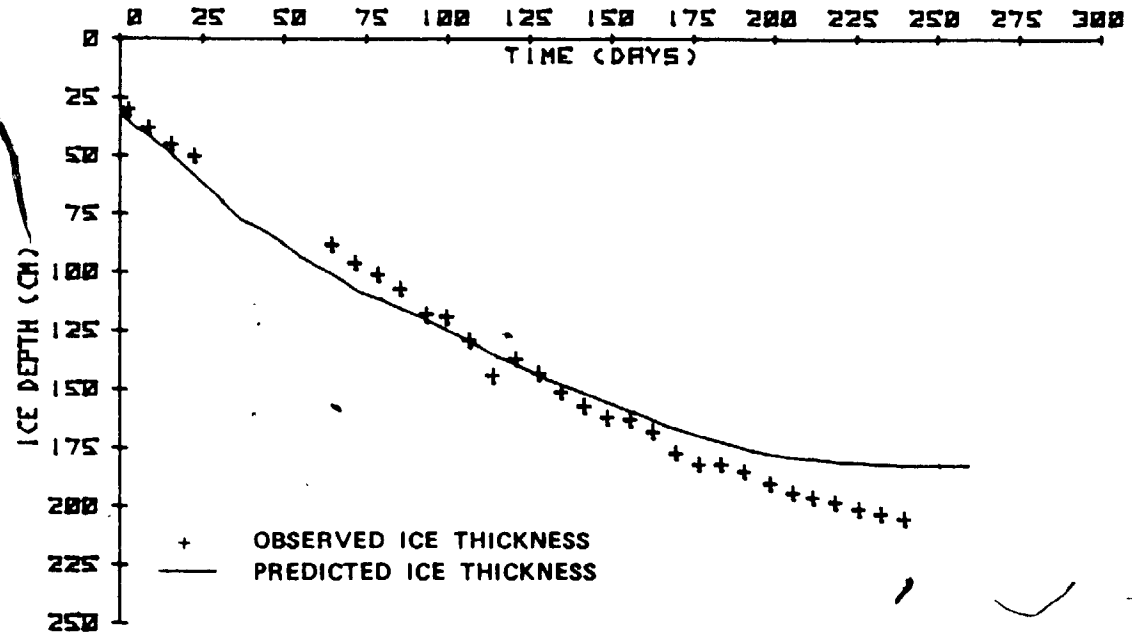

FIGURE 5.3(b) OBSERVED VERSUS PREDICTED ICE THICKNESS
EUREKA 1974 - 1975

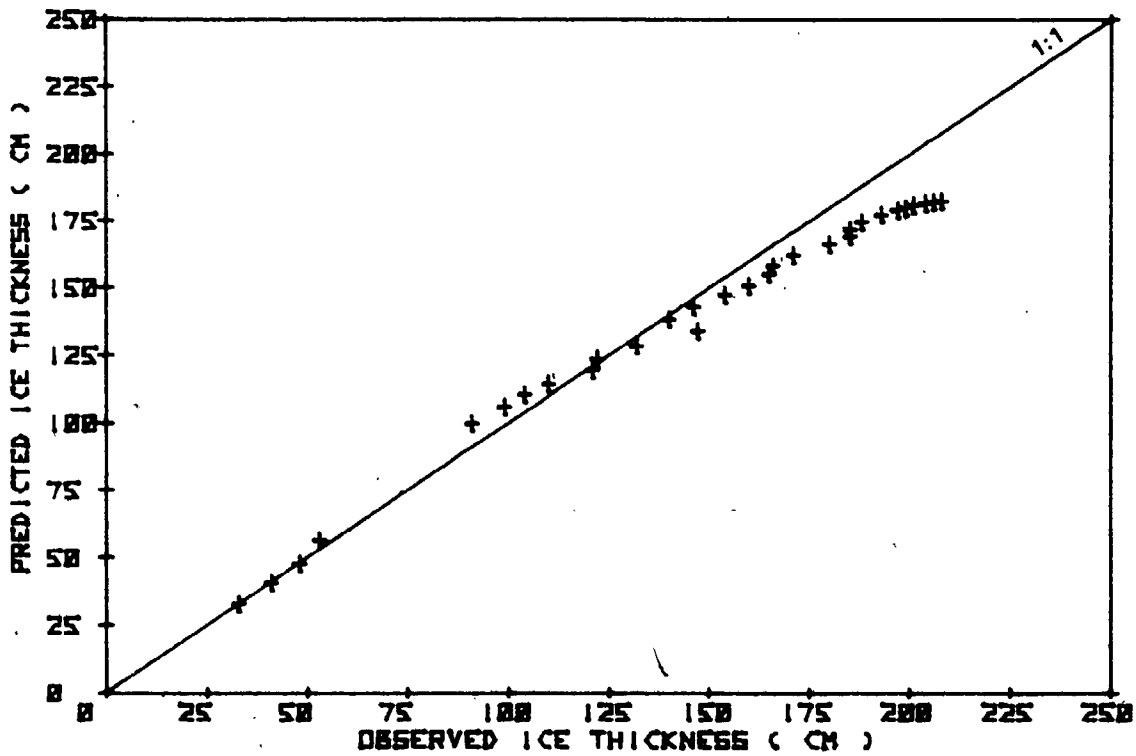

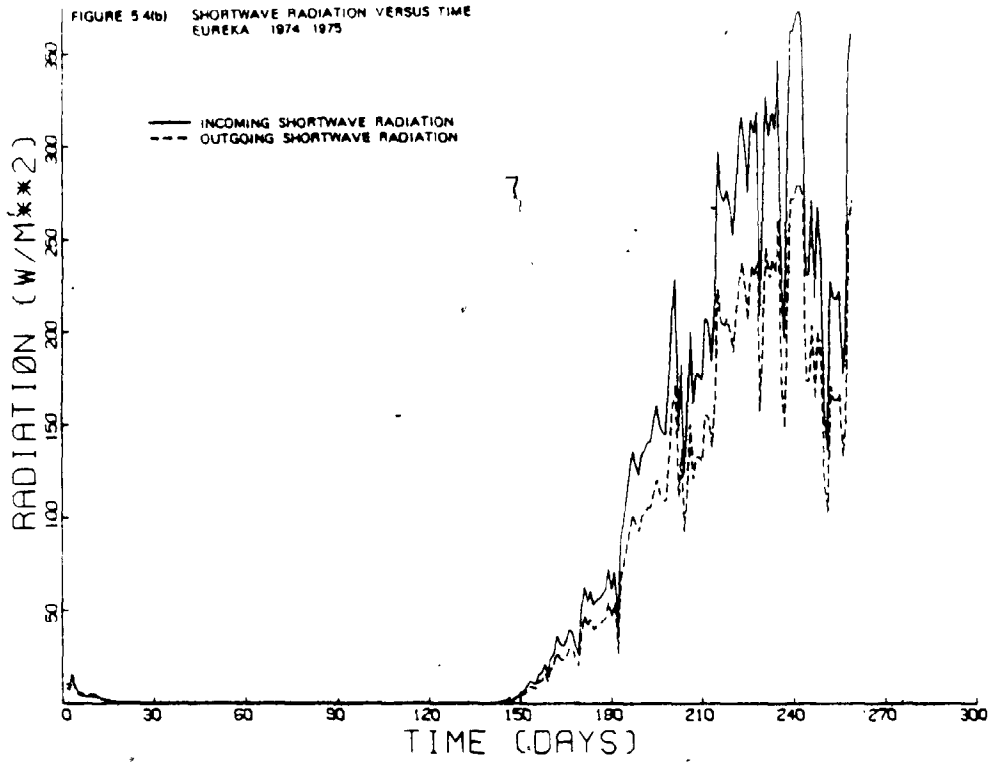
FIGURE 5.4(b) SHORTWAVE RADIATION VERSUS TIME
EUREKA 1974 1975
INCOMING SHORTWAVE RADIATION
OUTGOING SHORTWAVE RADIATION
RADIATIØN (W/M**2)
TIME (DAYS)
0
30
60
90
120
150
180
210
240
270
300
50
100
150
200
250
300
350

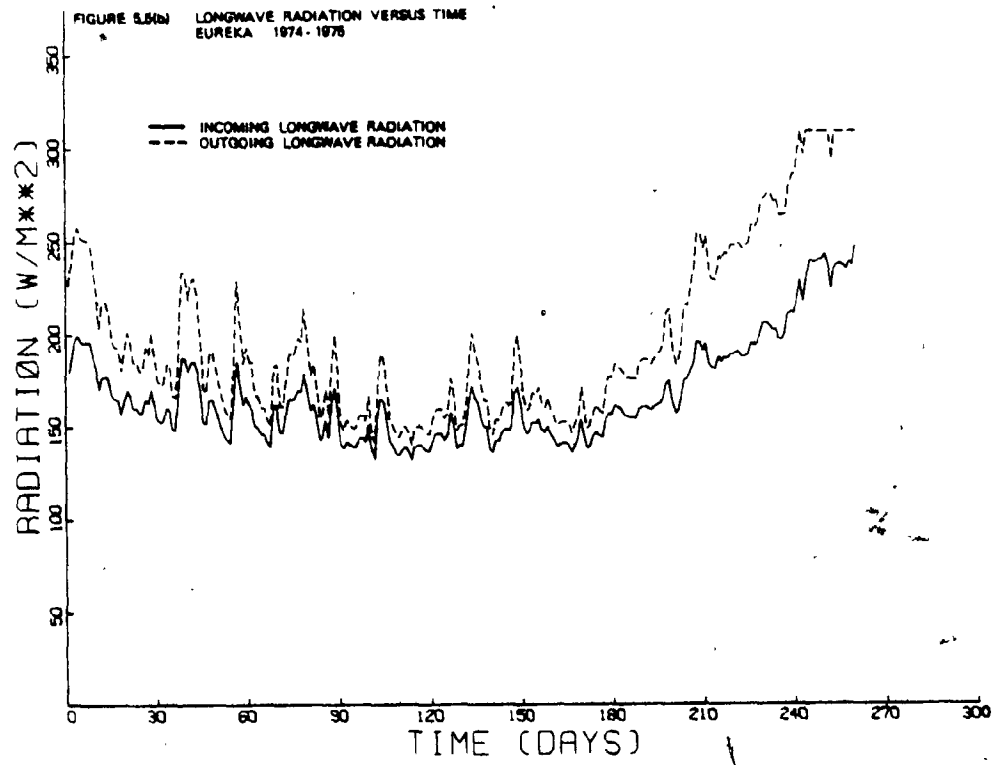
FIGURE 5.5(b) LONGWAVE RADIATION VERSUS TIME
EUREKA 1974 - 1975
INCOMING LONGWAVE RADIATION
OUTGOING LONGWAVE RADIATION
RADIATIØN (W/M**2)
TIME (DAYS)
0
30
60
90
120
150
180
210
240
270
300
50
100
150
200
250
300
350

FIGURE 5.6(b) ENERGY FLUXES VERSUS TIME
EUREKA 1974 - 1975

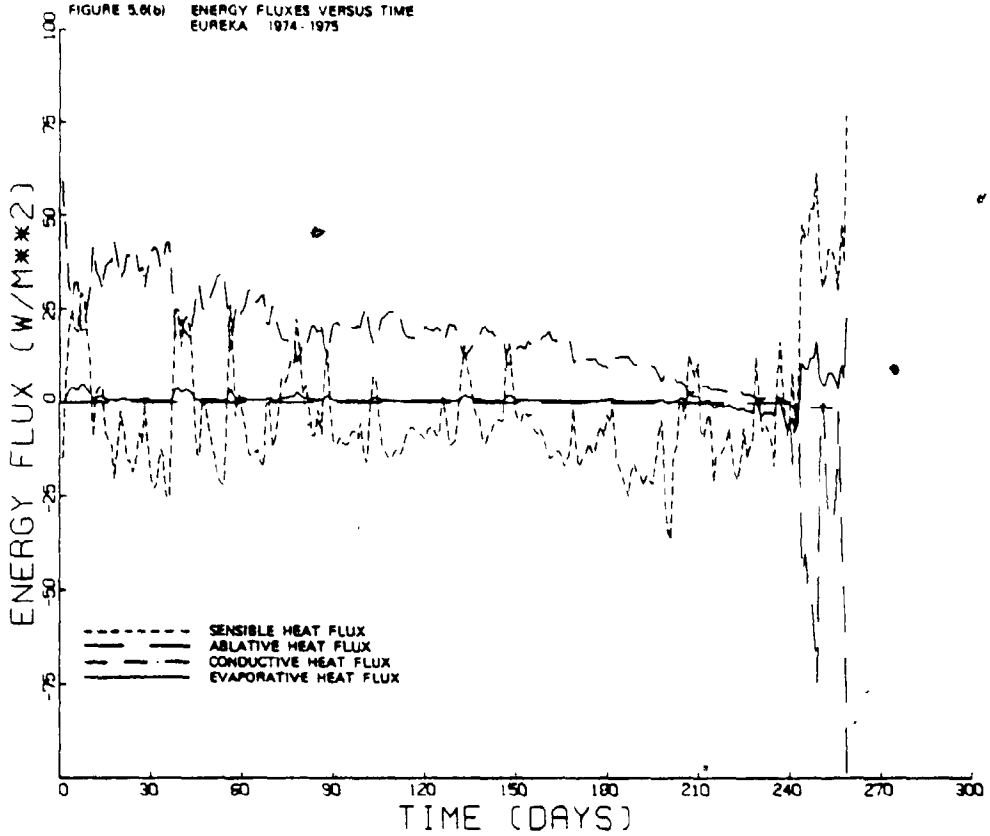

FIGURE 5.7(b) TEMPERATURES VERSUS TIME
EUREKA 1974 - 1975

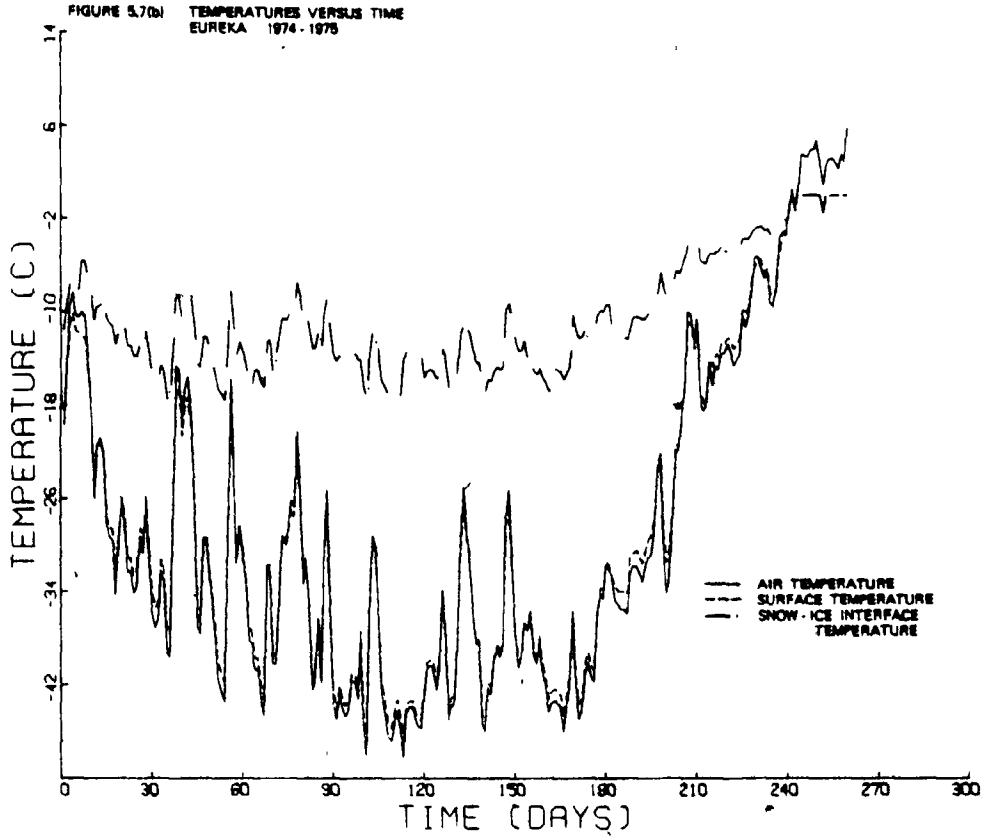

FIGURE 5.8(b) ICE SALINITY VERSUS TIME
EUREKA 1974 - 1975

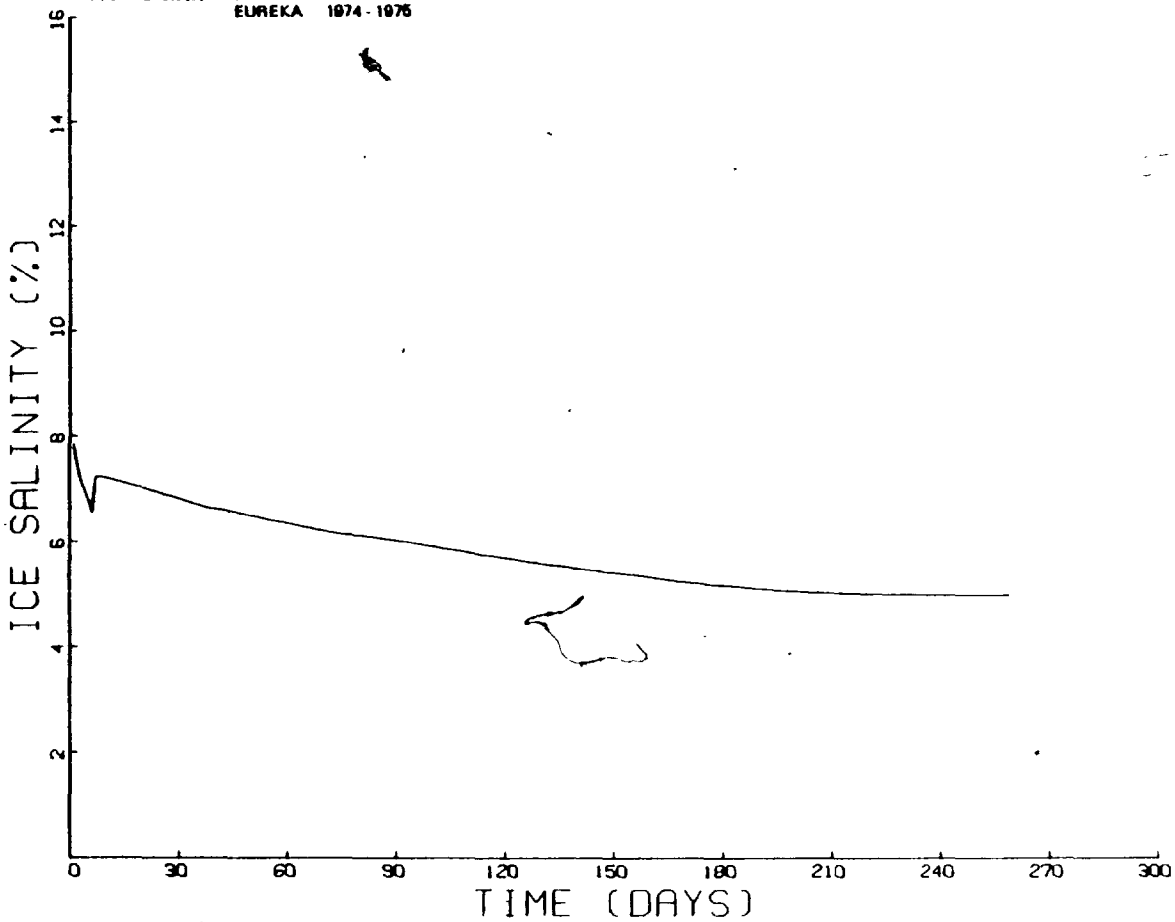

FIGURE 5.2(c) ICE THICKNESS VERSUS TIME
EUREKA 1975 - 1976

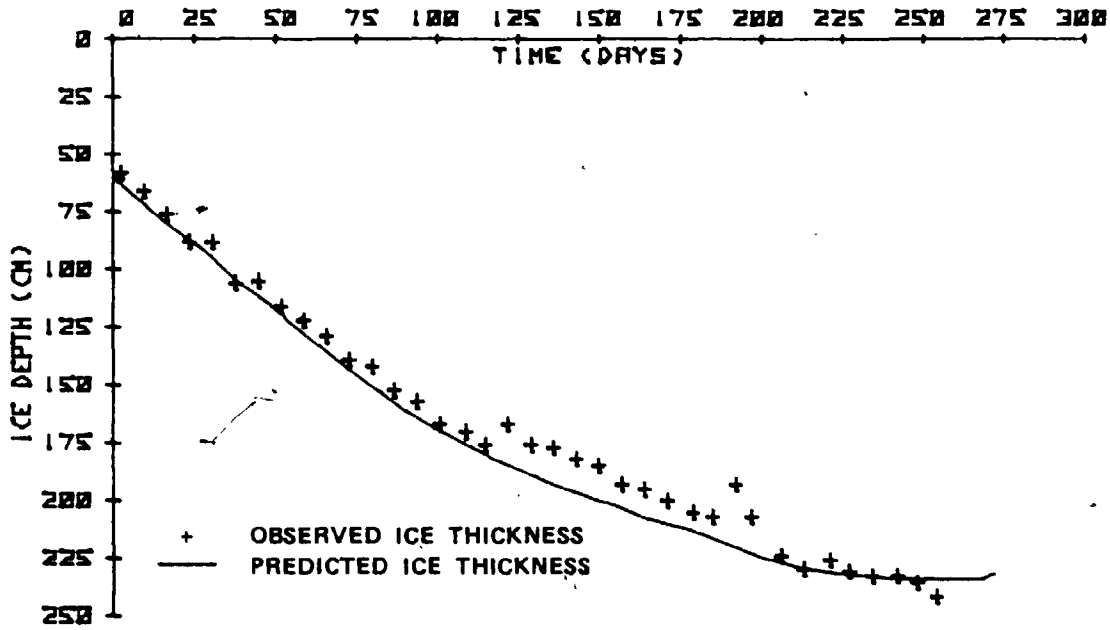

FIGURE 5.3(c) OBSERVED VERSUS PREDICTED ICE THICKNESS
EUREKA 1975 - 1976

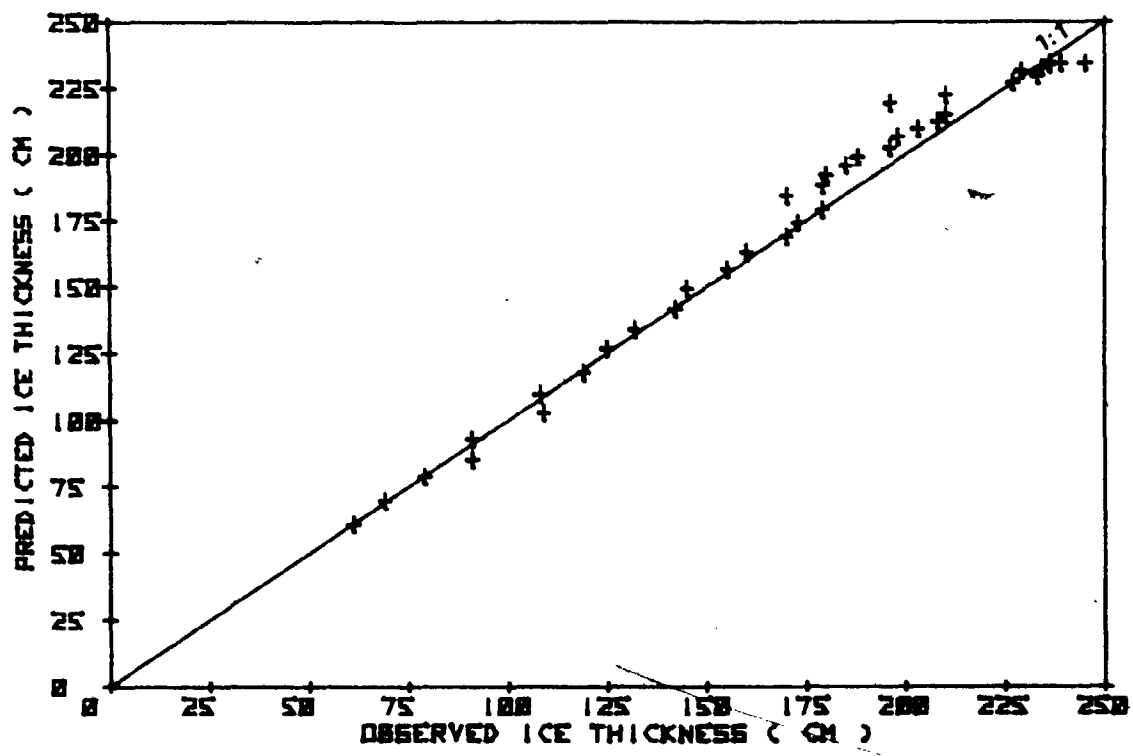

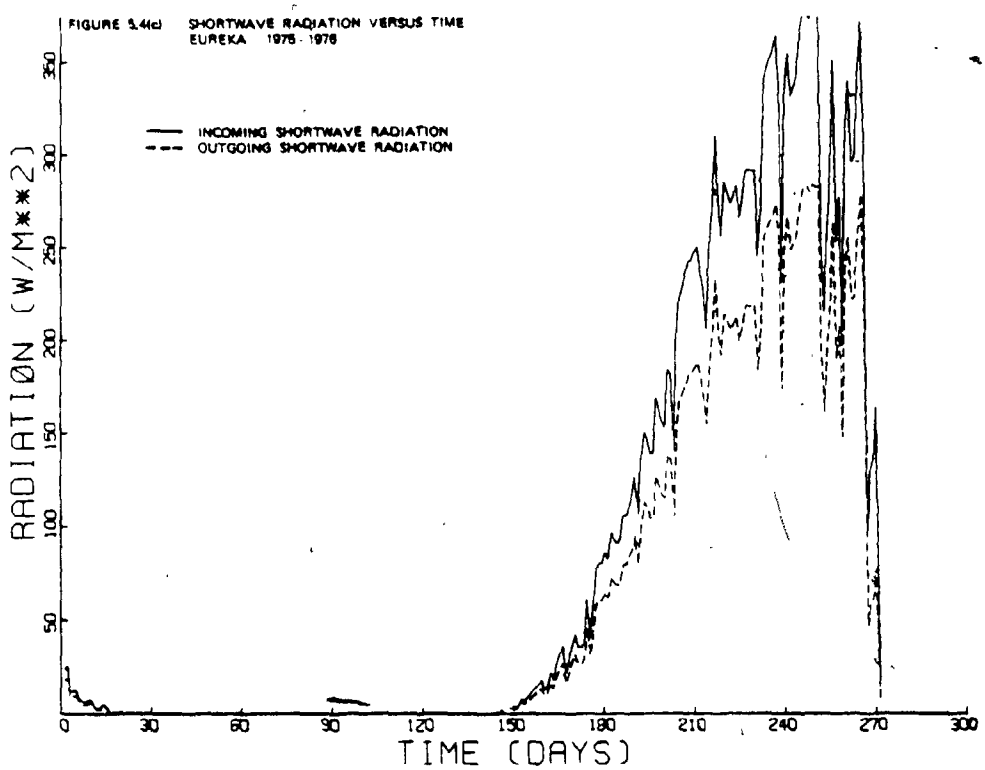
FIGURE 5.4(c) SHORTWAVE RADIATION VERSUS TIME
EUREKA 1975 - 1976
INCOMING SHORTWAVE RADIATION
OUTGOING SHORTWAVE RADIATION
RADIATIØN (W/M**2)
50
100
150
200
250
300
350
0
30
60
90
120
150
180
210
240
270
300
TIME (DAYS)

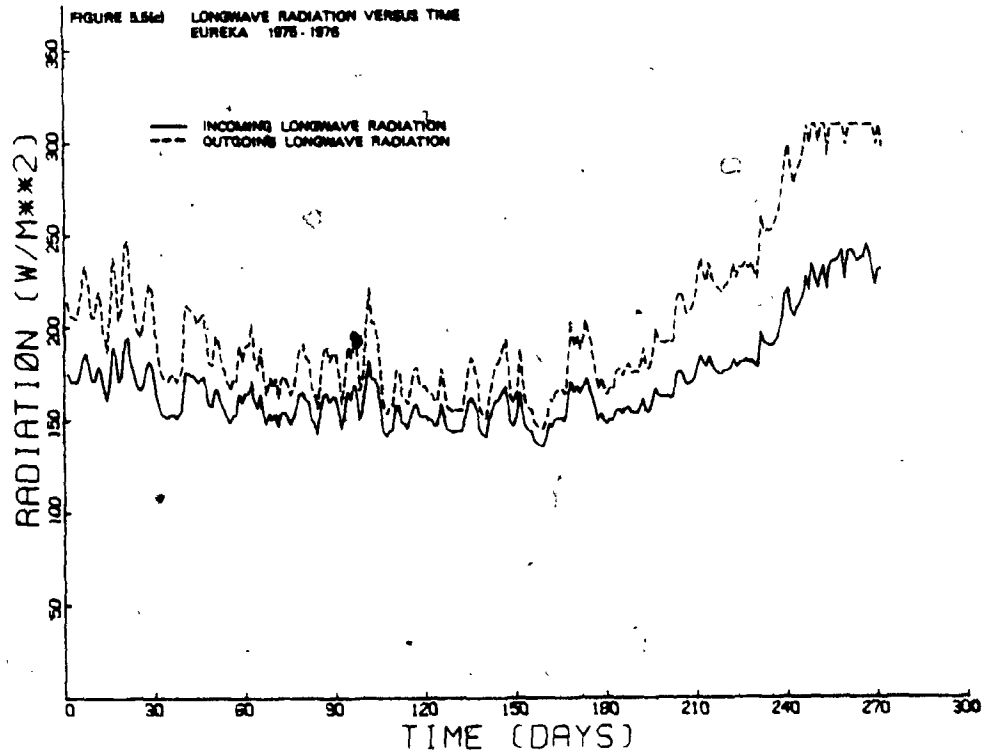
FIGURE 5.5(c) LONGWAVE RADIATION VERSUS TIME
EUREKA 1975 - 1976
INCOMING LONGWAVE RADIATION
OUTGOING LONGWAVE RADIATION
RADIATIØN (W/M**2)
50
100
150
200
250
300
350
0
30
60
90
120
150
180
210
240
270
300
TIME (DAYS)

FIGURE 5.6(c) ENERGY FLUXES VERSUS TIME
EUREKA 1975 1976

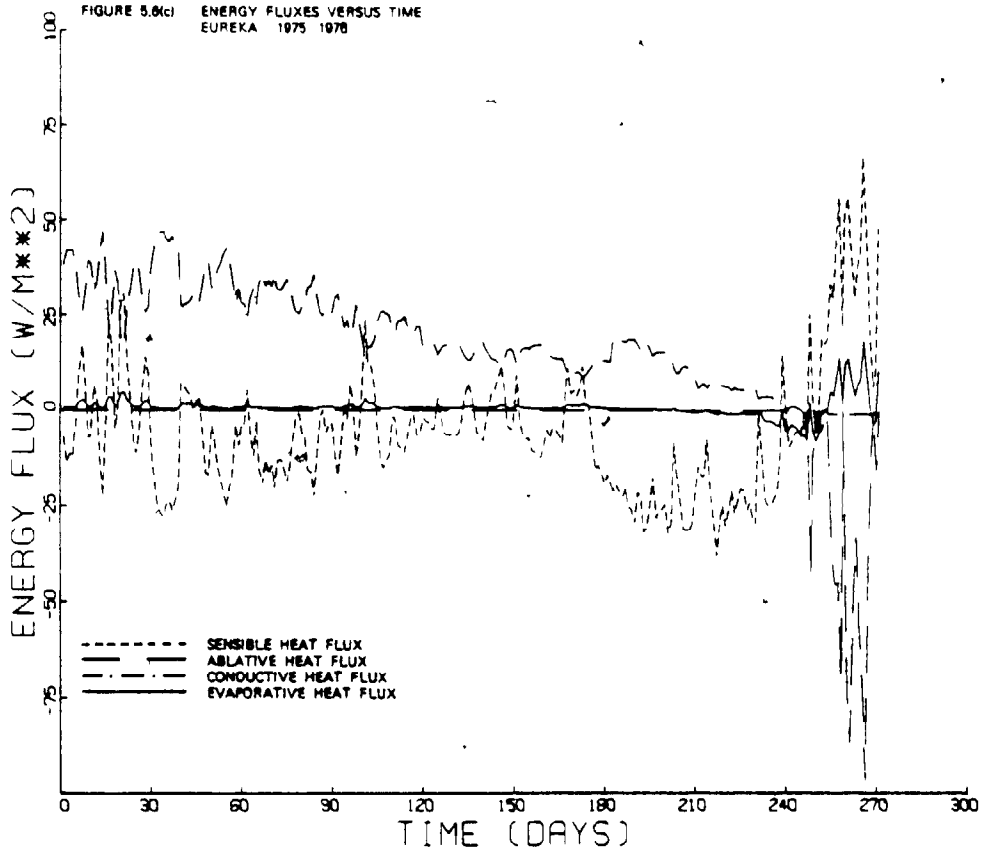

FIGURE 5.7(c) TEMPERATURES VERSUS TIME
EUREKA 1975 - 1976

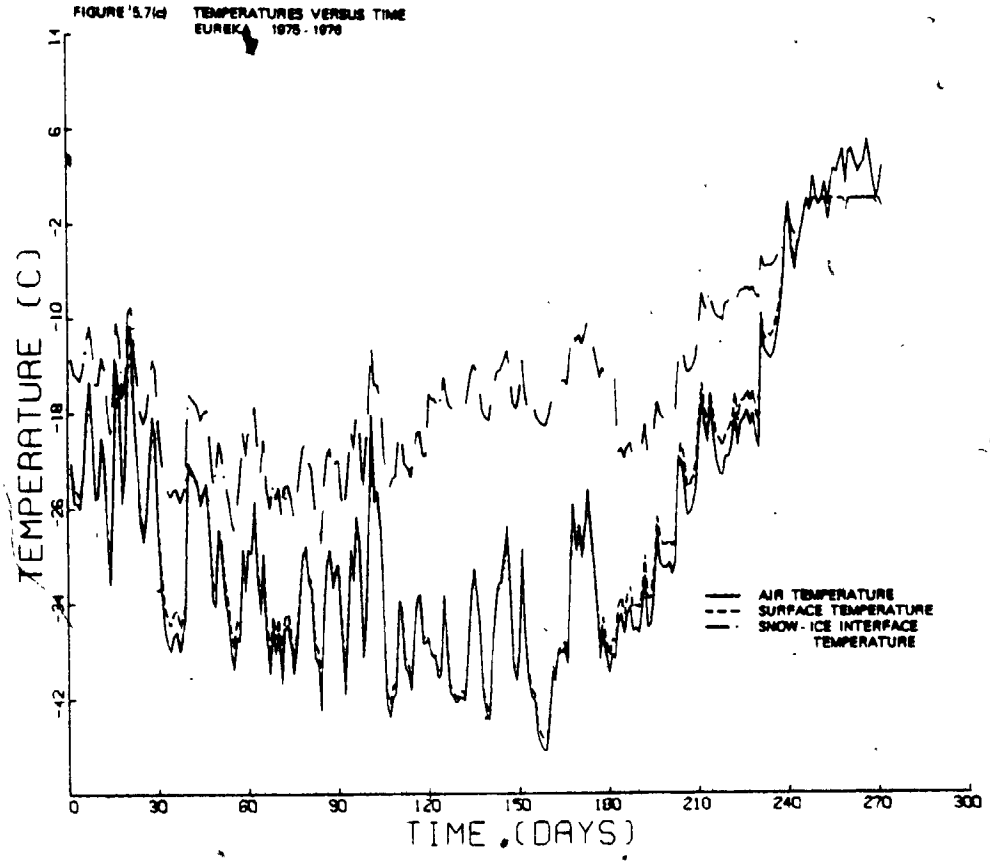

FIGURE 5.8(c) ICE SALINITY VERSUS TIME
EUREKA 1975 - 1976

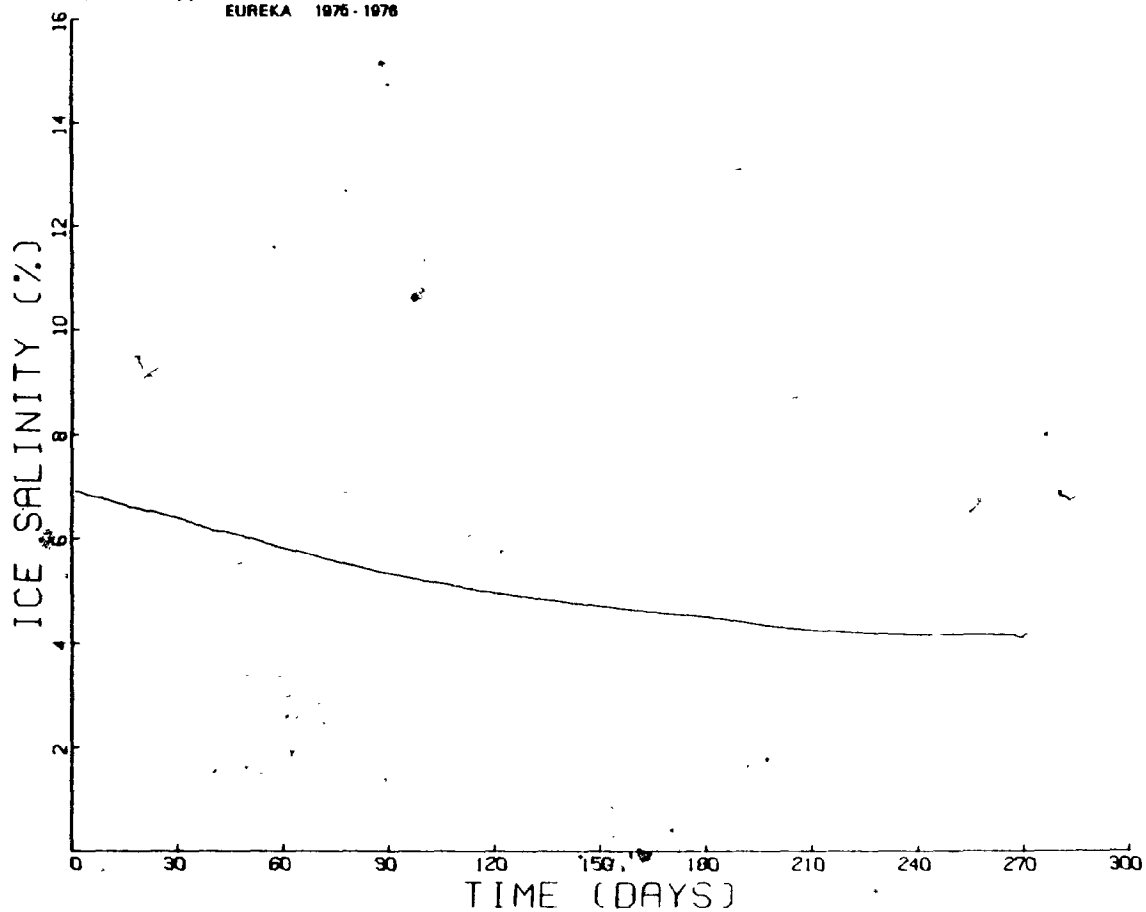

FIGURE 5.2(d) ICE THICKNESS VERSUS TIME
FROBISHER BAY 1973 - 1974

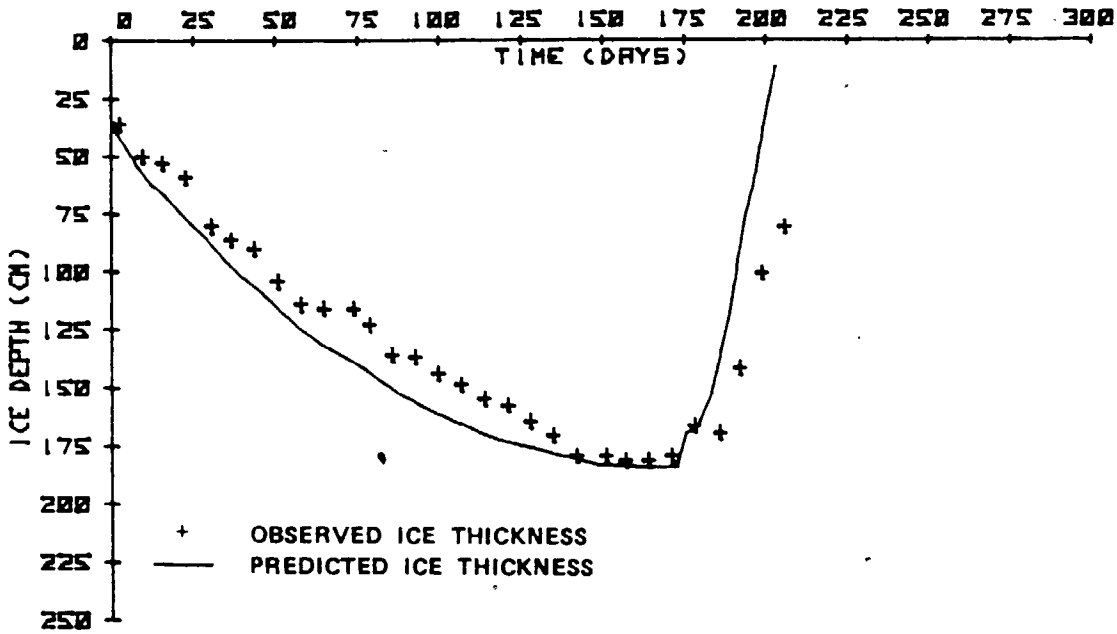

FIGURE 5.3(d) OBSERVED VERSUS PREDICTED ICE THICKNESS
FROBISHER BAY 1973 - 1974

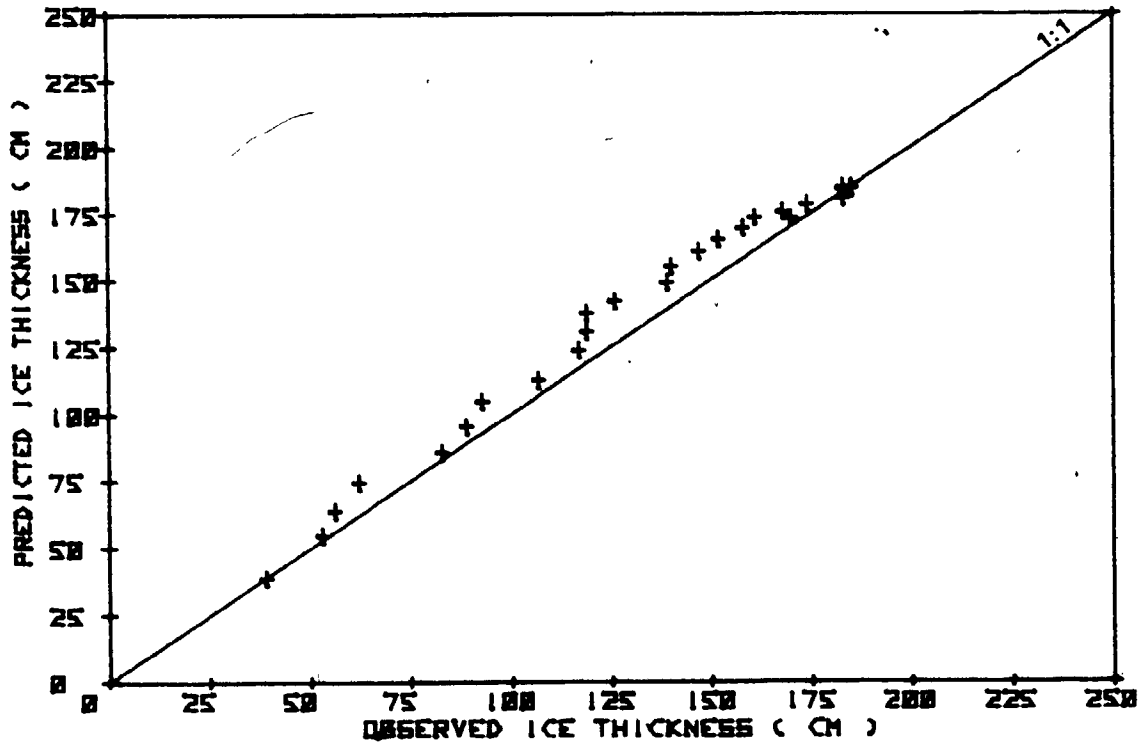

FIGURE 5.4(d) SHORTWAVE RADIATION VERSUS TIME
FROBISHER BAY 1973 - 1974

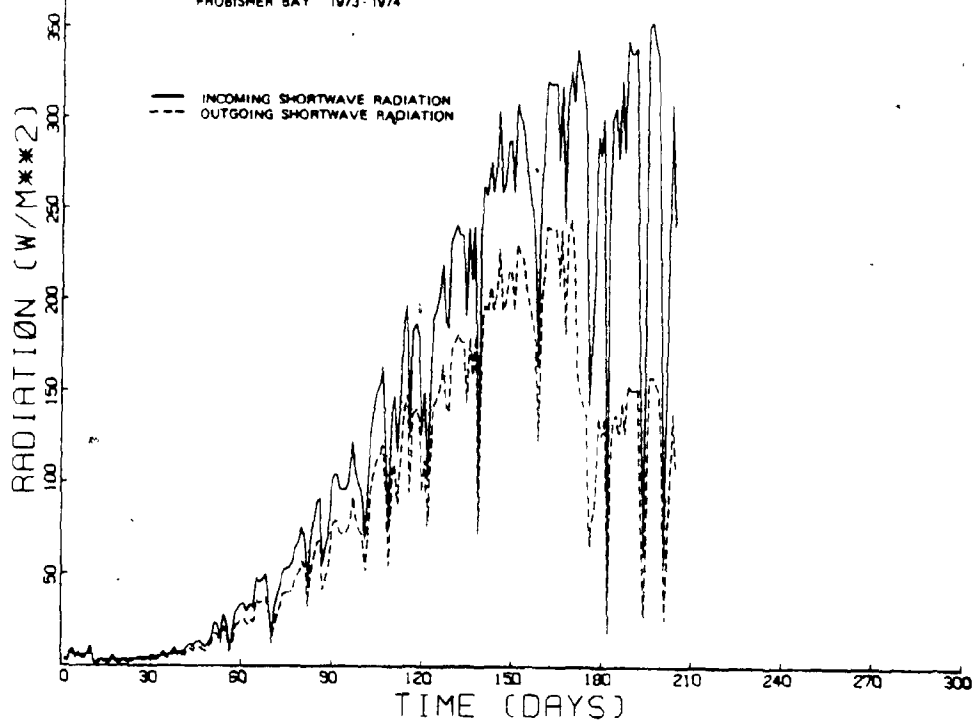

FIGURE 5.5(d) LONGWAVE RADIATION VERSUS TIME
FROBISHER BAY 1973 - 1974

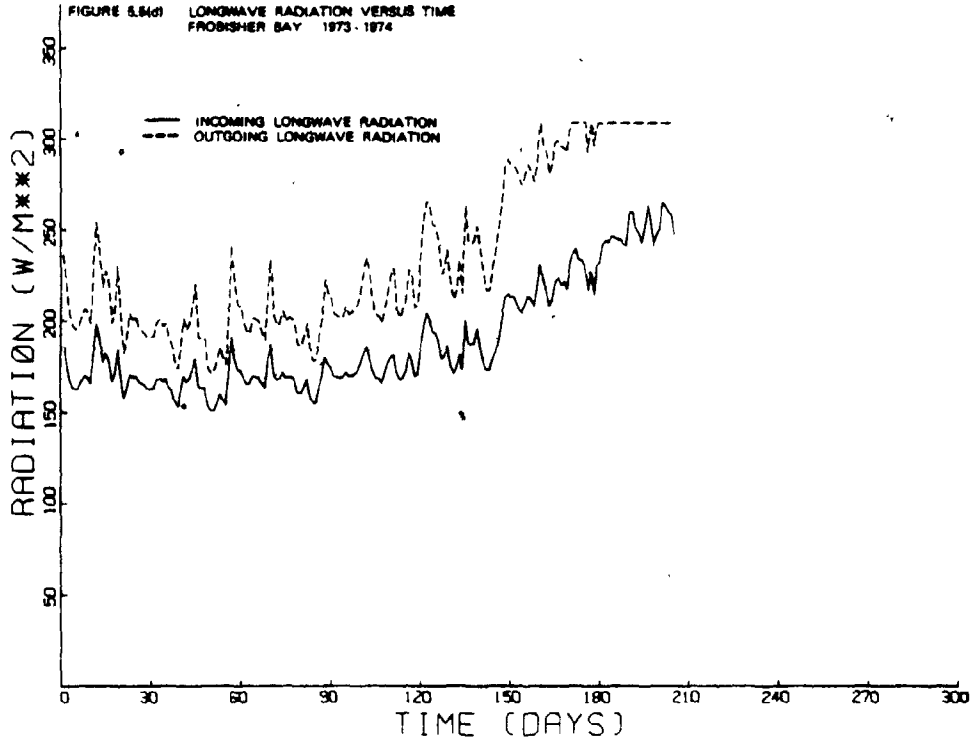

FIGURE 5.6(d) ENERGY FLUXES VERSUS TIME
FROBISHER BAY 1973 1974

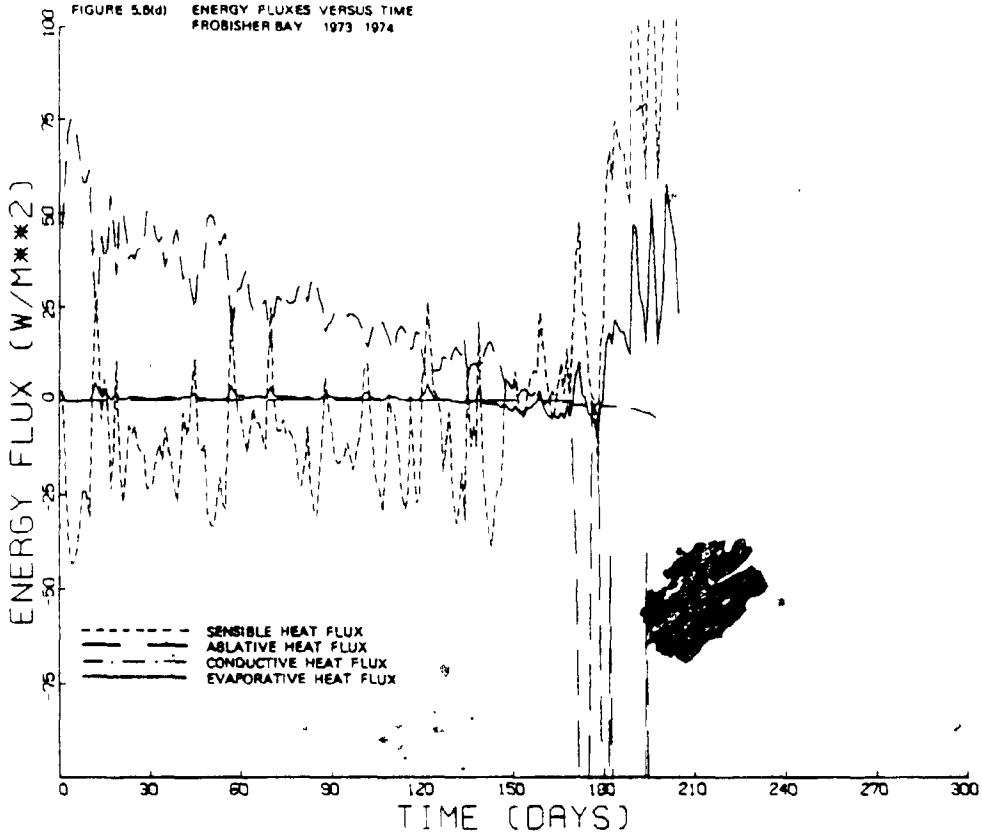

FIGURE 5.7(d) TEMPERATURES VERSUS TIME
FROBISHER BAY 1973 - 1974

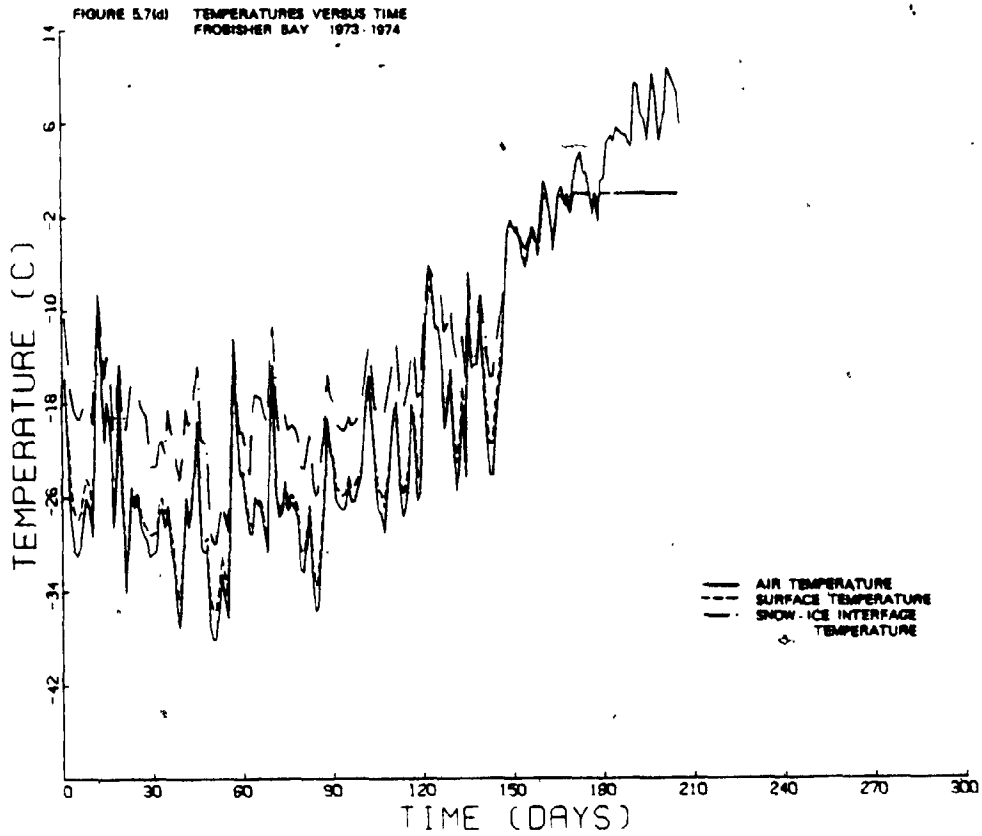

FIGURE 5.8(d) ICE SALINITY VERSUS TIME
FROBISHER BAY 1973 - 1974

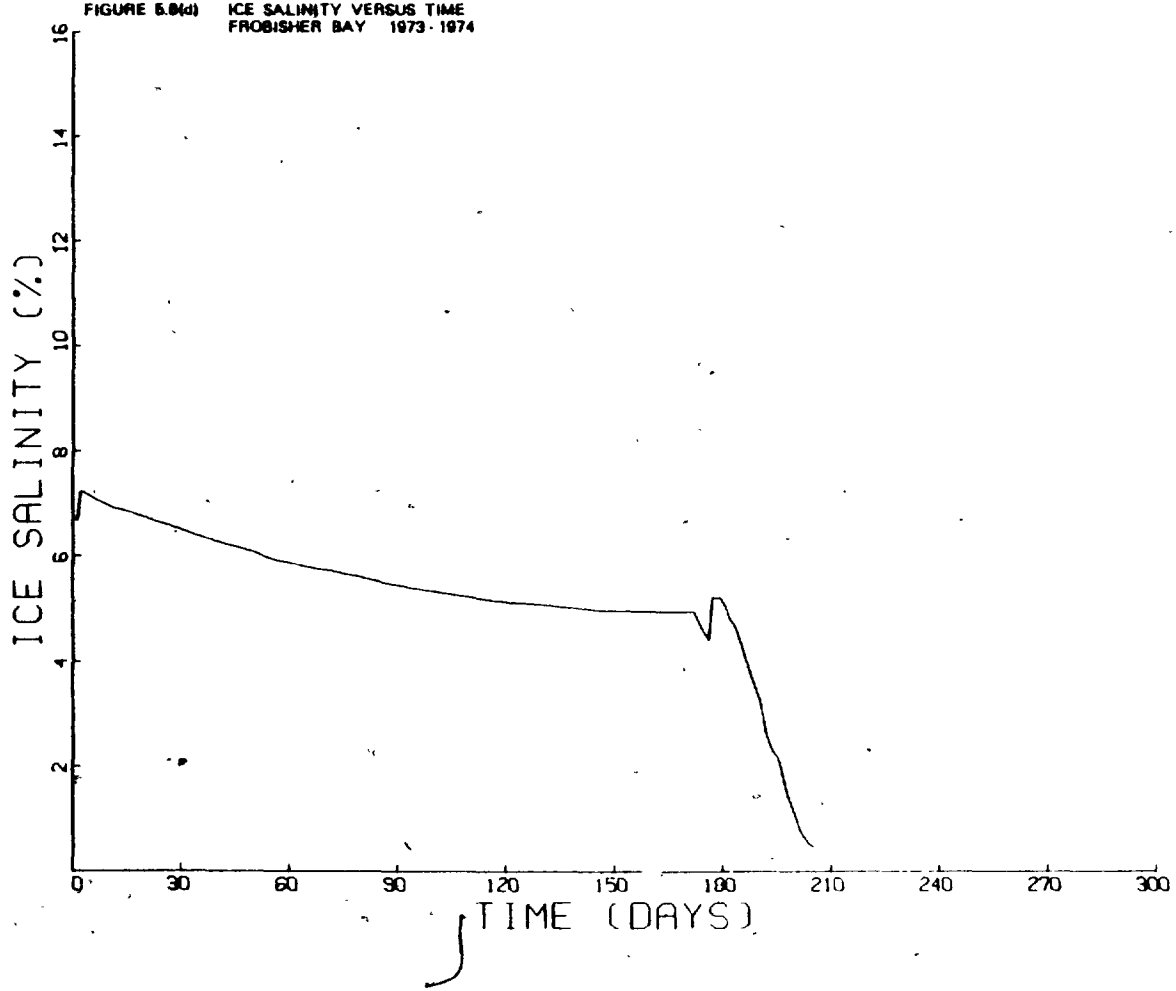

FIGURE 5.2(e) ICE THICKNESS VERSUS TIME
FROBISHER BAY 1974-1975

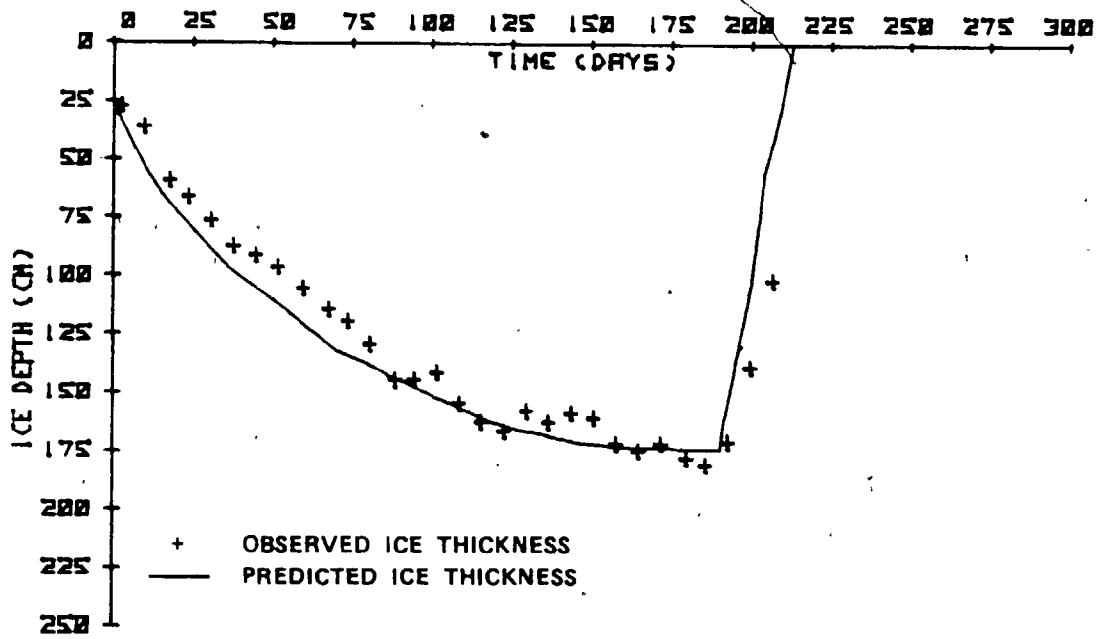

FIGURE 5.3(e) OBSERVED VERSUS PREDICTED ICE THICKNESS
FROBISHER BAY 1974-1975

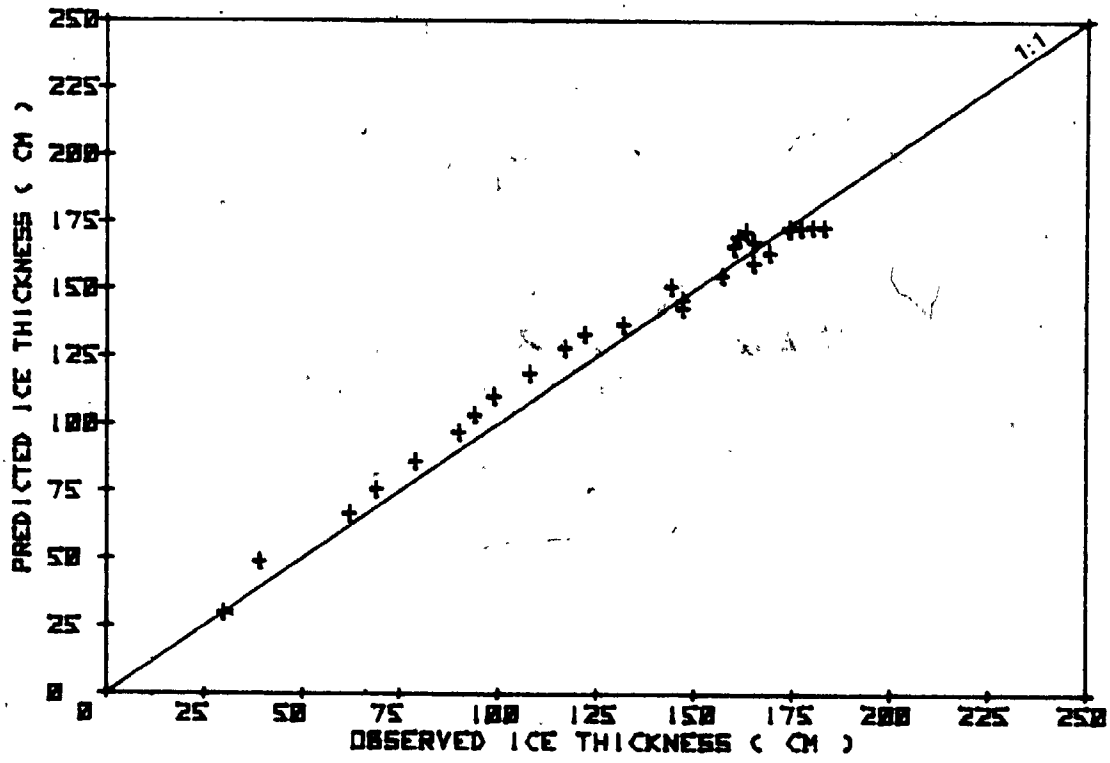

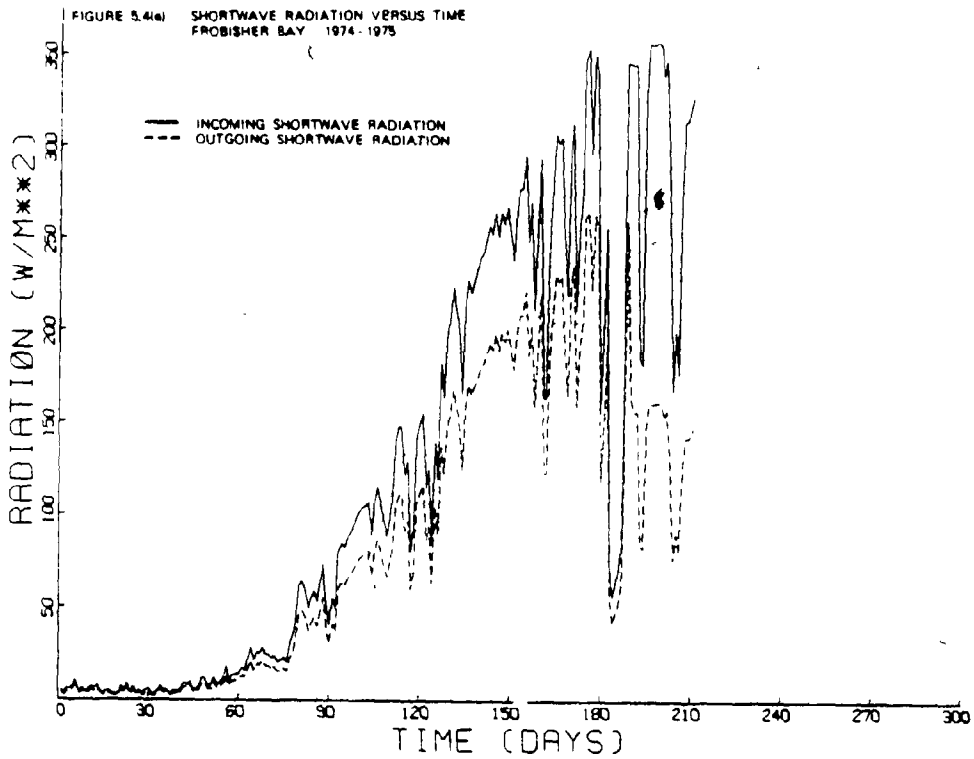
FIGURE 5.4(a) SHORTWAVE RADIATION VERSUS TIME
FROBISHER BAY 1974 - 1975
INCOMING SHORTWAVE RADIATION
OUTGOING SHORTWAVE RADIATION
RADIATIØN (W/M**2)
50
100
150
200
250
300
350
0
30
60
90
120
150
180
210
240
270
300
TIME (DAYS)

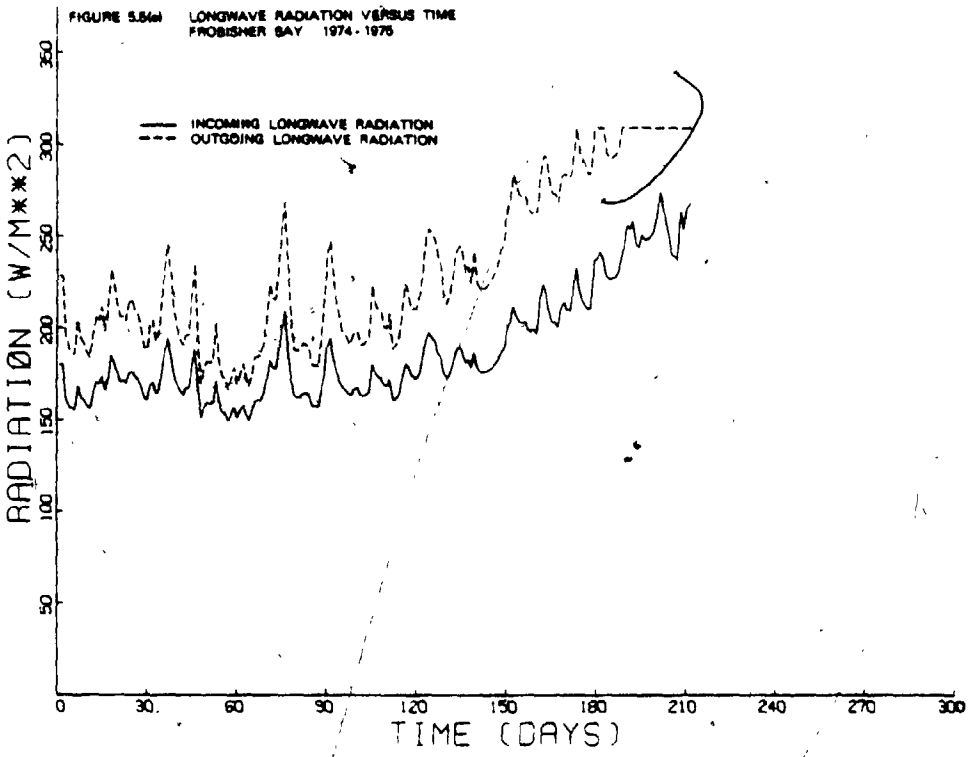
FIGURE 5.5(a) LONGWAVE RADIATION VERSUS TIME
FROBISHER BAY 1974 - 1975
INCOMING LONGWAVE RADIATION
OUTGOING LONGWAVE RADIATION
RADIATIØN (W/M**2)
50
100
150
200
250
300
350
0
30
60
90
120
150
180
210
240
270
300
TIME (DAYS)

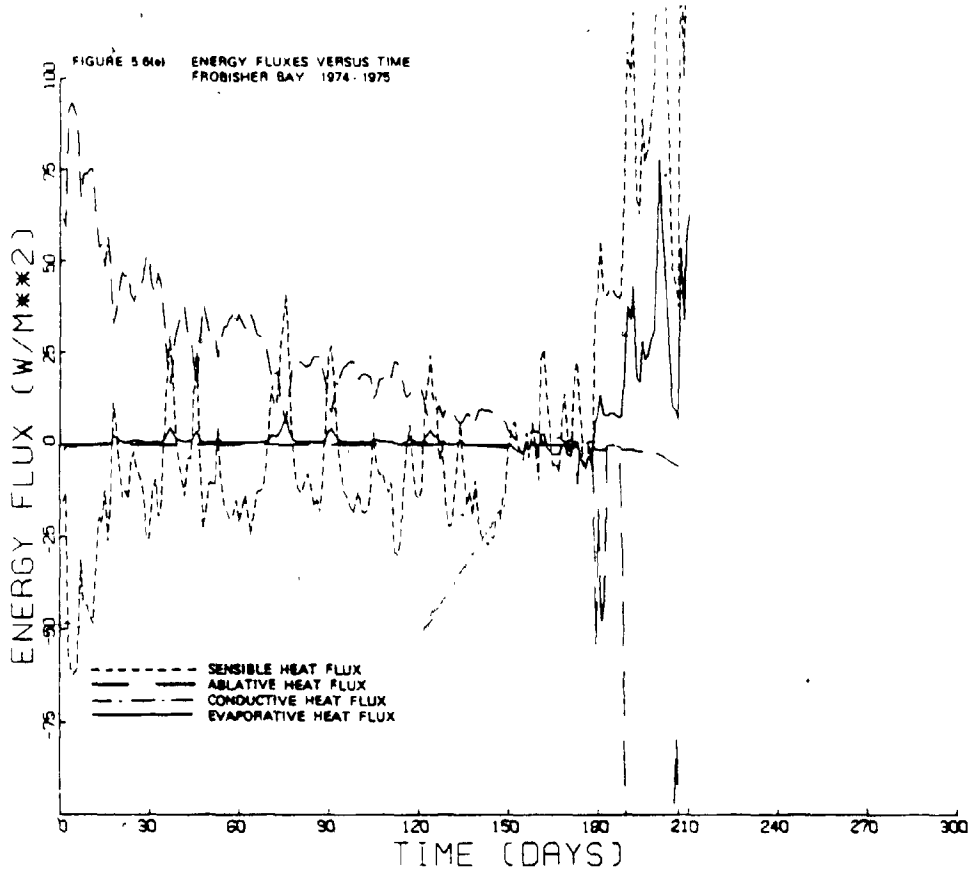
FIGURE 5.6(a) ENERGY FLUXES VERSUS TIME
FROBISHER BAY 1974 - 1975
ENERGY FLUX (W/M**2)
100
75
50
25
0
-25
-50
-75
SENSIBLE HEAT FLUX
ABLATIVE HEAT FLUX
CONDUCTIVE HEAT FLUX
EVAPORATIVE HEAT FLUX
0
30
60
90
120
150
180
210
240
270
300
TIME (DAYS)

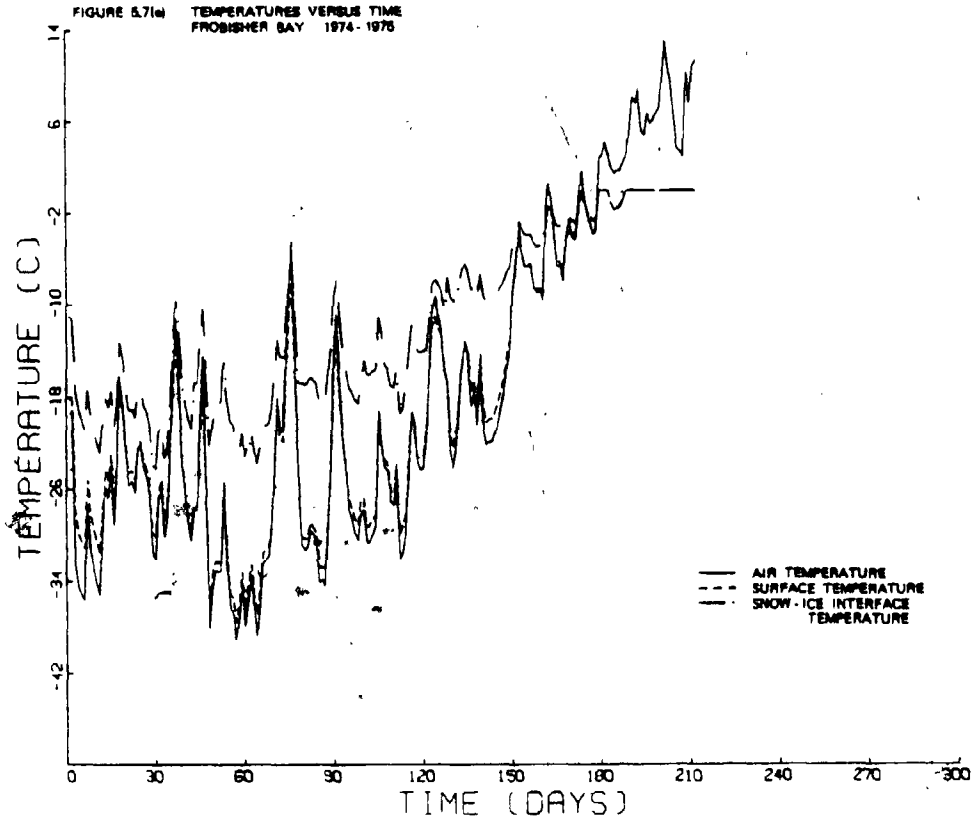
FIGURE 5.7(a) TEMPERATURES VERSUS TIME
FROBISHER BAY 1974 - 1975
TEMPERATURE (C)
14
6
-2
-10
-18
-26
-34
-42
AIR TEMPERATURE
SURFACE TEMPERATURE
SNOW - ICE INTERFACE TEMPERATURE
0
30
60
90
120
150
180
210
240
270
300
TIME (DAYS)

FIGURE 5.8(a) ICE SALINITY VERSUS TIME
FROBISHER BAY 1974 - 1976

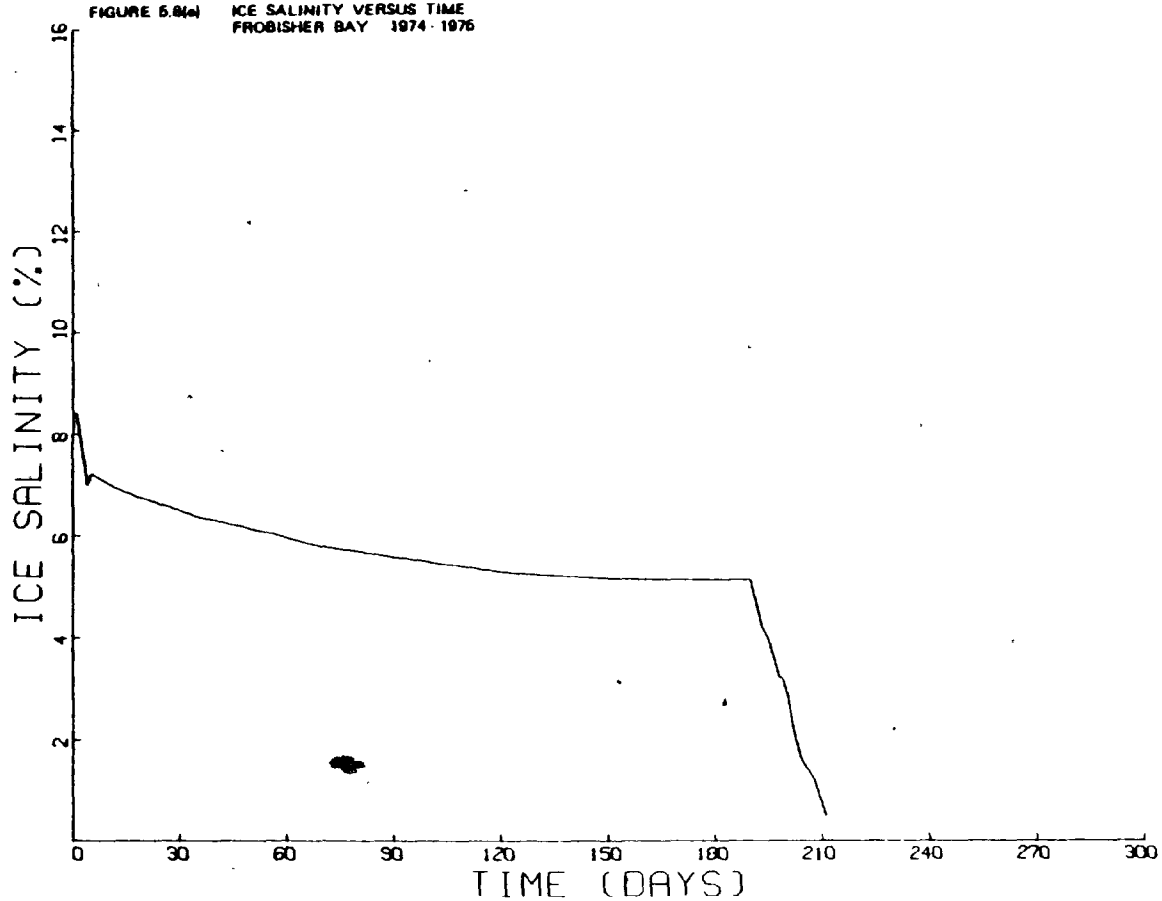

FIGURE 5.2(f) ICE THICKNESS VERSUS TIME
FROBISHER BAY 1975 - 1976

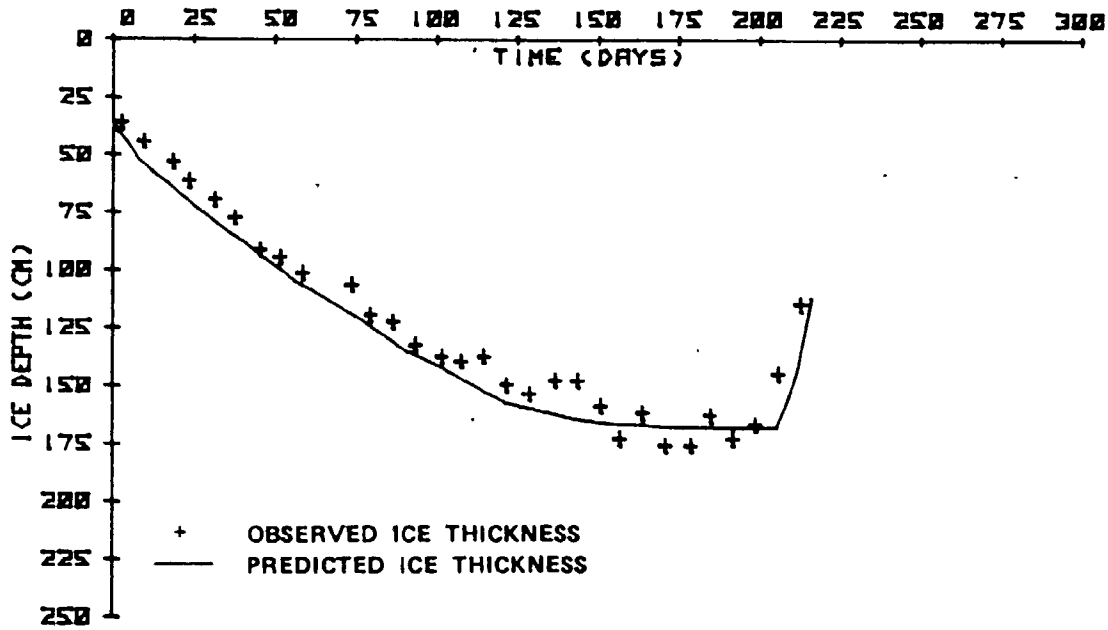

FIGURE 5.3(f) OBSERVED VERSUS PREDICTED ICE THICKNESS
FROBISHER BAY 1975 - 1976

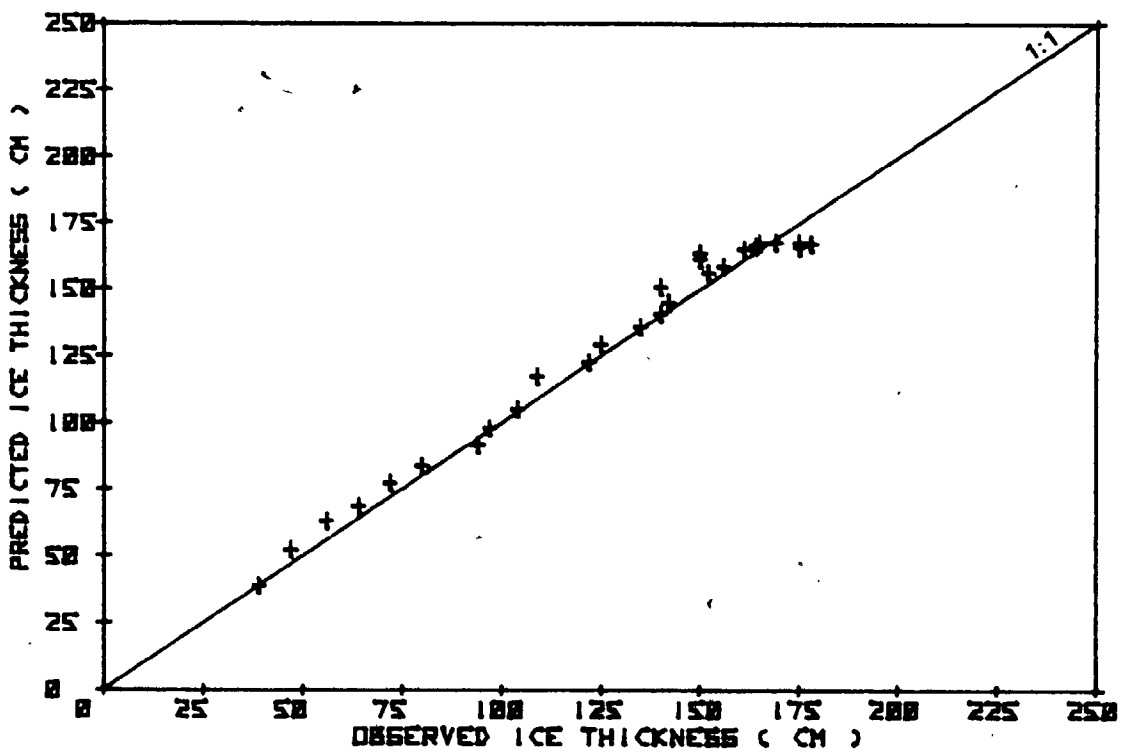

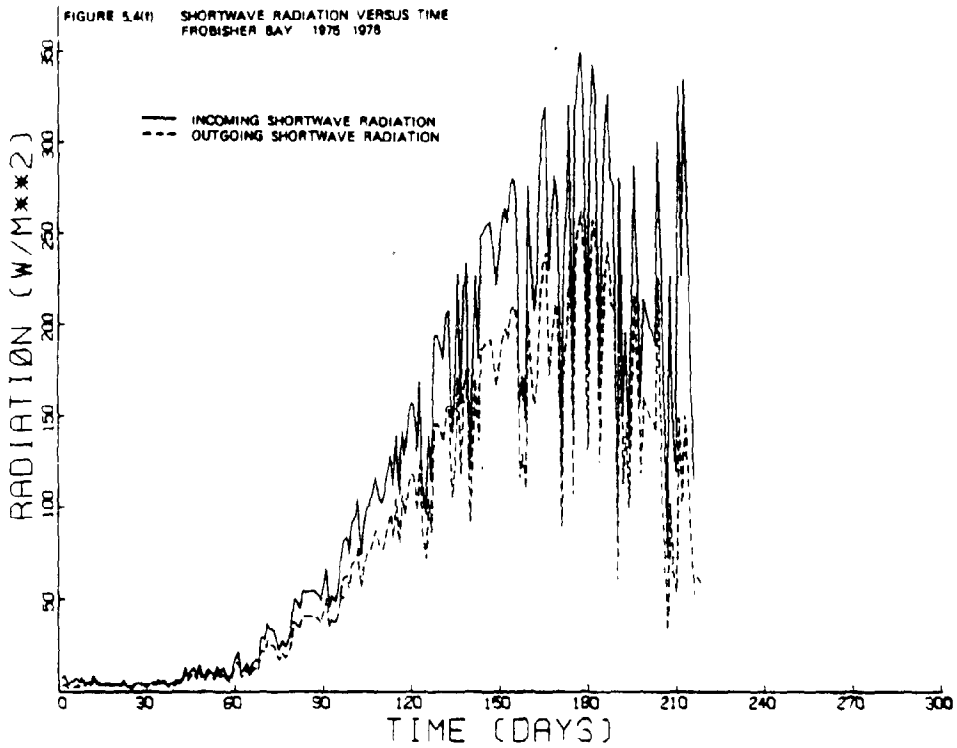
FIGURE 5.4(1) SHORTWAVE RADIATION VERSUS TIME
FROBISHER BAY 1975 1976
INCOMING SHORTWAVE RADIATION
OUTGOING SHORTWAVE RADIATION
RADIATIØN (W/M**2)
TIME (DAYS)

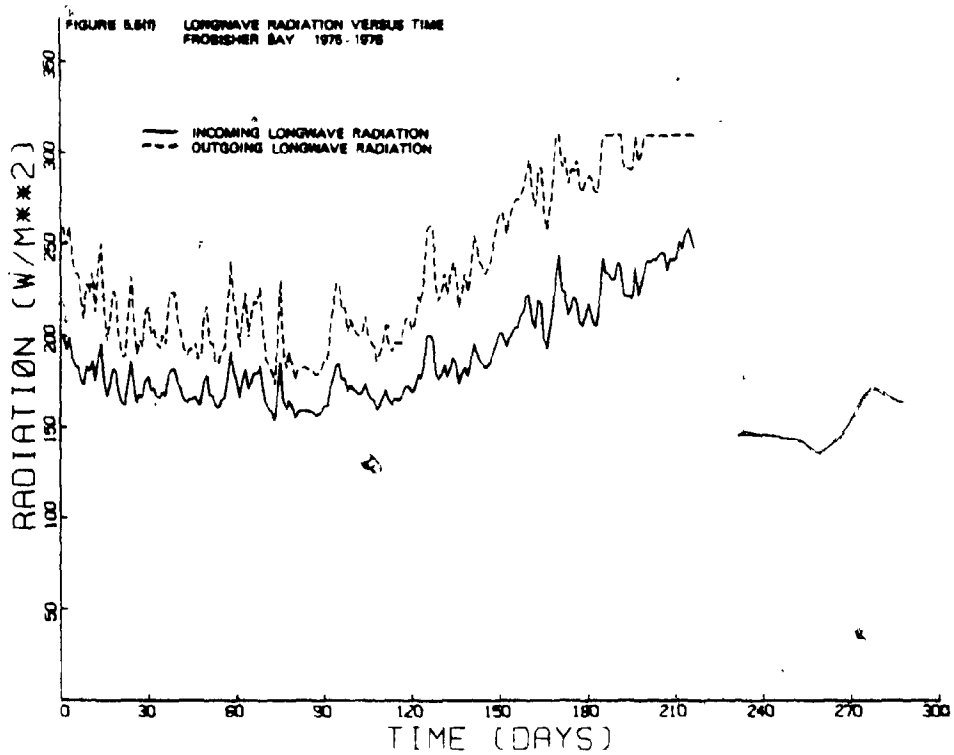
FIGURE 5.5(1) LONGWAVE RADIATION VERSUS TIME
FROBISHER BAY 1975 - 1976
INCOMING LONGWAVE RADIATION
OUTGOING LONGWAVE RADIATION
RADIATIØN (W/M**2)
TIME (DAYS)

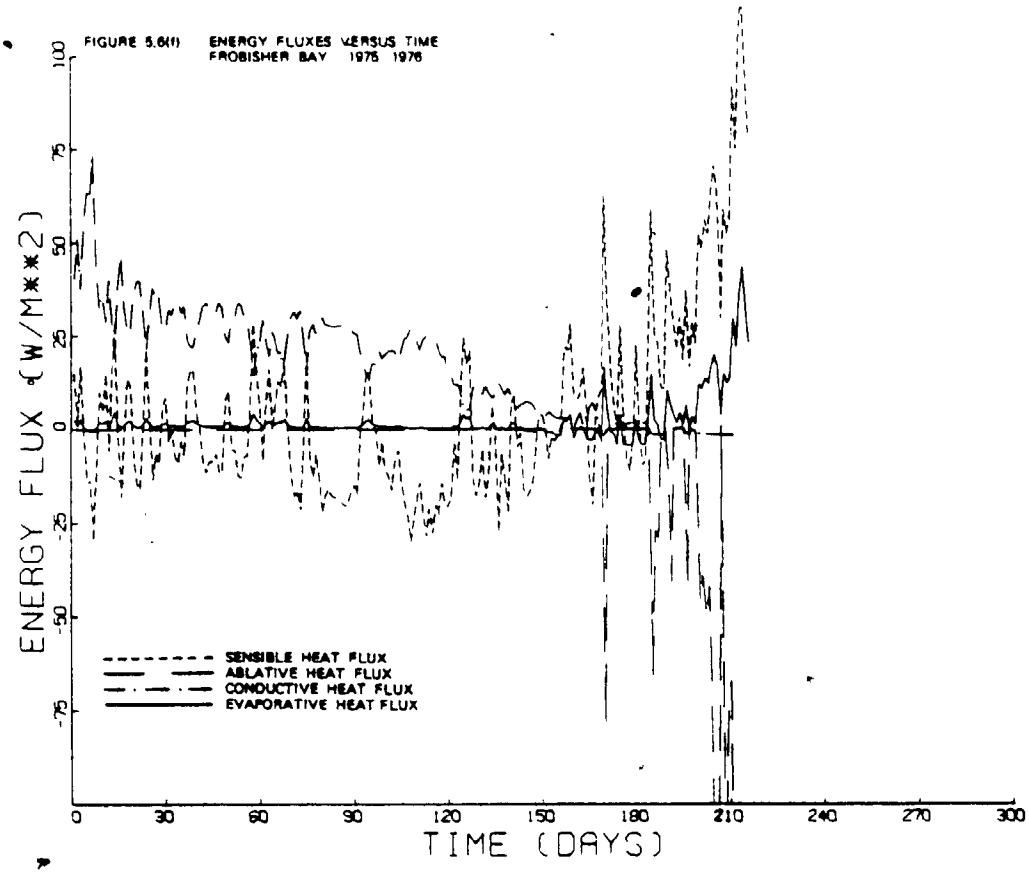
FIGURE 5.6(i) ENERGY FLUXES VERSUS TIME
FROBISHER BAY 1975 1976
ENERGY FLUX (W/M**2)
100
75
50
25
0
-25
-50
-75
SENSIBLE HEAT FLUX
ABLATIVE HEAT FLUX
CONDUCTIVE HEAT FLUX
EVAPORATIVE HEAT FLUX
0
30
60
90
120
150
180
210
240
270
300
TIME (DAYS)

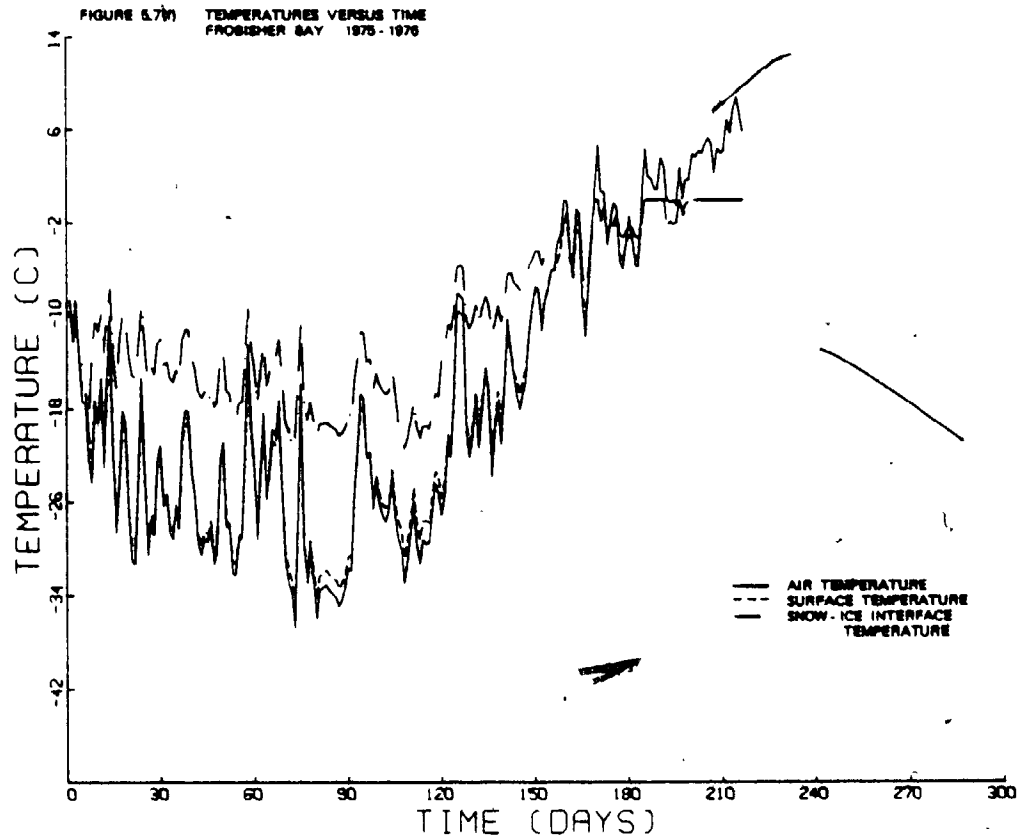
FIGURE 5.7(i) TEMPERATURES VERSUS TIME
FROBISHER BAY 1975 - 1976
TEMPERATURE (C)
14
6
-2
-10
-18
-26
-34
-42
AIR TEMPERATURE
SURFACE TEMPERATURE
SNOW - ICE INTERFACE TEMPERATURE
0
30
60
90
120
150
180
210
240
270
300
TIME (DAYS)

FIGURE 5.8(f) ICE SALINITY VERSUS TIME
FROBISHER BAY 1975 - 1976

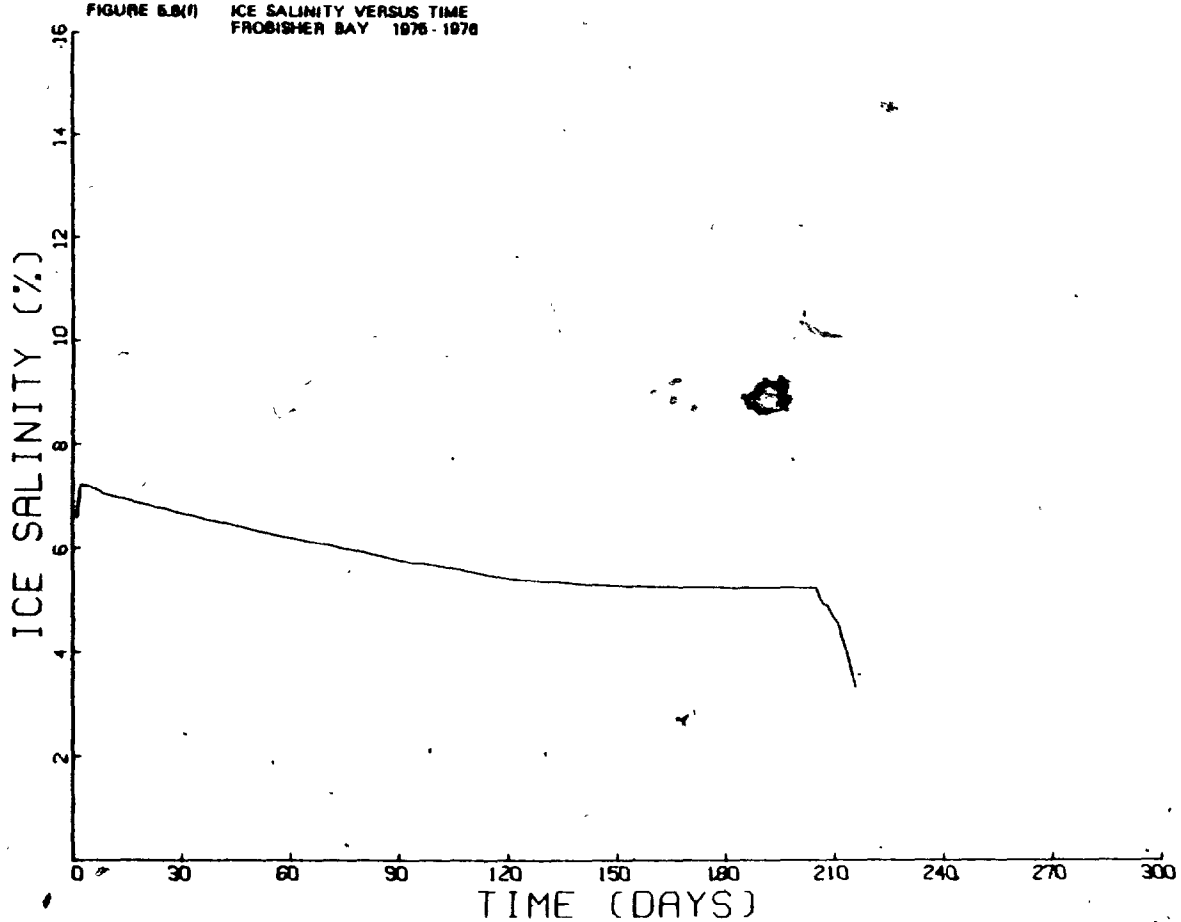

FIGURE 5.2(g) ICE THICKNESS VERSUS TIME
RESOLUTE 1973 - 1974

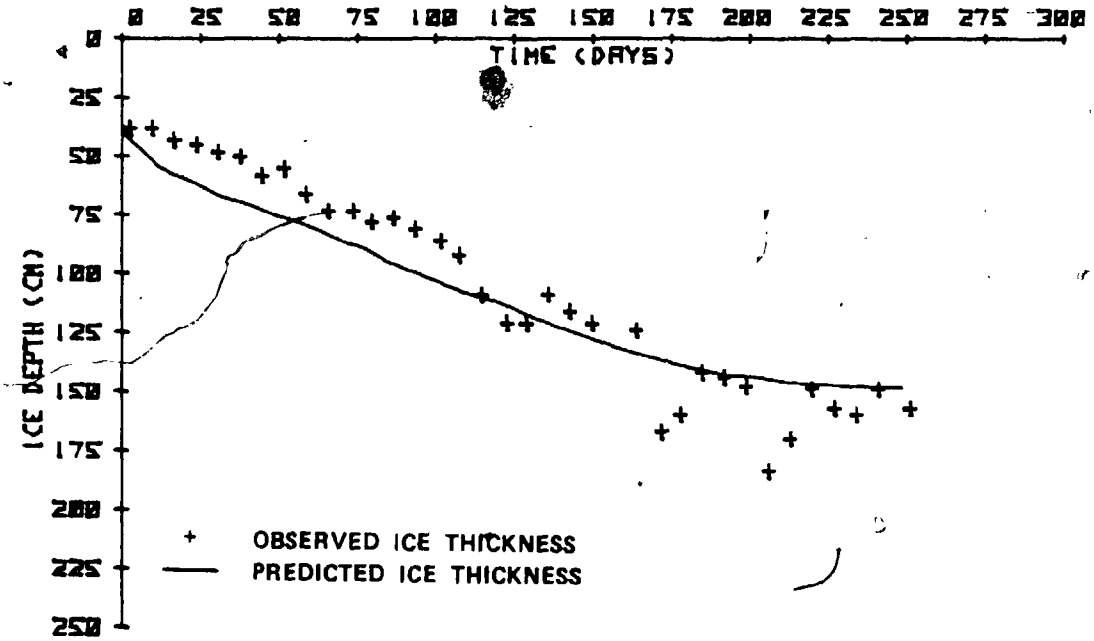

FIGURE 5.3(g) OBSERVED VERSUS PREDICTED ICE THICKNESS
RESOLUTE 1973 - 1974

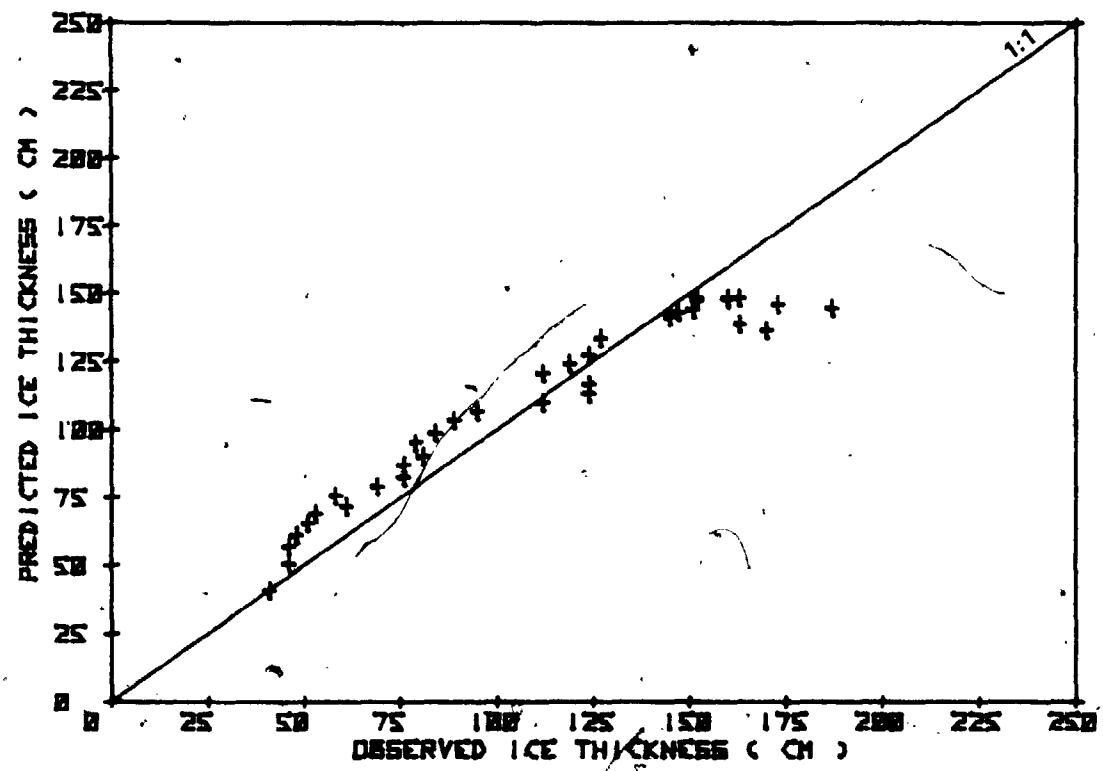

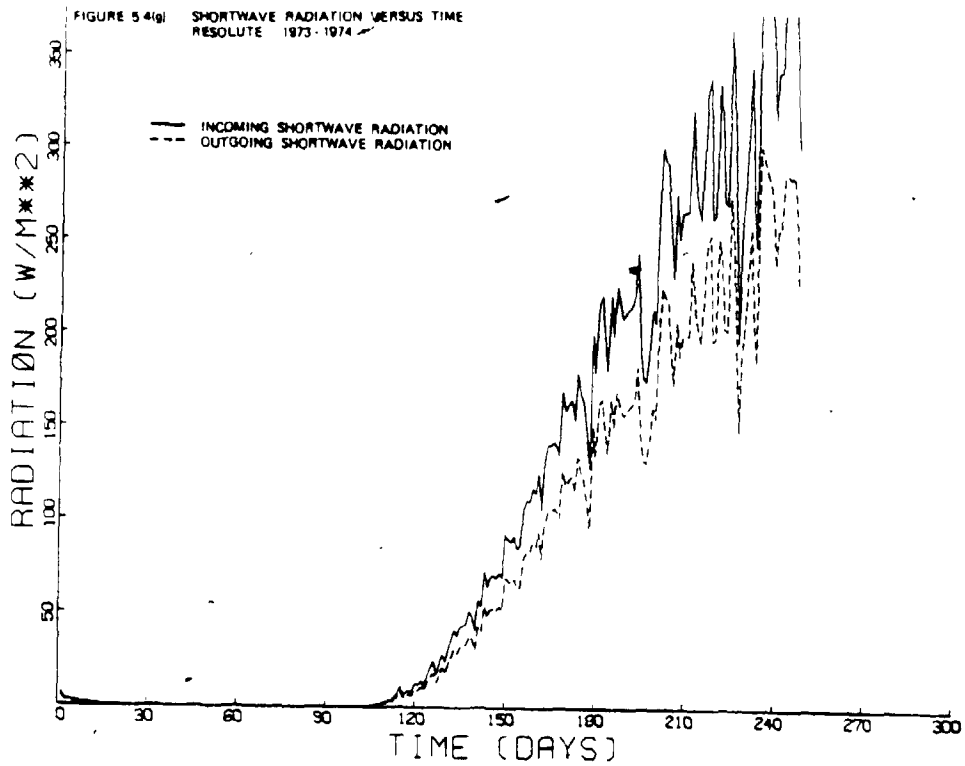
FIGURE 5.4(g) SHORTWAVE RADIATION VERSUS TIME
RESOLUTE 1973 - 1974
INCOMING SHORTWAVE RADIATION
OUTGOING SHORTWAVE RADIATION
RADIATIØN (W/M**2)
50
100
150
200
250
300
350
0
30
60
90
120
150
180
210
240
270
300
TIME (DAYS)

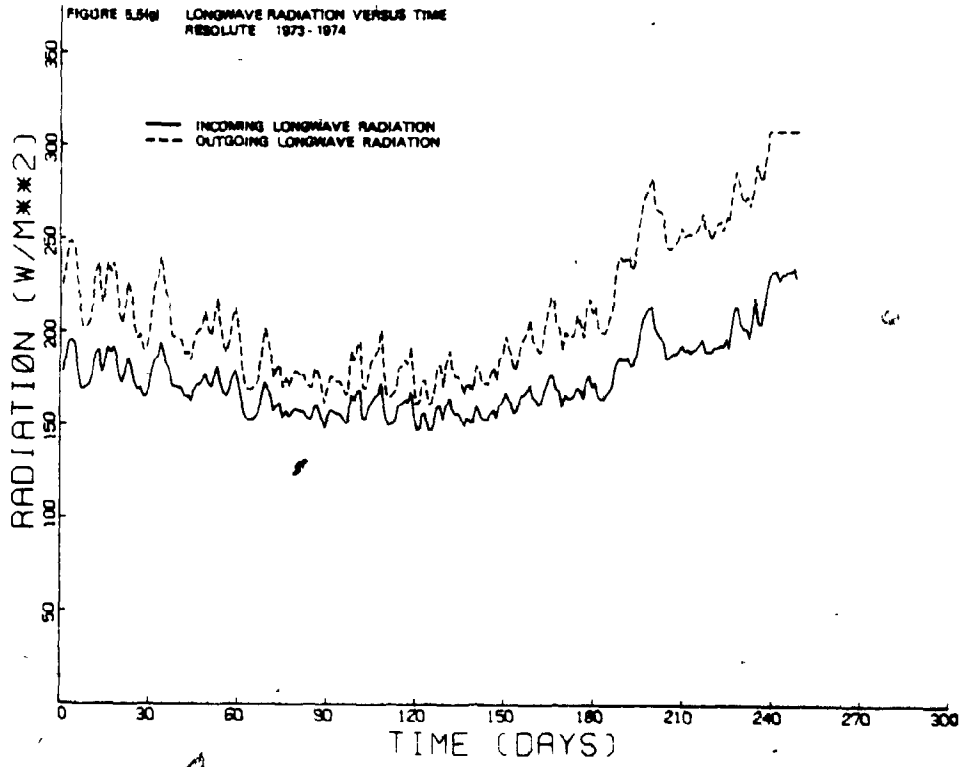
FIGURE 5.5(g) LONGWAVE RADIATION VERSUS TIME
RESOLUTE 1973 - 1974
INCOMING LONGWAVE RADIATION
OUTGOING LONGWAVE RADIATION
RADIATIØN (W/M**2)
50
100
150
200
250
300
350
0
30
60
90
120
150
180
210
240
270
300
TIME (DAYS)

FIGURE 5.6(g) ENERGY FLUXES VERSUS TIME
RESOLUTE 1973 1974

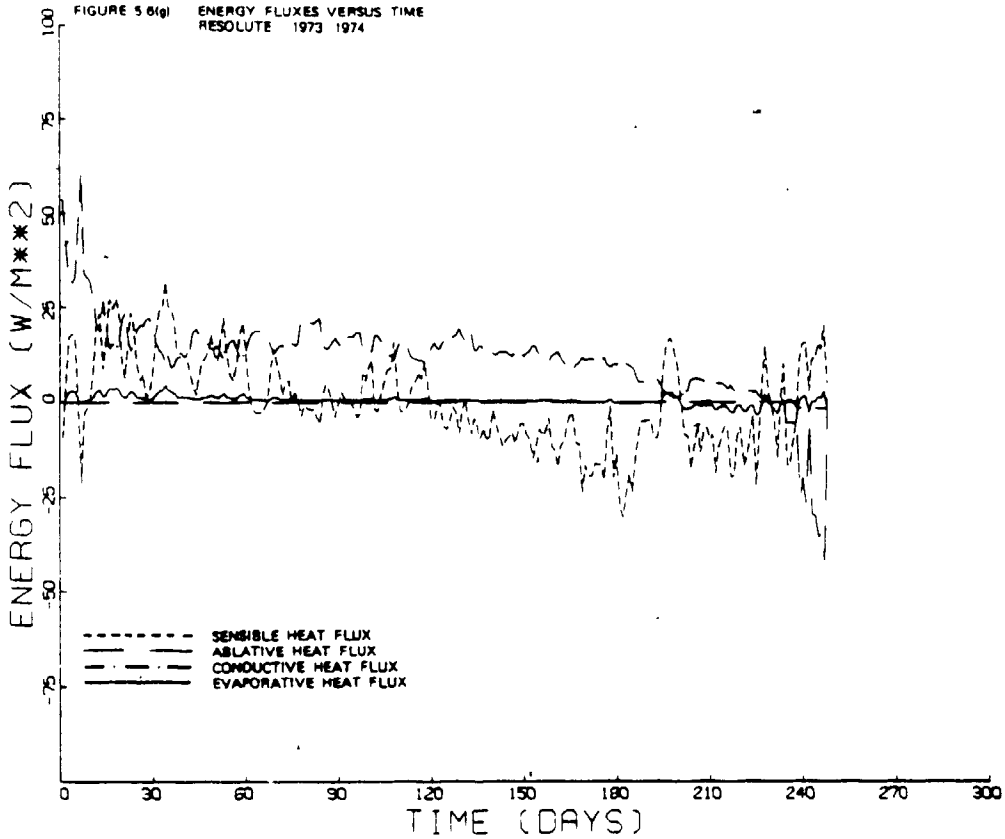

FIGURE 5.7(g) TEMPERATURES VERSUS TIME
RESOLUTE 1973 - 1974

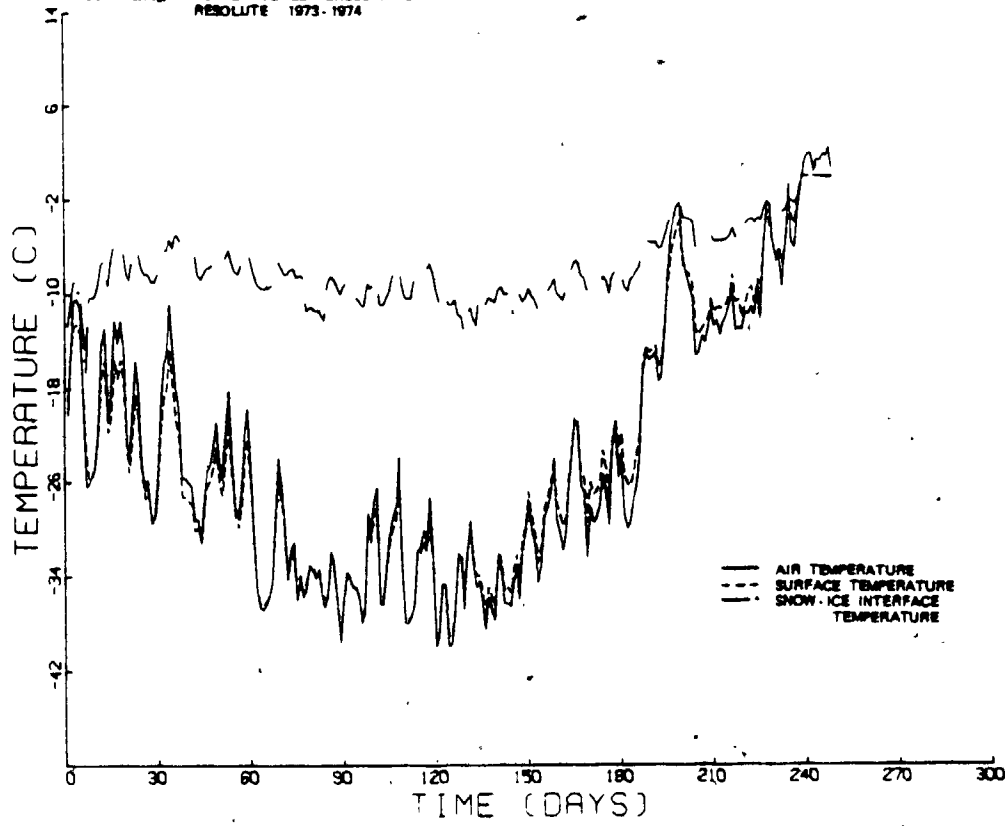

FIGURE 6.34(a) ICE SALINITY VERSUS TIME
RESOLUTE 1973 - 1974

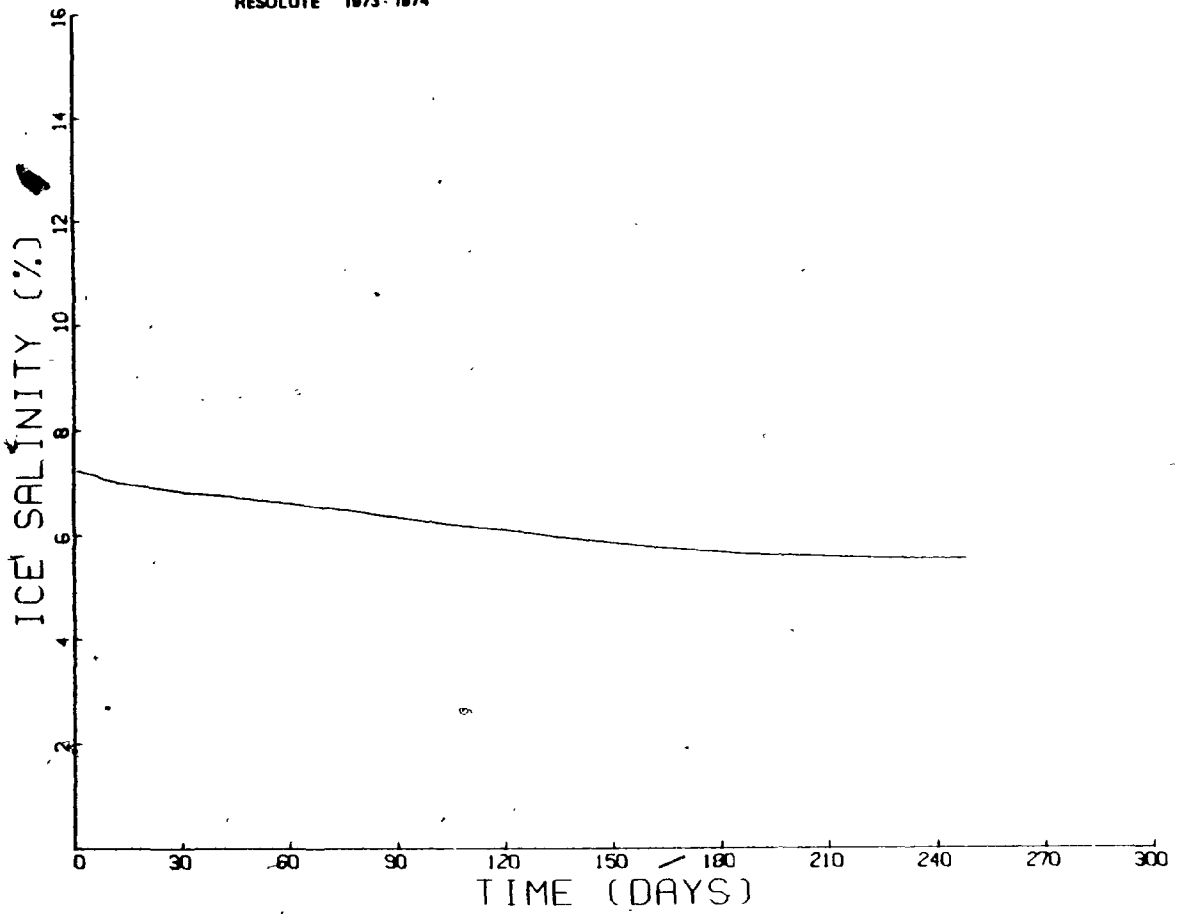

FIGURE 5.2(h) ICE THICKNESS VERSUS TIME
RESOLUTE 1974 - 1975

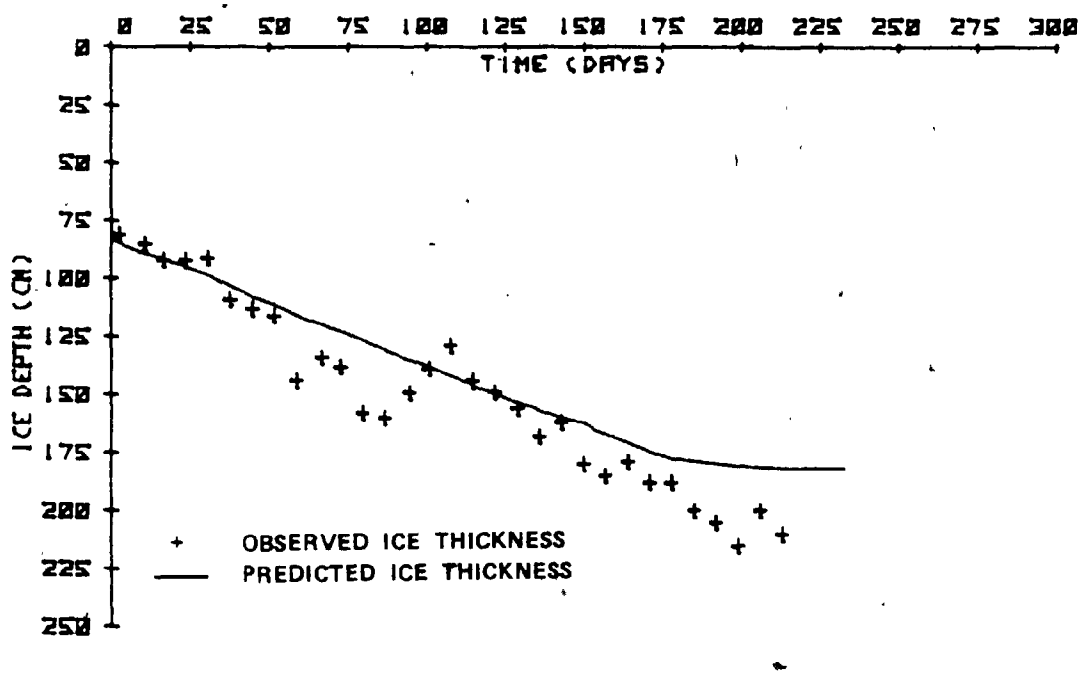

FIGURE 5.3(h) OBSERVED VERSUS PREDICTED ICE THICKNESS
RESOLUTE 1974 - 1975

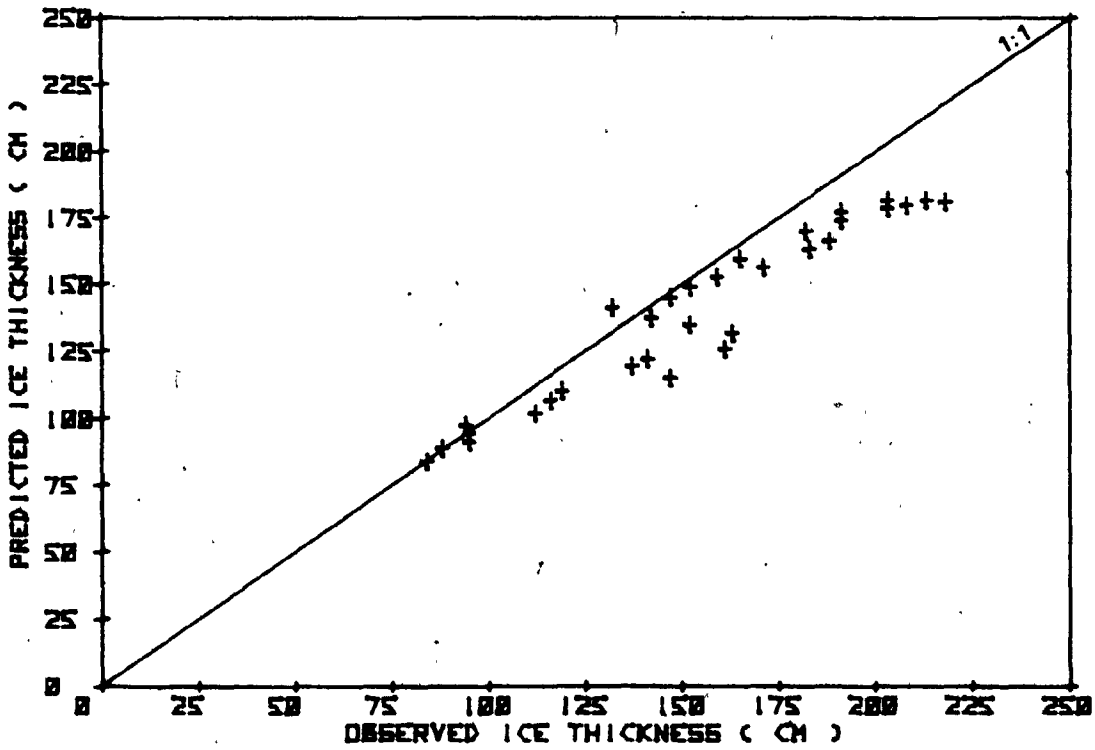

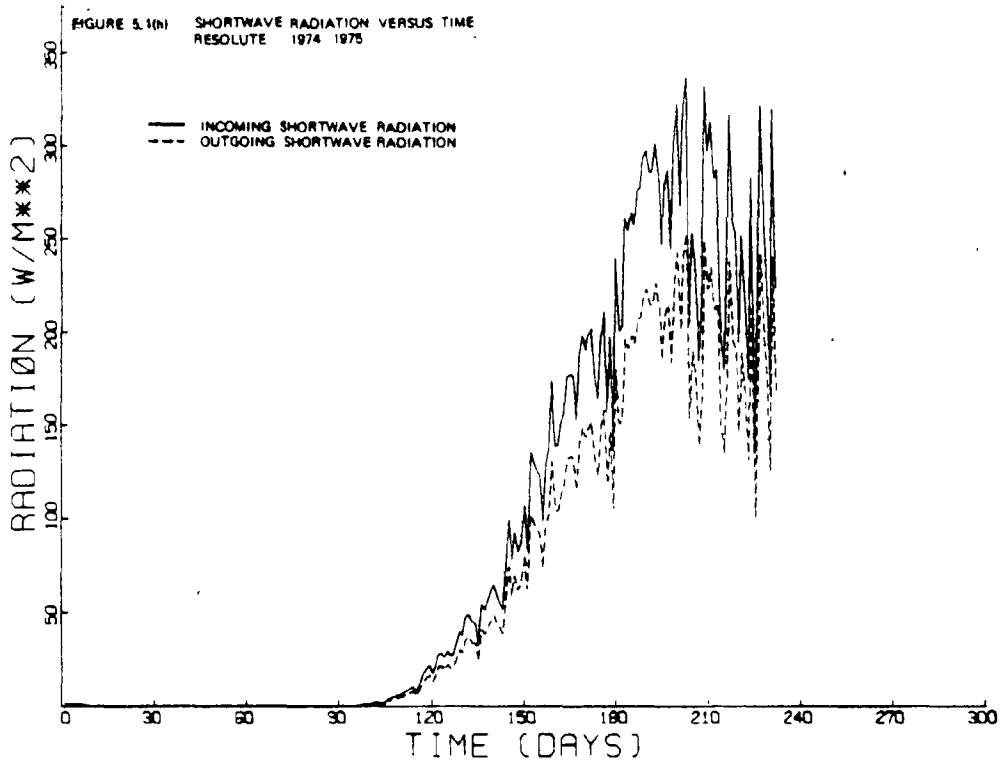
FIGURE 5.1(h) SHORTWAVE RADIATION VERSUS TIME
RESOLUTE 1974 1975
INCOMING SHORTWAVE RADIATION
OUTGOING SHORTWAVE RADIATION
RADIATION (W/M**2)
TIME (DAYS)
0
30
60
90
120
150
180
210
240
270
300
50
100
150
200
250
300
350

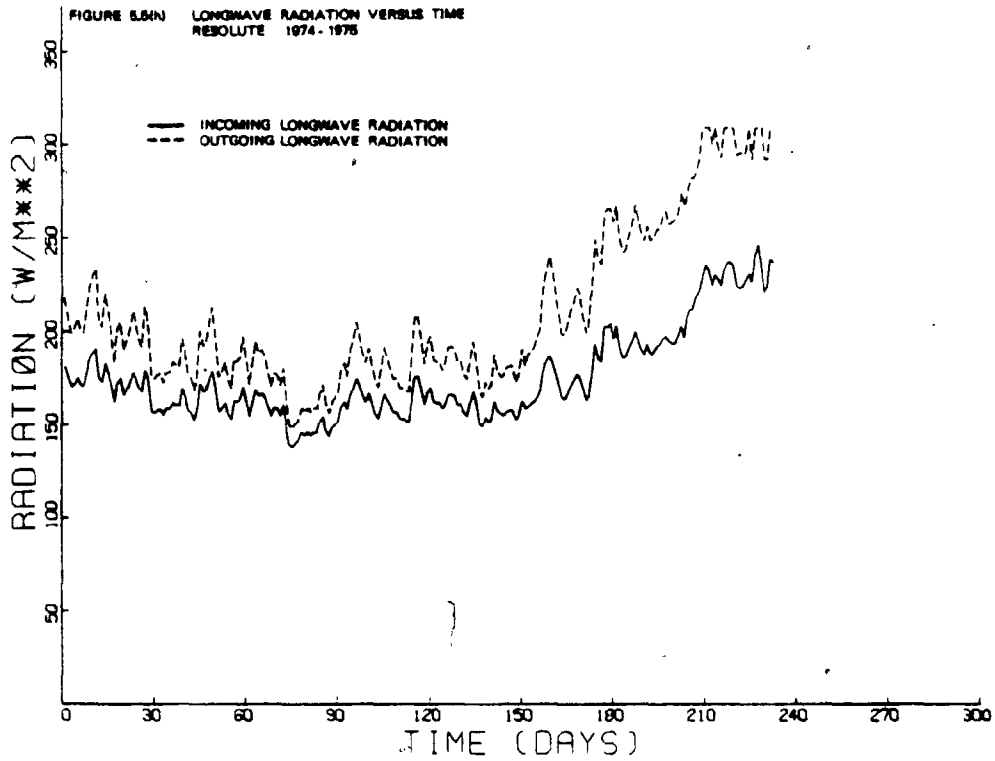
FIGURE 5.5(h) LONGWAVE RADIATION VERSUS TIME
RESOLUTE 1974 - 1975
INCOMING LONGWAVE RADIATION
OUTGOING LONGWAVE RADIATION
RADIATION (W/M**2)
TIME (DAYS)
0
30
60
90
120
150
180
210
240
270
300
50
100
150
200
250
300
350

FIGURE 5.6(h) ENERGY FLUXES VERSUS TIME
RESOLUTE 1974 1975

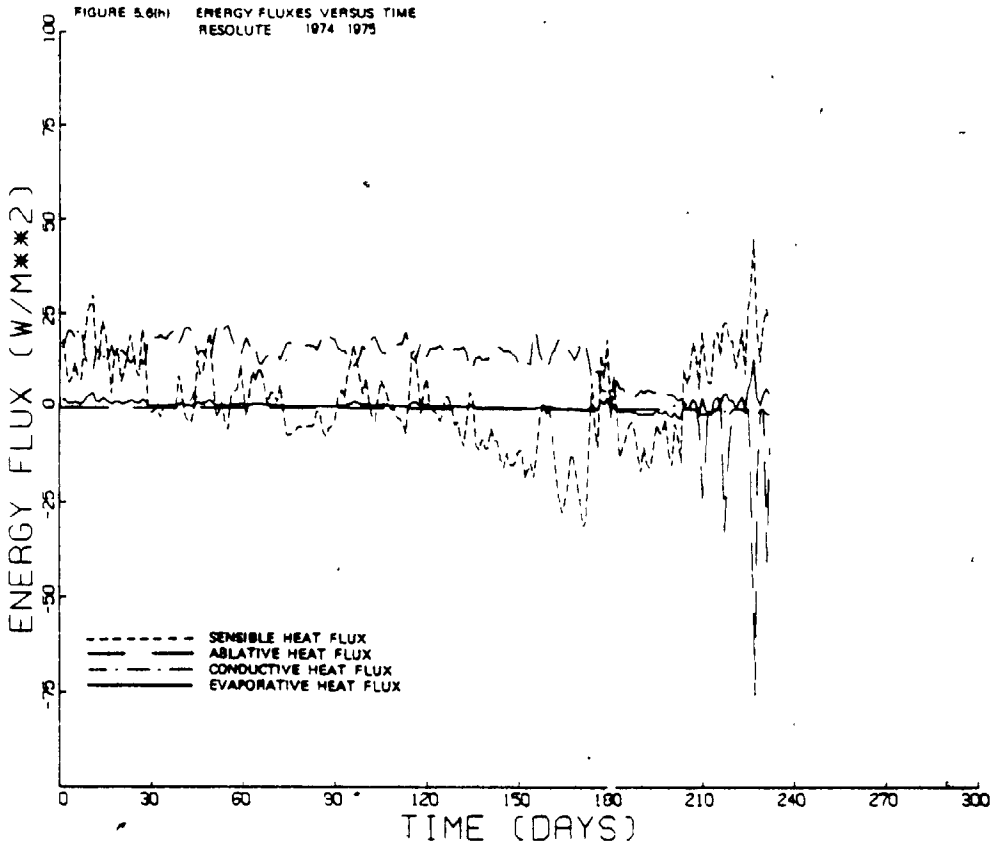

FIGURE 5.7(h) TEMPERATURES VERSUS TIME
RESOLUTE 1974 - 1975

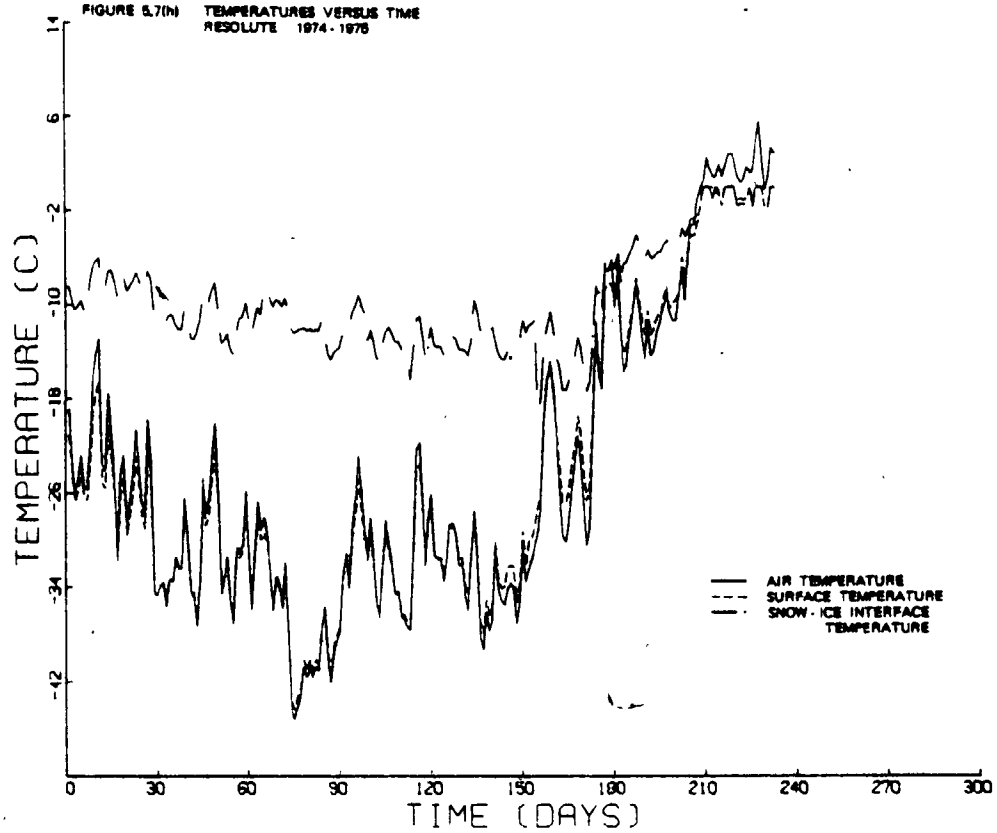

FIGURE 5.8(h) ICE SALINITY VERSUS TIME
RESOLUTE 1974 - 1975

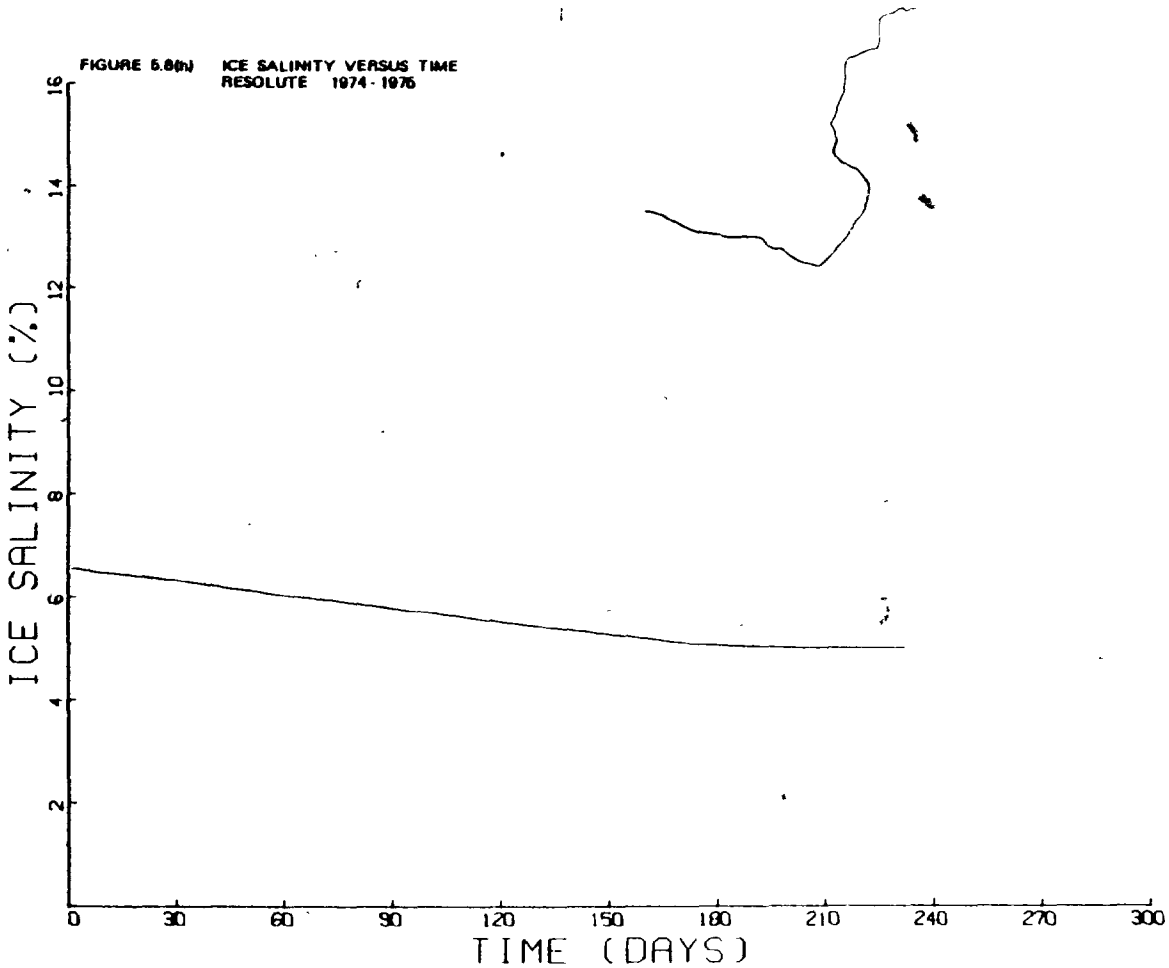

FIGURE 5.2(i) ICE THICKNESS VERSUS TIME
RESOLUTE 1975 - 1976

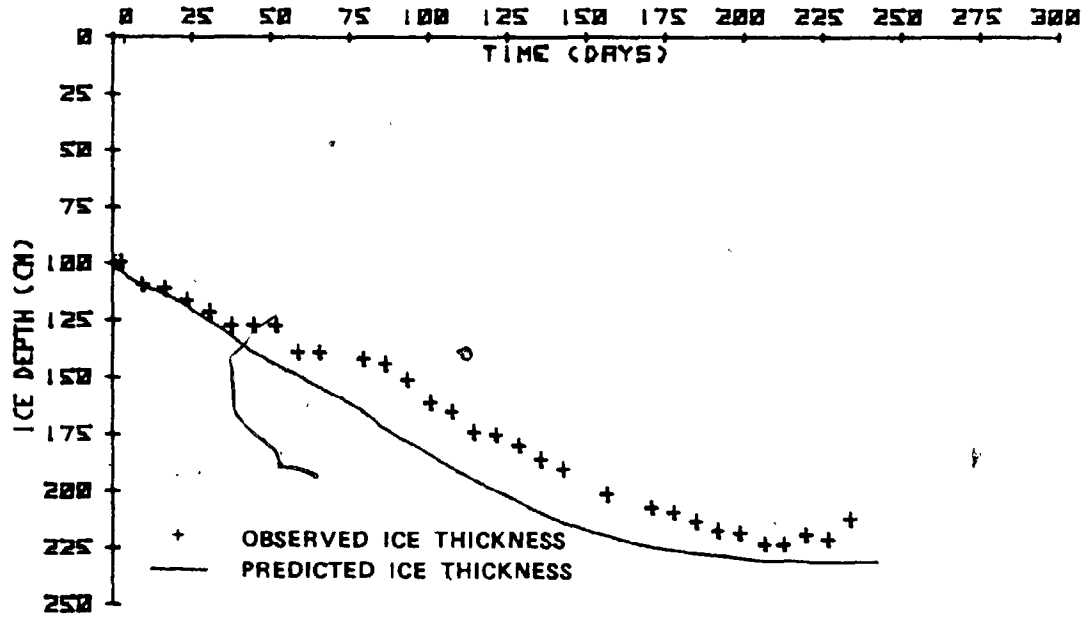

FIGURE 5.3(i) OBSERVED VERSUS PREDICTED ICE THICKNESS –
RESOLUTE 1975 - 1976

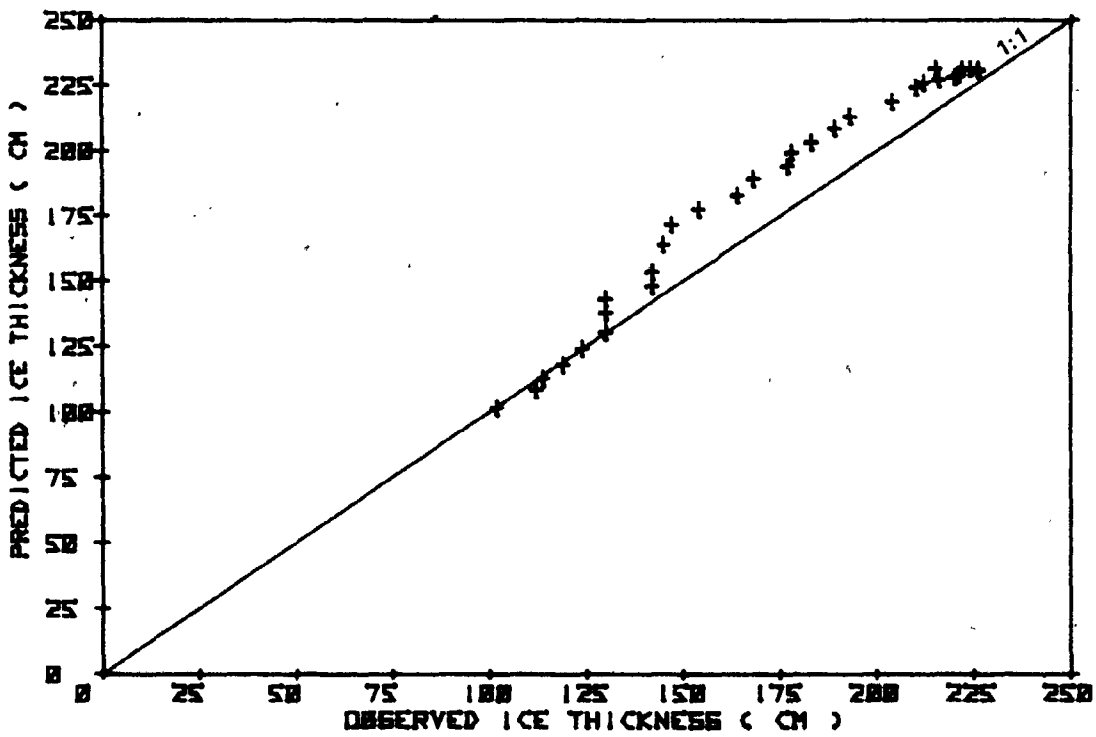

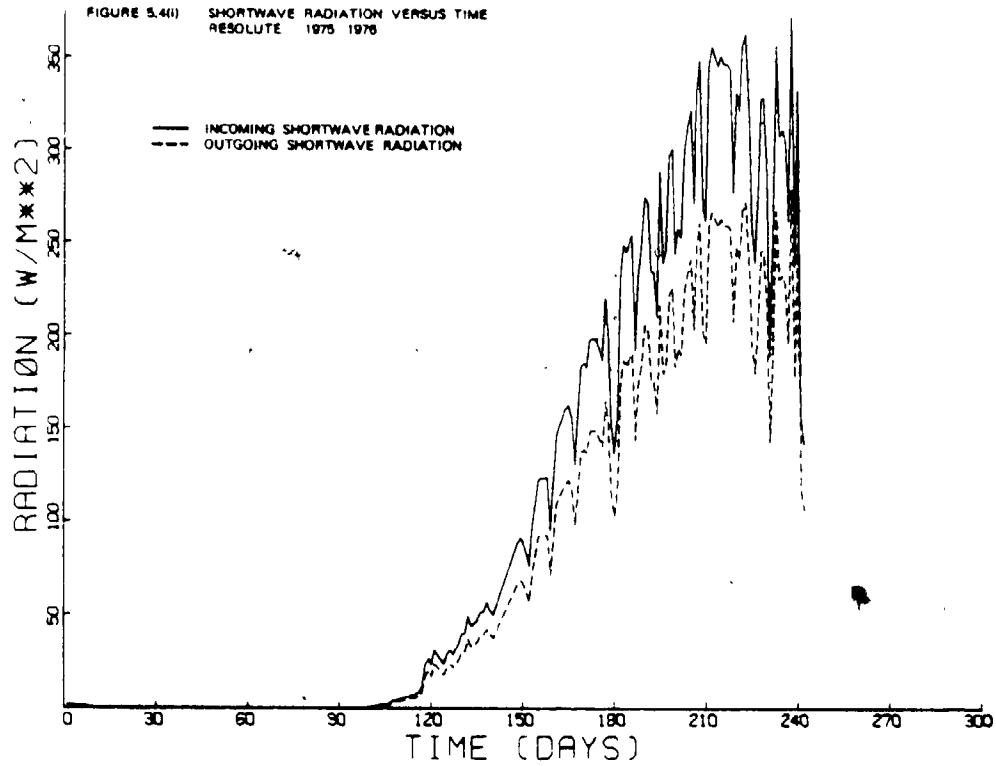
FIGURE 5.4(i) SHORTWAVE RADIATION VERSUS TIME
RESOLUTE 1975 1976
INCOMING SHORTWAVE RADIATION
OUTGOING SHORTWAVE RADIATION
RADIATIØN (W/M**2)
50
100
150
200
250
300
350
0
30
60
90
120
150
180
210
240
270
300
TIME (DAYS)

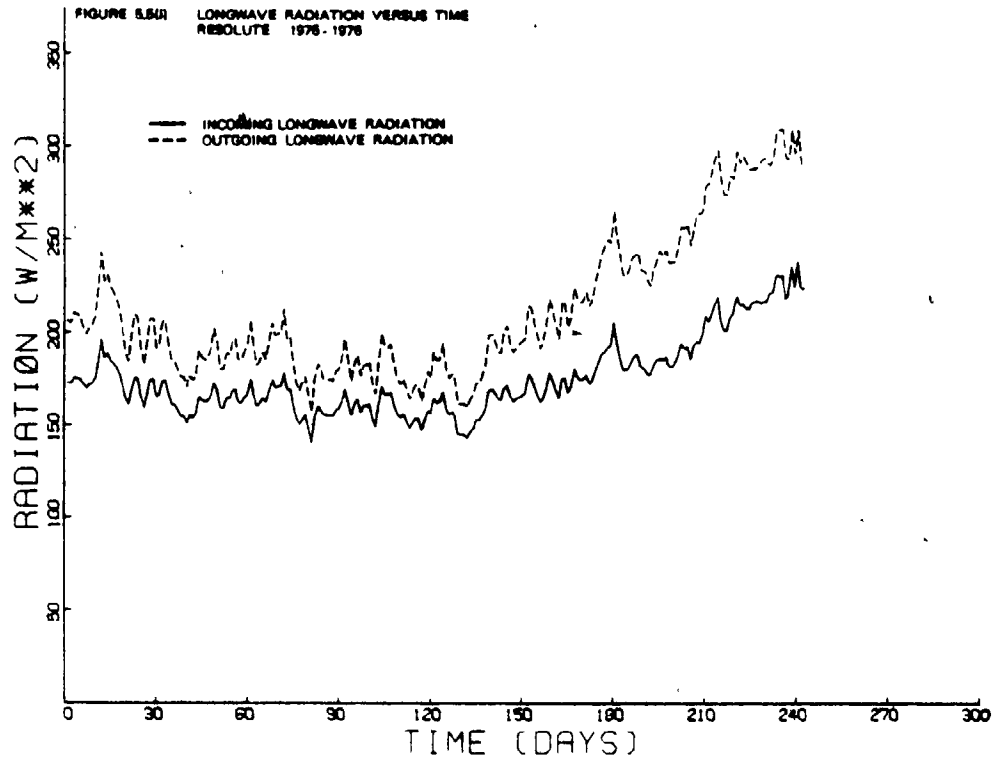
FIGURE 5.5(i) LONGWAVE RADIATION VERSUS TIME
RESOLUTE 1975 - 1976
INCOMING LONGWAVE RADIATION
OUTGOING LONGWAVE RADIATION
RADIATIØN (W/M**2)
50
100
150
200
250
300
350
0
30
60
90
120
150
180
210
240
270
300
TIME (DAYS)

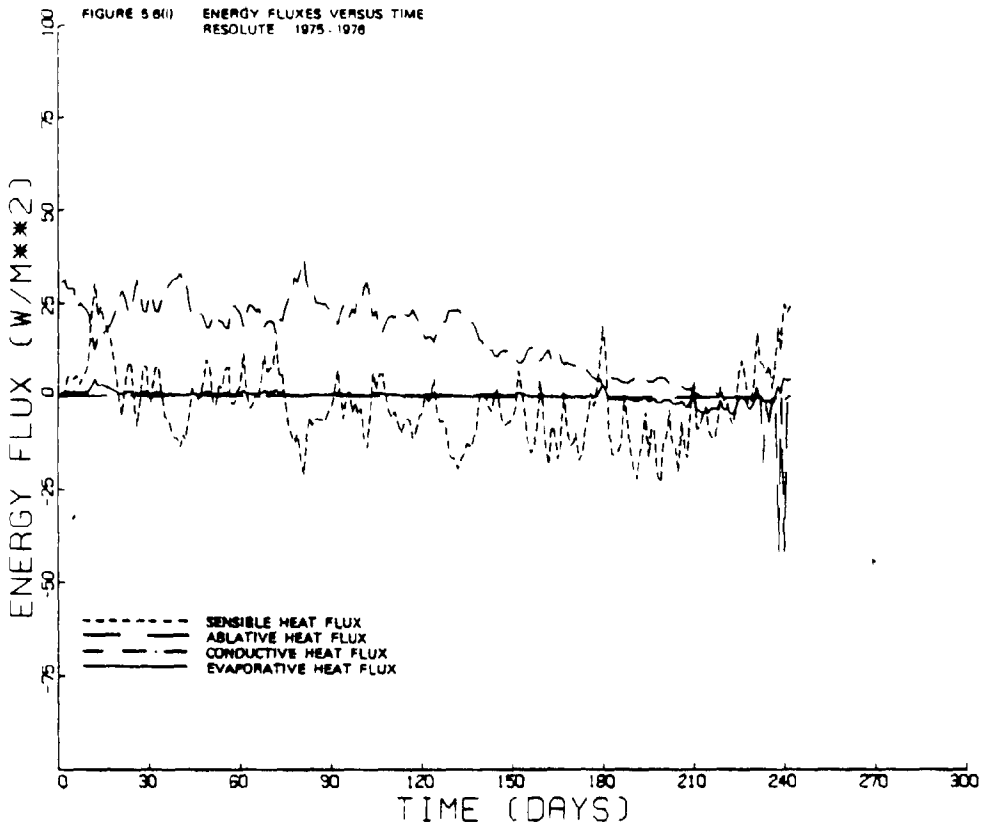
FIGURE 5.6(i) ENERGY FLUXES VERSUS TIME
RESOLUTE 1975 - 1976
ENERGY FLUX (W/M**2)
100
75
50
25
0
-25
-50
-75
SENSIBLE HEAT FLUX
ABLATIVE HEAT FLUX
CONDUCTIVE HEAT FLUX
EVAPORATIVE HEAT FLUX
0
30
60
90
120
150
180
210
240
270
300
TIME (DAYS)

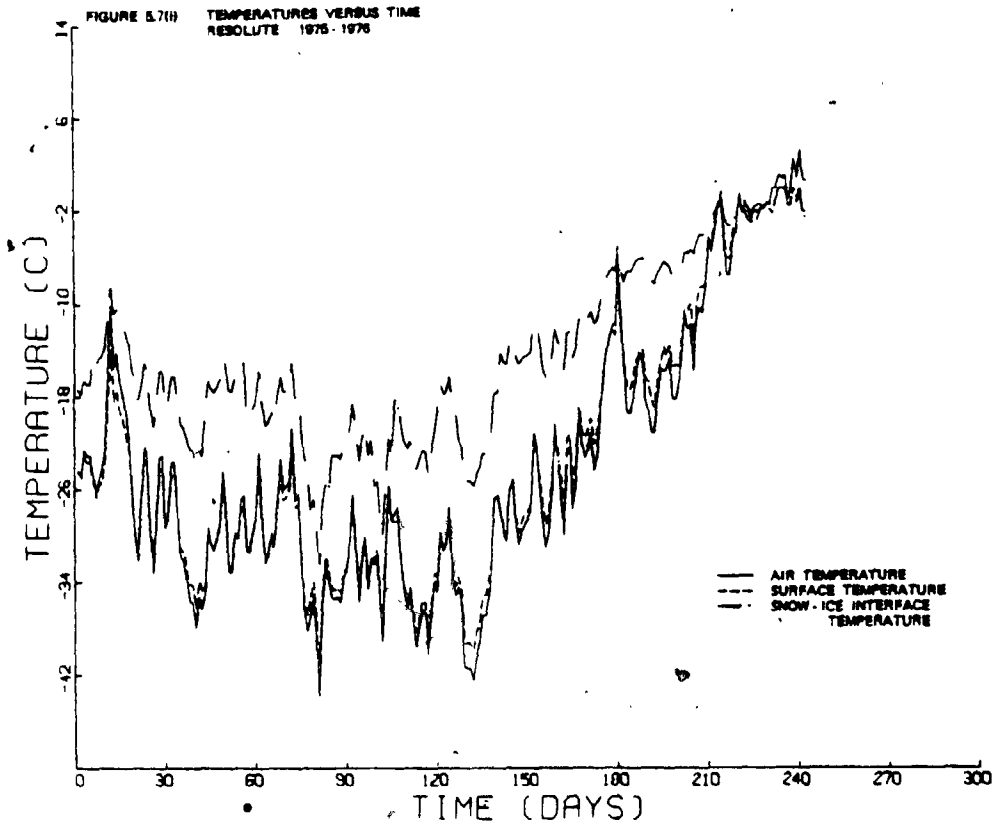
FIGURE 5.7(i) TEMPERATURES VERSUS TIME
RESOLUTE 1975 - 1976
TEMPERATURE (C)
14
6
-2
-10
-18
-26
-34
-42
AIR TEMPERATURE
SURFACE TEMPERATURE
SNOW - ICE INTERFACE TEMPERATURE
0
30
60
90
120
150
180
210
240
270
300
TIME (DAYS)

FIGURE 6.8(ii) ICE SALINITY VERSUS TIME
RESOLUTE 1975 - 1976

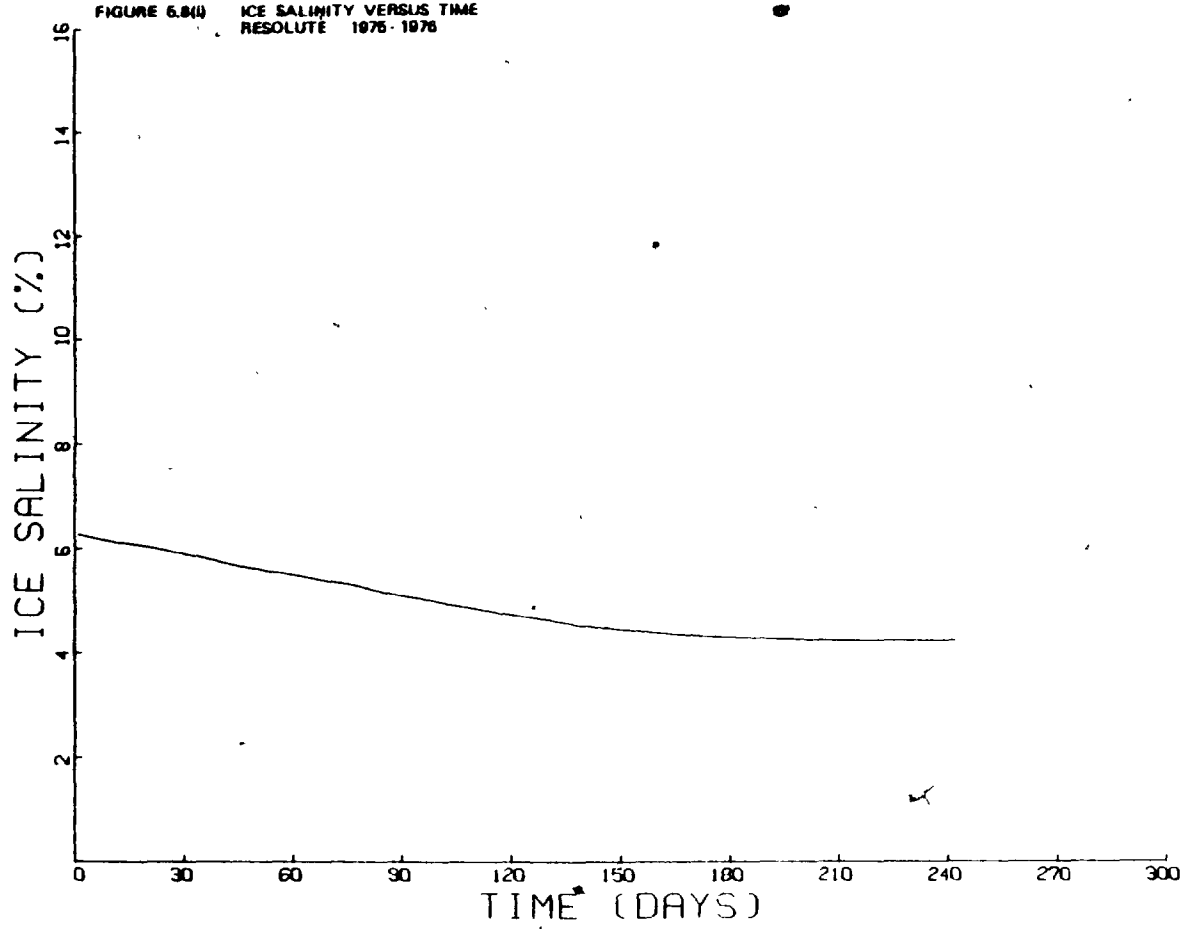

CHAPTER 6

DISCUSSION

6.1 Conceptual and Physical Limitations of the Model

A better understanding of the applicability of the model to specific situations is gained through the identification of both the physical and conceptual limitations. The action also serves to pinpoint areas where further developmental work is required to produce an improved model of sea ice behaviour.

The model represents ice growth for the one dimensional situation. Horizontal gradients and transfers are not modelled as they are assumed not to exist. While this may be true of the temperature field and heat conduction, horizontal advection is present in the atmosphere. The variable distribution of ice thickness groups and leads ensures this.

There is no attempt to include the effects of mechanical stresses. Ice thicknesses are affected as evidenced by pressure ridges (compression) and leads (contraction). Wind induced cracking can break up both a young ice sheet and a decayed older sheet. The wind may then clear a region of ice by transporting it in a downwind direction.

The model does not have the ability to predict the time of formation of an ice cover. This requires a theoretical model of the ocean coupled with an atmospheric model. This would also remove the restrictions of an isohaline, isothermal layer at the base of an ice sheet. The development of such a model would entail an equivalent amount of work, if not more, to that required to prepare this model. In such a situation, we are no longer dealing with a 'simple' model.

The use of the Fourier steady state heat conduction equation may result in an oversimplification of the system during certain periods of the year. The use of the parabolic heat conduction equation would be more realistic and allow the inclusion of internally generated heat such as that due to radiation penetration and the latent heat associated with brine concentration by freezing.

Ice thermal properties are strongly affected by salinity when warm ice temperatures exist in conjunction with high salinities. The interaction between the temperature and salinity fields, as originally intended it should be modelled, has not been accomplished. The failure to produce a model that allows the prediction of salinity variations from a knowledge of ice thickness, ice temperature and the existing salinity profile meant that only a bulk salinity effect could be introduced. The question of salinity variations in time

and space, like the ocean model, requires an intensive study to untangle its complexities. The model has at least allowed the average salinity to be specified in a realistic manner within the model and not treated as an external input with a constant value.

The solution of the parabolic heat conduction equation and allowances for salinity redistribution and its effect on the temperature field would be enhanced by modelling involving finite difference or finite element techniques. This would also allow variations in internal properties as a function of location within the ice sheet to be included. This would be more realistic than the bulk substrate format adopted for this work.

During ablation it is assumed that the meltwater is removed from the surface of the ice. There is no attempt made to include the changes induced by the existence of ponded water on the surface. Its presence may substantially change both the radiation and energy flux components relative to the clear ice situation (most notably the evaporative heat flux and net shortwave radiation (see Langleben (1966) for the effect on meltwater ponds on the surface albedo)) as well as acting as a heat storage reservoir.

The specifications of the variables and the functional relationships amongst themselves could benefit by reinterpretation and redefinition. They are based on the present state of knowledge and will surely be improved as more is learned of their behaviour. Just as this work represents a more realistic definition of some of these variables than found in the preceeding work, so can be said of the work to follow this.

It should be remembered that there is no guarantee that better results can be obtained by the implementation of the above recommendations. In view of the natural variability in ice conditions we may only secure an increased understanding and not necessarily a better predictive tool. Complex models suffer in that they may be so elaborately constructed that they become impractical to change (see Walker's (1976) comments on the Maykut and Untersteiner (1969) model), require excessive time and cost to run, and are limited in their usefulness in applied situations. Despite the limitations discussed, this model has proved to be a useful tool to study the growth and decay of first year sea ice. In summary we may list some of its abilities and advantages:

- the model is conceptually and computationally simple
- the surface temperature and the climatological variables influencing it have been modelled in a realistic fashion consistent with the energy conservation approach

- the model allows the energy and radiation fluxes to respond to changes in surface conditions
- the model is versatile in that changes required for a specific application may be implemented without major revisions
- the model allows annual ice growth to be simulated at very low cost in terms of time and money
- the model has been verified in its ability to predict ice growth with respect to both magnitude and phase.

6.2 Concluding Remarks

A model of the growth and decay of sea ice was developed because of its need in the physical and applied sciences. A good understanding of the atmosphere-ice-ocean interaction was obtained through the development of a computer simulation model utilizing an energy conservation methodology. The model allowed the computation of the energy and radiation fluxes at the ice surface, their dependence on the characteristics of the surface and the atmosphere and the resultant ice growth.

The ice growth predicted by the model was tested against observations at three arctic locations over three consecutive growth seasons. The model provided estimates of ice thickness at each site that were equivalent to the observed thicknesses within the range of their natural variability. The simulated thicknesses were comparable with the observations in respect to both magnitude and phase.

The radiation and energy flux predictions could not be evaluated directly because of the lack of real world observations. However, very close agreement was found with the results of two other climate simulation models. Qualitative agreement was also obtained between the model and observations over ice in the Beaufort Sea indicating that the fluxes produced by the model were not contradictory with respect to the magnitude of the observed fluxes.

The model is available now as a tool to explore and assess the consequences of changes in the state of the atmosphere and the properties of the snow and ice medium. This, in conjunction with the implementation of some of the recommendations of 6.1, remains as the next step in the evolution of our knowledge of the behaviour of sea ice and its growth.

APPENDIX A

BRINE DRAINAGE

APPENDIX A Brine Drainage

A.1. Towards A Gravity Drainage Model

Even after eliminating brine pocket diffusion (due to its very low rate), hydrostatic flushing (because of its limitation to periods when ponded surface meltwater occurs) and brine expulsion (due to its small influence for ice thicknesses in excess of 40 cm, Cox and Weeks, 1975) the problem of modelling brine drainage is not without its difficulties. A gravity drainage model is complicated by the existence of two radically different drainage pathways--the first being the somewhat interconnected volumes occupied by the brine and the second being the extensive drainage channel network.

In the case of the drainage network the ice is considered porous and the difference between the hydrostatic head of seawater and that of the interior brine creates the pressure gradient force which drives the brine downward. An unstable vertical density distribution exists within the brine of a growing ice sheet because the density of the brine in equilibrium with ice is determined by its temperature. Observations in laboratory ice indicate that an oscillatory flow develops in the channels in which brine pours out of the channel to be replaced by seawater flowing up into the ice (Eide and Martin,

1975). Acting as a pumping mechanism these oscillations will replace high salinity brine with lower salinity sea water resulting in lower overall ice salinities.

When considering gravity drainage without a hydrostatic linkage to the underlying sea water the denser brine in the colder regions moves downward through the ice under its own weight. The rate of gravity drainage is dependent on both ice permeability and the temperature gradient, increasing with an increase in either of these variables (Cox and Weeks, 1975). The permeability of ice is related to the ice microstructure and as yet only poorly understood. Qualitatively, it has been linked to the brine volume (as defined by Assur, 1958) as laboratory experiments have indicated an increase in gravity drainage with an increase in temperature gradient (Cox and Weeks, 1975).

A simple one-dimensional continuity model to evaluate salinity changes within an ice sheet of constant thickness was attempted by relating ice permeability functionally to the brine volume. It had been hoped to duplicate the characteristic C-shaped curve and the overall decrease in salinity with time observed in first year ice. Results were generally poor with one exception where the observed features were duplicated but the functional relation employed could not be rationalized in a proper physical sense.

Approaching the problem of salinity redistribution within ice from a one-dimensional viewpoint may be an unrealistic proposition. Weeks and Lee (1962) have demonstrated the lateral variability of salinity within an apparently homogeneous ice sheet. The distribution of brine channels within an ice sheet suggests strong variations in ice salinity depending on whether or not, and where such a channel or its feeders are intersected. It remains for future research to detail the relative importance of the mechanisms described and provide a sound mathematical basis for their evaluation.

A.2. Testing Tsurikov's Theory of Brine Migration

Testing Tsurikov's (1967) theory of brine migration was accomplished using first year sea ice data collected by the Polar Continental Shelf Project at a location on Eclipse Sound near Pond Inlet, N.W.T. Using this data set the state variables (salinity, depth, time and temperature) were decomposed into the required differential terms. These terms, which were produced by the use of a spline function differentiation were compared with the components of the exact differential equation. The difference in these terms is a measure of the degree of departure of the observed distribution from the theoretical distribution. Components of the error term include 1) deviation of the actual processes from the modelled process, 2) observational or instrumentational errors, and 3) errors generated by the differentiation technique. To adequately assess the relation between the theoretical and observed results, the latter two components must be minimized. Errors in (2) include the effects of core handling, storage and salinity determination uncertainties. It is difficult to evaluate these effects but if a regular set of procedures are employed then one might expect a reasonably constant residual due to these effects. Errors due to (3) are highly dependent on the method of numerical differentiation employed and Tagaki (1967) has shown that differentiation involving a cubic spline function introduces

minimal errors (see also Grenville (1967)).

Tsurikov's formula expresses the variation in salinity of the ice layer on the condition that the migration of the brine pockets is due to the inflow and outflow of heat and not ion diffusion. Equation (3.2) may be rewritten as

$$\frac{dS}{dt} + \frac{a}{nr^2 L_f \Delta T_f} (S) \frac{dS}{dZ} \frac{dT}{dZ} = 0 \qquad (A.1)$$

From the real world data set we expect that error will be introduced from various sources such that

$$\frac{dS}{dt} + \frac{a}{nr^2 L_f \Delta T_f} (S) \frac{dS}{dZ} \frac{dT}{dZ} = D \qquad (A.2)$$

where D is a residual term. If this is squared and integrated over the profile depth we obtain the integral residual R.

$$R = \int_0^H D^2 dZ \qquad (A.3)$$

Ten profiles from March-April 1977 were selected to evaluate the residual D and the integral residual R. The analysis employed data from 45 depth levels sampled at 2.5 cm intervals. For each profile (at a fixed time t) the value of the first derivative of salinity with respect to depth was calculated at each level resulting in 45 values of dS/dZ for each profile. Values of dS/dt at each time t were then calculated for each depth level.

Setting

$$\frac{a}{nr^2 L_f \Delta T_f} = k = 100 \qquad (A.4)$$

as suggested by Tsurikov (1967) provided very high residuals. A search was then instituted to determine the value which minimized D. A value of k equals zero was found implying that the rate of change of salinity with time was zero. Average ice salinity decays in an approximately exponential form (Assur and Weeks (1963), Tsurikov (1967)) such that towards the end of the growth period the average salinity changes only very little. If the layer by layer variation is analogous then dS/dt at the time of year of the profiles may be very small and tend to zero, supporting the observations. However, one would also expect that the dS/dt and dS/dZ terms consistently have the same sign; this was observed only 50% of the time with these data.

Ten profiles were then selected for testing from the early portion of the growth season (November 1977 - January 1978) where significant salinity changes are expected. The results showed k to vary over several orders of magnitude with no apparent trend.

The results of these studies indicate that

1. the k factor is more variable than suggested and should not be treated as a constant, or
2. The data and the analysis technique are not of a sufficient quality to assess the validity of Tsurikov's theory, or
3. Tsurikov's governing differential equation is wrong, or
4. other more important salinity redistribution mechanisms are at work.

The very poor correlation amongst the observed data and the predicted behaviour of sea ice salinity suggests that the governing relationships as given by Tsurikov do not provide a sufficient answer to the question of salinity redistribution in sea ice.

APPENDIX B

LISTING OF COMPUTER PROGRAM: ICE

```
C*****     PROGRAM  ICE     *****
C
C     THIS COMPUTER PROGRAM SIMULATES THE GROWTH OF FIRST YEAR SEA ICE
C     USING AN ENERGY CONSERVATION APPROACH.DOCUMENTATION FOR THIS
C     PROGRAM MAY BE FOUND IN 'AN EQUILIBRIUM SURFACE TEMPERATURECLIMATE
C     MODEL APPLIED TO THE GROWTH OF FIRST YEAR SEA ICE',MASTER'S THESIS,
C     DEPT. OF GEOGRAPHY,CARLETON UNIVERSITY,BY J.D.MILLER ,1979.
C
C*****PROGRAM DEVISED AND COMPILED BY J.D.MILLER
C     USE OF THIS PROGRAM (OR DERIVATIVE) IS NOT ALLOWED WITHOUT THE
C     WRITTEN PERMISION OF THE AUTHOR.
C     COMMERCIAL USE STRICTLY FORBIDDEN
C     COPYRIGHT 1979 BY J.D.MILLER
C*********************************************************************
      REAL SNODEN,SNODEP,AIRDEN,CAPAIR,LVAP,DRAGH,DRAGE
     1,INDT,BETA,KNOT,EPSLON,SIGMA,A,B,C,SALWTR,TAIR,
     2TAIRC,PRESUR,WIND,KDOWN,KUP,LDOWN,LUP,HEAT,EVAP,DELTAQ,FICE
     3,HICE,HWICE,ALPHAI,SAL,TFREEZ,KICE,KBROW,BD(10)
      REAL SNOW,SNOMLT,ICEMLT,DLDICE,AA(10),DEPTHS,SALTY,MLTH
      INTEGER KOUNT
C*****I N I T I A L I Z E   C O N S T A N T S
      KOUNT=0
      AIRDEN=1.32
      LFUSW=65.*4.18*1000.
      LFUSS=334400.
      CAPAIR=1010.
      LVAP=2533455.
      DRAGH=0.0010
      DRAGE=0.0005
      INDT=0.17
      IIESF=0
      BETA=0.117
      KNOT=2.03
      EPSLON=0.97
      SIGMA=5.57E-08
      A=-0.0137
      B=-0.051990
      C=-7.225E-5
      SNODEP=0.
      KOUNTR=0
C *****I N P U T   S I T E   N A M E
      READ(105,2200) (BD(I),I=1,10)
C *****I N P U T   S I M U L A T I O N   S T A R T I N G   D A T E ****
      READ(105,2200) (AA(I),I=1,10)
C *****I N P U T   O C E A N   S A L I N I T Y *****
```

```
      READ(105,2005) SALWTR
C *****I N P U T  I C E  A N D  S N O W  D E P T H *****
      READ(105,3005) DEPTHS,SNOW
C*****I N P U T  W I N D  S P E E D  A N D  P R E S S U R E
      READ(105,3005) WIND,PRESUR
C*****I N P U T  S N O W  D E N S I T Y
      READ(105,2005) SNODEN
      HICE=DEPTHS/100.
      SNODEP=SNOW/100.
      OLDICE=HICE
C*****E C H O  P R I N T
      WRITE(108,2202) (BH(I),I=1,10)
      WRITE(108,2201) (AA(I),I=1,20)
      WRITE(108,4005) SALWTR
      WRITE(108,5005) DEPTHS
      WRITE(108,6005) SNOW
      WRITE(108,2203) WIND,PRESUR
      WRITE(108,7007) SNODEN
      WRITE(108,7005)
      TFREEZ=273.+(A+B*SALWTR+C*SALWTR**2.)
C*******R E A D  I N  D A T A ************
   99 READ(105,1000) TAIRC,KDOWN,SNOW
      IF(TAIRC.EQ.999) GOTO 999
      SNODEP=SNODEP+SNOW/100.
      SNOWW=SNODEP*100.
C*****E S T I M A T E  A V E R A G E  I C E  S A L I N I T Y
      IF(ITEST) 21,21,22
   21 SAL=14.24-19.39*HICE
      IF(HICE.GT.0.40) SAL=7.88-1.59*HICE
      GOTO 111
   22 SALTY=SAL
      MLTR=OLDICE+0.01
      SAL=0.5+(SALTY-0.5)/(MLTR-0.10)*(HICE-0.10)
  111 KOUNTR=KOUNTR+1
      U=293.
      L=223
      TEQ=(U+L)/2.
      HHICE=HICE*100.
      TAIR=TAIRC+273.
C*****I C E  A L B E D O
      IF(ITEST) 56,56,59
   56 CALL ALBEDO(HICE,ALPHAI)
      GO TO 55
   59 ALPHAI=0.45
C*****S T A R T  S E A R C H  F O R  E Q.  S F C E.  T E M .  *******
   55 KICE=KNOT+(BETA*SAL)/(TEQ-273.)
      TSFCE=TEQ-273.
      IF(TEQ.GE.272.0) KICE=1.322
      FICE=KICE*(TFREEZ-TEQ)/HICE
C*****S N O W  A L B E D O
      IF(SNODEP.LE.0.) GOTO 44
```

```
      IF(ITEST) 39,39,34
   39 ALPHAI=0.75
      GOTO 210
   34 ALPHAI=0.45
C*****S N O W  P A C K  E F F E C T S ******
  210 KSNOW=2.0530E-02+4.21657E-04*SNDEN-1.0909E-08*SNDEN**2. +
     I 2.1838E-09*SNDEN**3.
C           VAN DUSEN'S FORMULA .... SEE YEN (1969)
      INDT=0.0
      FICE=(TFREEZ-TEQ)*(KICE*KSNOW)/(KSNOW*HICE+KICE*SNDEP)
C           FROM FLUX IN ICE = FLUX IN SNOW
   44 CONTINUE
C*****E N E R G Y  B A L A N C E  T E R M S *
      KUP=KDOWN*ALPHAI
      LDOWN=SIGMA*TAIR**4.*(1-0.261*EXP(-7.77E-4*(TAIRC**2.)))
      LDOWN=LDOWN*EPSLON
C           INCOMING LONGWAVE ESTIMATE FROM IDSO AND JACKSON (1969)
   33 HEAT=AIRDEN*CAPAIR*DRAGH**IND*(TAIR-TEQ)
      KOUNT=KOUNT+1
      IF(KOUNT.GT.100) GOTO 200
      QSFCE=EXP(24.294-(6138./TEQ))
C           VAPOUR PRESSURE FROM  CLAUSIUS-CLAPEYRON FORMULA
      QAIR=EXP(21.644-(5418.7/TAIR))
      QSFCE=QSFCE*0.622/PRESUR
      QAIR=QAIR*0.622/PRESUR
      DELTAQ=0.9*QAIR-QSFCE
      LUP=EPSLON*SIGMA*TEQ**4.
      EVAP=AIRDEN*LVAP*DRAGE**IND*DELTAQ
   29 SHORTW=(1-ALPHAI)*(1-INDT)*KDOWN
      LONGW=LDOWN-LUP
      BALNCE=SHORTW+LONGW+(FICE+HEAT+EVAP)
      IF(ABS(BALNCE).LT.0.5) GOTO 199
      IF(BALNCE.LT.0.0) GOTO 57
      L=TEQ
      TEQ=(TEQ+U)/2.
      GOTO 55
   57 U=TEQ
      TEQ=(TEQ+L)/2.
      GOTO 55
  199 I=KOUNTR
      IF(TEQ.GE.273.) GOTO 217
C*****O U T P U T  S O L U T I O N  P A R A M E T E R S
      MELT=0.
      DU=(KICE*SNDEP)/(KSNOW*HICE)
      TINT=(TEQ+DU*TFREEZ)/(1+DU)-273.
      WRITE(108,2002)I,TAIRC,SNOWW,KDOWN,KUP,LDOWN,LUP,EVAP,
     1HEAT,FICE,MELT,ISFCE,TINT,HHICE,SAL
      DICE=(FICE*86400)/(LFUSW*920.)
      ITEST=0
      HICE=HICE+DICE
      GOTO 300
```

```
 217  TEW=273.
C          SET UPPER SURFACE TEMPERATURE AT 273 KELVIN
      TSFCE=TEW-273.
      TINT=TSFCE
      HEAT=AIRDEN*CAPAIR*DRAGH*WIND*(TAIR-TEW)
      DELTAW=0.9*WAIR-(P.108*0.622/PRESUR)
      EVAP=AIRDEN*LVAP*DRAGE*WIND*DELTAW
      FICE=KICE*(271.-273.)/HICE
      LDOWN=0.736*SIGMA*TAIR**4.
      LUP=SIGMA*273.**4.
      BALNCE=(1-ALPHAI)*(1-INOT)*KDOWN+LDOWN-LUP+FICE+HEAT+EVAP
      IF(SNODEP.LE.0.) GOTO 221
C*****C A L U L A T E   S N O W M E L T
      SNOMLT=((FICE-BALNCE)*86400)/(LFUSS*SNODEN)
      MELT=FICE-BALNCE
      TINT=TSFCE
      WRITE(106,2002)I,TAIRC,SNOHW,KDOWN,KUP,LDOWN,LUP,EVAP,
     1HEAT,FICE,MELT,TSFCE,TINT,HHICE,SAL
      SNODEP=SNODEP+SNOMLT
      OLDICE=HICE
      IF(SNODEP.LE.0.) SNODEP=0.
      GOTO 300
C*****C A L C U L A T E   I C E   M E L T
 221  ICEMLT=((FICE-BALNCE)*86400)/(920.*LFUSW)
      MELT=FICE-BALNCE
      TINT=TSFCE
      WRITE(108,2002)I,TAIRC,SNOHW,KDOWN,KUP,LDOWN,LUP,EVAP,
     1HEAT,FICE,MELT,TSFCE,TINT,HHICE,SAL
      OLDICE=HICE
      HICE=HICE+ICEMLT
      ITEST=1
      SNODEP=0.
      IF(HICE.LE.0.) GOTO 88
      GOTO 300
 300  KOUNT=0
      GOTO 99
 200  WRITE(108,1111) ITW
 1111 FORMAT(' ','PROGRAM STOPPED..>50  ITERATIONS',' TEW=',F10.2)
      KOUNT=0
      GO TO 99
 1000 FORMAT(3G.0)
 2002 FORMAT(' ',I5,6F8.1,4F9.1,2F9.2,F9.1,F9.2)
 2005 FORMAT(1G.0)
 2200 FORMAT(10A4)
 2201 FORMAT(' ',6X,'STARTING DATE IS',3X,10A4//)
 3005 FORMAT(2G.0)
 4005 FORMAT(' ','       OCEAN SALINITY',F10.1,5X,'(P.P.T.)')
 5005 FORMAT(' ','       INITIAL ICE DEPTH ',F10.1,5X,' (CM)')
 6005 FORMAT(' ',6X,'INITIAL SNOW DEPTH',F10.1,5X,'(CM)'///)
 7007 FORMAT(' ',6X,'SNOW DENSITY IS ',F6.1,' KG/M**3'/)
 2202 FORMAT(' ',5X,' SITE LOCATION IS ',2X,10A4//)
```

```
2603 FORMAT(' ',5X,' WIND SPEED  ',F6.1,'    M/S '/6X
     1,' MEAN PRESSURE',F8.1,'   MB.'//)
7003 FORMAT(' ',2X,'DAY',3X,'T AIR',4X,'SNOW',2X,'K DOWN',4X,
     1'K UP',2X,'L DOWN',4X,'L UP',5X,'LVAP',5X,'HEAT',4X,
     2'F ICE',5X,'MELT',3X,'T SFCE',4X,'T INT',2X,'THICKNESS',
     33X,'SALINITY'//)
999  OUTPUT ' '
C*****S I T E  O B S E R V A T I O N S
     WRITE(108,9999)
     WRITE(108,9998)
 87  READ(105,1000) DAY,HHICE,SNOW
     IF(DAY.EQ.999) GOTO 1999
     WRITE(108,9090) DAY,HHICE,SNOW
     GOTO 87
 88  HICE=0.
752  READ(105,1000) TAIRC,KDOWN,SNOW
     IF(TAIRC.NE.999) GOTO 752
     GOTO 87
9090 FORMAT(' ',5X,F5.0,5X,F5.1,5X,F5.1)
9998 FORMAT(' ',7X,'DAY',6X,'ICE',/X,'SNOW'/14X,
     1'THICKNESS',3X,'DEPTH'//)
9999 FORMAT(' ','THE FOLLOWING TABLE PRESENTS THE RECORDED ICE THICKNES
    1S INFORMATION FOR THE STATION'/)
1999 OUTPUT ' '
     OUTPUT '            I HOPE YOU ENJOYED THE SEA-ICE GAME'
     OUTPUT '            THIS EXERCISE HAS BROUGHT TO YOU IN PART BY:'
     OUTPUT '                    CARLETON UNIVERSITY AND'
     OUTPUT '                    THE NATIONAL RESEARCH COUNCIL OF CANADA'
9901 END
     SUBROUTINE ALBEDO(HICE,ALPHAI)
     HICE=HICE*100.
     IF(HICE.GE.100) GO TO 55
     IF(HICE.GE.5.) GO TO 44
     ALPHAI=0.04*HICE+0.07
     GO TO 66
 44  A1=2.4668E-01
     A2=7.0486E-03*HICE
     A3=-8.6082E-05*HICE*HICE
     A4=3.8112E-07*HICE**3.
     ALPHAI=A1+A2+A3+A4
     GO TO 66
 55  ALPHAI=0.47
 66  CONTINUE
     HICE=HICE/100.
     RETURN
     END
```

APPENDIX C

SAMPLE COMPUTER INPUT

APPENDIX C

SAMPLE COMPUTER INPUT

Card Number	Input	Format	Quantity
1	Frobisher Bay N.W.T. (A.E.S.)	10A4	Location
2	November 28 1975	10A4	Starting date
3	32.0	1G.0	Ocean salinity ($^{o}/oo$)
4	39.4	2G.0	Initial ice and snow thickness (cm)
5	0.0	2G.0	Wind speed (m/s) and atmospheric pressure (mb)
6	310.	1G.0	Snow density (kg/m^3)
7	- 8.6 7.3 0.	3G.0	Air temperature (^{o}C), incoming shortwave radiation (W/m^2), change in snow thickness (cm)
7	-12.2 8.7 0.	3G.0	(as above)
7	- 8.6 3.4 0.	3G.0	(as above)
7	-13.9 5.3 0.	3G.0	(as above)
7	-17.5 5.8 0.	3G.0	(as above)
	⋮		
8	999 0 0	3G.0	End of data flag.

APPENDIX D

SAMPLE COMPUTER OUTPUT

SITE LOCATION IS FROBISHER BAY N.W.T. (A.E.S.)

STARTING DATE IS NOVEMBER 28 1975

OCEAN SALINITY 32.0 (P.P.T.)
INITIAL ICE DEPTH 39.4 (CM)
INITIAL SNOW DEPTH .0 (CM)

WIND SPEED 10.0 M/S
MEAN PRESSURE 1000.0 MB.

SNOW DENSITY IS 310.0 KG/M**3

DAY	T AIR	SNOW	K DOWN	K UP	L DOWN	L UP	EVAP	HEAT	F ICE	MELT	T SFCE	T INT	THICKNESS	SALINITY
1	-8.6	.0	7.3	3.0	199.0	259.6	2.3	14.9	39.4	.0	-9.72	-9.72	39.4	6.60
2	-12.2	.0	8.7	3.6	191.8	249.5	.7	1.7	50.9	.0	-12.32	-12.32	40.8	7.23
3	-8.6	.0	3.4	1.4	199.0	259.0	2.7	17.0	37.2	.0	-9.68	-9.68	42.5	7.20
4	-13.9	.0	5.3	2.2	188.8	244.0	.5	-1.9	54.0	.0	-13.76	-13.76	43.8	7.18
5	-17.5	.0	5.8	2.5	182.9	234.2	-.4	-14.5	63.5	.0	-16.42	-16.42	45.7	7.15
6	-17.5	.0	7.3	3.1	182.9	233.9	-.3	-13.5	60.9	.0	-16.49	-16.49	47.9	7.12
7	-22.5	.0	4.8	2.1	175.3	220.4	-.9	-29.8	73.7	.0	-20.26	-20.26	50.0	7.09
8	-24.4	5.0	7.7	5.8	172.4	209.0	.6	-10.4	44.1	.0	-23.62	-13.37	52.5	7.04
9	-17.2	5.0	2.9	2.2	183.3	228.6	2.0	10.1	32.1	.0	-17.96	-10.50	54.0	7.02
10	-19.2	5.0	5.3	4.0	180.2	223.1	1.5	4.3	34.9	.0	-19.52	-11.42	55.2	7.00
11	-15.3	5.0	3.9	2.9	186.4	234.2	2.5	14.9	28.4	.0	-16.42	-9.83	56.4	6.98
12	-23.1	5.0	6.7	6.5	174.4	212.3	.8	-6.2	40.2	.0	-22.63	-13.30	57.3	6.97
13	-15.3	5.0	4.8	3.6	186.4	234.0	2.6	15.4	27.8	.0	-16.45	-9.99	58.7	6.95
14	-10.0	5.0	3.9	2.9	196.1	250.1	4.6	28.8	19.4	.0	-12.16	-7.65	59.7	6.93
15	-22.2	5.0	2.9	2.2	175.7	214.3	1.1	-2.1	37.9	.0	-22.04	-13.23	60.4	6.92
16	-28.6	5.0	4.8	3.6	166.1	197.1	.4	-18.2	47.1	.0	-27.24	-16.29	61.7	6.90
17	-24.2	8.0	4.4	3.3	172.7	207.2	1.1	-.5	32.5	.0	-24.16	-12.07	63.3	6.87
18	-18.1	8.0	3.9	2.9	181.9	224.4	2.3	13.8	25.0	.0	-19.13	-9.85	64.4	6.86
19	-19.2	8.0	3.4	2.5	180.2	221.2	2.1	11.3	26.1	.0	-20.05	-10.33	65.3	6.84
20	-27.5	8.0	3.4	2.5	167.8	198.0	.8	-7.4	35.9	.0	-26.95	-13.62	66.2	6.83
21	-31.1	8.0	3.9	2.9	162.2	188.5	.5	-15.1	39.8	.0	-29.97	-15.16	67.4	6.81
22	-31.4	8.0	6.3	4.7	161.7	187.8	.5	-16.0	39.8	.0	-30.20	-15.41	68.8	6.79
23	-23.9	8.0	2.4	1.8	173.2	207.6	1.3	1.8	30.8	.0	-24.03	-12.56	70.2	6.76
24	-15.3	8.0	2.4	1.8	186.4	232.4	3.2	21.2	20.7	.0	-16.89	-9.19	71.3	6.75

25	-25,1	8,0	5,4	2,5	174,4	204,9	1,4	5,5	29,5	,0	-23,55	-12,57	72,0	6,74
26	-30,6	8,0	4,8	3,6	163,0	189,7	,5	-13,6	37,8	,0	-29,58	-15,53	73,0	6,72
27	-27,5	8,0	4,4	3,3	167,8	197,8	,8	-6,4	34,0	,0	-27,02	-14,38	74,3	6,70
28	-28,9	8,0	4,4	3,3	165,7	193,9	,7	-9,0	35,4	,0	-28,23	-15,08	75,5	6,68
29	-22,2	8,0	2,9	2,2	175,7	212,3	1,6	5,8	27,6	,0	-22,63	-12,37	76,7	6,66
30	-21,1	8,0	3,4	2,5	177,4	215,3	1,8	8,5	26,3	,0	-21,74	-11,98	77,6	6,65
31	-26,4	8,0	4,4	3,3	169,5	200,6	1,0	-3,3	31,9	,0	-26,15	-14,29	78,6	6,63
32	-25,3	8,0	4,8	3,6	171,1	203,5	1,1	-,4	30,5	,0	-25,27	-13,92	79,7	6,61
33	-28,6	8,0	4,4	3,3	166,1	194,6	,8	-7,5	33,9	,0	-28,04	-15,43	80,7	6,60
34	-29,2	8,0	6,3	4,7	165,2	193,0	,7	-9,1	34,3	,0	-28,52	-15,77	81,9	6,58
35	-26,4	8,0	4,8	3,6	169,5	200,5	1,0	-2,8	31,1	,0	-26,19	-14,65	83,1	6,56
36	-28,3	8,0	6,3	4,7	166,6	195,3	,8	-6,9	32,9	,0	-27,79	-15,57	84,1	6,54
37	-20,0	8,0	2,9	2,2	179,0	218,2	2,1	12,0	23,9	,0	-20,90	-12,00	85,3	6,52
38	-18,1	8,0	4,8	3,6	181,9	223,8	2,5	16,0	21,8	,0	-19,30	-11,19	86,1	6,51
39	-18,3	8,0	3,9	2,9	181,6	223,3	2,4	15,3	21,9	,0	-19,45	-11,31	86,9	6,50
40	-23,3	8,0	6,3	4,7	174,1	209,0	1,4	4,3	27,0	,0	-23,62	-13,59	87,6	6,49
41	-25,6	8,0	5,8	4,3	170,7	202,5	1,1	-,4	29,3	,0	-25,57	-14,70	88,6	6,47
42	-29,4	8,0	6,3	4,7	164,9	192,3	,7	-8,7	33,0	,0	-28,75	-16,49	89,6	6,46
43	-30,6	8,0	13,1	9,8	163,[illegible]	189,3	,6	-11,8	33,9	,0	-29,71	-17,10	90,7	6,44
44	-29,2	8,0	7,3	5,5	165,2	192,8	,7	-8,3	32,3	,0	-28,58	-16,57	91,9	6,42
45	-29,4	8,0	11,1	8,3	164,9	192,3	,7	-8,7	32,3	,0	-28,75	-16,74	93,0	6,40
46	-28,1	8,0	13,1	9,8	166,9	195,9	,8	-6,4	30,7	,0	-27,62	-16,20	94,1	6,38
47	-31,4	8,0	8,2	6,1	161,7	186,8	,6	-11,8	34,0	,0	-30,52	-17,88	95,2	6,37
48	-30,3	8,0	15,0	11,3	163,5	190,0	,6	-11,0	32,5	,0	-29,48	-17,39	96,3	6,35
49	-22,2	8,0	7,3	5,5	175,7	211,7	1,7	7,9	24,5	,0	-22,79	-13,70	97,5	6,33
50	-20,8	8,0	8,7	6,5	177,8	215,9	1,9	10,5	22,9	,0	-21,59	-13,00	98,3	6,32
51	-28,1	8,0	12,1	9,1	166,9	195,7	,8	-5,7	29,9	,0	-27,67	-16,55	99,1	6,30
52	-28,3	8,0	9,7	7,3	166,6	195,0	,9	-5,4	30,0	,0	-27,90	-16,75	100,1	6,29
53	-32,2	8,0	7,7	5,8	160,5	184,5	,6	-12,5	33,7	,0	-31,27	-18,74	101,2	6,27
54	-32,2	8,0	14,0	10,5	160,5	184,6	,5	-13,1	33,4	,0	-31,22	-18,80	102,3	6,25
55	-29,4	8,0	9,7	7,3	164,9	191,9	,8	-7,0	30,5	,0	-28,87	-17,52	103,5	6,23
56	-28,9	8,0	13,5	10,1	165,7	193,5	,8	-7,0	29,8	,0	-28,38	-17,30	104,6	6,22
57	-21,7	8,0	8,7	6,5	176,5	213,2	1,8	8,8	22,9	,0	-22,36	-13,85	105,6	6,20
58	-12,5	8,0	6,8	5,1	191,3	240,7	4,3	26,5	14,2	,0	-14,04	-9,37	106,4	6,19
59	-19,2	8,0	10,2	7,6	180,2	220,3	2,3	14,8	20,5	,0	-20,31	-12,71	106,9	6,18
60	-22,8	8,0	17,4	13,0	174,8	210,2	1,5	5,9	23,6	,0	-23,24	-14,46	107,6	6,17
61	-29,2	8,0	21,3	16,0	165,2	192,8	,7	-8,3	29,4	,0	-28,58	-17,65	108,4	6,16
62	-22,8	8,0	9,7	7,3	174,8	209,9	1,6	7,3	23,5	,0	-23,35	-14,61	109,4	6,14
63	-18,3	8,0	11,6	8,7	181,6	223,1	2,5	16,3	19,2	,0	-19,52	-12,38	110,2	6,13
64	-25,8	8,0	15,5	11,6	170,4	201,8	1,1	-,2	26,0	,0	-25,79	-16,13	110,9	6,12
65	-23,3	8,0	9,7	7,3	174,1	208,5	1,5	6,0	23,6	,0	-23,75	-14,96	111,8	6,10
66	-19,7	8,0	15,0	11,3	179,5	219,0	2,1	12,9	20,2	,0	-20,67	-13,16	112,6	6,09
67	-20,3	8,0	17,4	13,0	178,6	217,3	2,0	11,4	20,7	,0	-21,16	-13,48	113,3	6,08
68	-17,2	8,0	15,5	11,6	183,3	226,4	2,8	18,5	17,8	,0	-18,58	-11,96	114,0	6,07
69	-24,7	8,0	29,5	22,1	172,0	205,3	1,2	,1	24,3	,0	-24,71	-15,67	114,6	6,06
70	-31,1	8,0	27,6	20,7	162,2	187,8	,6	-12,3	30,0	,0	-30,17	-19,02	115,5	6,04
71	-33,1	8,0	36,8	27,6	159,0	183,0	,4	-17,9	31,5	,0	-31,76	-20,04	116,5	6,03
72	-33,9	10,0	33,4	25,0	157,7	180,2	,4	-18,2	29,5	,0	-32,68	-19,00	117,6	6,01
73	-36,9	10,0	32,9	24,7	152,7	172,6	,3	-21,8	31,8	,0	-35,27	-20,50	118,6	5,99
74	-26,9	10,0	27,6	20,7	168,7	198,7	1,0	-2,0	23,5	,0	-26,75	-15,81	119,7	5,98
75	-15,8	10,0	22,3	16,7	185,6	230,6	3,1	21,2	14,6	,0	-17,39	-10,60	120,5	5,96

76	-30.0	10.0	27.6	20.7	164.0	190.2	.7	-7.9	25.9	.0	-29.41	-17.38	121.0	5.96
77	-33.1	10.0	24.2	18.1	159.0	181.9	.5	-12.9	28.3	.0	-32.13	-18.96	121.9	5.94
78	-29.7	10.0	26.6	19.9	164.4	190.8	.8	-8.5	25.5	.0	-29.21	-17.37	122.9	5.93
79	-32.8	10.0	32.9	24.7	159.5	182.8	.5	-13.1	27.8	.0	-31.82	-18.90	123.8	5.91
80	-36.1	10.0	50.3	37.7	154.0	175.0	.3	-22.4	30.1	.0	-34.42	-20.44	124.7	5.90
81	-33.6	10.0	48.4	36.3	158.2	181.4	.4	-17.5	28.0	.0	-32.29	-19.28	125.8	5.88
82	-33.3	10.0	44.5	33.4	158.7	181.9	.5	-15.8	27.7	.0	-32.11	-19.24	126.8	5.86
83	-33.1	10.0	54.7	41.0	159.0	183.0	.4	-17.9	27.3	.0	-31.76	-19.09	127.7	5.85
84	-33.6	10.0	53.7	40.3	158.2	181.5	.4	-18.1	27.6	.0	-32.24	-19.42	128.7	5.83
85	-33.9	10.0	54.2	40.6	157.7	180.8	.4	-18.7	27.7	.0	-32.50	-19.63	129.6	5.82
86	-34.2	10.0	54.4	40.8	157.2	180.1	.4	-19.6	27.8	.0	-32.73	-19.81	130.6	5.80
87	-35.0	10.0	54.7	41.0	155.9	177.9	.3	-20.6	28.3	.0	-33.45	-20.29	131.5	5.79
88	-34.4	10.0	52.3	39.2	156.9	179.5	.4	-19.6	27.7	.0	-32.93	-20.04	132.5	5.77
89	-33.3	10.0	48.4	36.3	158.7	182.1	.4	-16.6	26.8	.0	-32.05	-19.58	133.5	5.76
90	-31.7	10.0	55.2	41.4	161.3	186.6	.5	-14.8	25.4	.0	-30.59	-18.77	134.4	5.74
91	-31.9	10.0	67.2	50.4	161.0	186.6	.4	-17.5	25.3	.0	-30.59	-18.82	135.3	5.73
92	-25.0	10.0	45.5	34.1	171.6	204.5	1.1	-.4	20.3	.0	-24.97	-15.54	136.1	5.72
93	-21.7	10.0	51.8	38.8	176.5	214.3	1.5	4.5	17.7	.0	-22.04	-13.84	136.8	5.70
94	-16.7	10.0	48.4	36.3	184.1	228.9	2.6	15.8	14.0	.0	-17.88	-11.39	137.5	5.69
95	-17.2	10.0	54.2	40.6	183.3	227.7	2.3	13.6	14.2	.0	-18.22	-11.60	137.9	5.69
96	-22.2	10.0	69.2	51.9	175.7	213.5	1.2	.9	17.7	.0	-22.27	-14.03	138.4	5.68
97	-21.7	10.0	81.8	61.3	176.5	215.5	1.2	-.2	17.2	.0	-21.69	-13.70	139.0	5.67
98	-26.7	10.0	83.7	62.8	169.0	201.3	.7	-10.0	20.8	.0	-25.95	-16.27	139.6	5.66
99	-23.9	10.0	73.5	55.1	173.2	208.8	1.0	-3.0	18.8	.0	-23.67	-14.94	140.4	5.65
100	-26.1	10.0	91.4	68.5	169.9	203.5	.6	-11.0	20.1	.0	-25.27	-15.92	141.0	5.64
101	-27.2	10.0	94.3	70.7	168.3	200.3	.6	-12.7	20.9	.0	-26.25	-16.53	141.7	5.63
102	-27.8	10.0	105.0	78.8	167.3	199.2	.4	-16.4	21.1	.0	-26.57	-16.76	142.4	5.62
103	-26.7	10.0	73.5	55.1	169.0	200.9	.7	-8.5	20.6	.0	-26.06	-16.46	143.2	5.60
104	-23.6	10.0	90.5	67.9	173.6	210.4	.9	-5.5	18.1	.0	-23.19	-14.77	143.9	5.59
105	-27.2	10.0	99.2	74.4	168.3	200.6	.5	-13.9	20.6	.0	-26.15	-16.59	144.5	5.58
106	-29.2	7.5	101.1	75.8	165.2	195.6	.3	-19.8	24.2	.0	-27.71	-19.28	145.2	5.57
107	-30.2	7.5	109.8	82.3	163.6	193.2	.2	-23.4	24.8	.0	-28.45	-19.80	146.0	5.56
108	-33.1	7.5	116.1	87.1	159.0	185.8	.1	-30.2	26.9	.0	-30.83	-21.45	146.9	5.54
109	-31.1	7.5	105.0	78.8	162.2	190.5	.2	-23.8	25.4	.0	-29.31	-20.46	147.8	5.53
110	-28.6	7.5	101.6	76.2	166.1	197.2	.3	-18.5	23.4	.0	-27.21	-19.07	148.7	5.52
111	-25.8	7.5	107.4	80.5	170.4	205.2	.5	-14.0	21.0	.0	-24.75	-17.43	149.5	5.50
112	-29.7	7.5	118.0	88.5	164.4	194.8	.2	-23.1	23.9	.0	-27.97	-19.64	150.2	5.49
113	-31.4	7.5	128.7	96.5	161.7	190.7	.1	-28.7	25.0	.0	-29.25	-20.54	151.1	5.48
114	-29.2	7.5	110.3	82.7	165.2	195.9	.3	-21.0	23.4	.0	-27.82	-19.47	151.9	5.46
115	-29.7	7.5	139.8	104.8	164.4	195.9	.0	-27.7	23.3	.0	-27.62	-19.50	152.7	5.45
116	-29.4	7.5	106.4	79.8	164.9	195.0	.3	-20.0	23.5	.0	-27.90	-19.72	153.6	5.44
117	-27.2	7.5	142.2	106.6	168.3	202.7	.1	-22.7	21.2	.0	-25.50	-18.10	154.4	5.43
118	-24.4	7.5	127.7	95.8	172.4	209.9	.4	-14.2	19.2	.0	-23.34	-16.64	155.1	5.41
119	-25.3	7.5	147.6	110.7	171.1	208.3	.1	-19.7	19.6	.0	-23.82	-16.99	155.8	5.40
120	-27.2	17.5	157.2	117.9	168.3	202.3	.2	-20.8	15.0	.0	-25.64	-13.45	156.4	5.39
121	-25.6	17.5	155.8	116.8	170.7	206.8	.3	-17.6	14.1	.0	-24.28	-12.81	157.0	5.38
122	-20.3	17.5	129.7	97.3	178.6	221.1	1.0	-2.9	11.5	.0	-20.08	-10.77	157.4	5.38
123	-22.2	17.5	169.3	127.0	175.7	217.3	.3	-13.7	12.1	.0	-21.17	-11.32	157.8	5.37
124	-16.9	17.5	108.4	81.3	183.8	230.5	1.7	7.2	9.8	.0	-17.44	-9.50	158.3	5.36
125	-8.1	17.5	95.3	71.5	200.1	258.7	4.0	24.6	5.1	.0	-9.95	-5.83	158.6	5.36
126	-8.3	17.5	139.3	104.5	199.6	260.1	2.7	17.3	4.8	.0	-9.60	-5.66	158.8	5.36

127	-8.6	17.5	114.6	85.8	199.0	257.9	3.3	20.8	5.2	.0	-10.16	-5.94	158.9	5.35
128	-20.0	17.5	194.0	145.5	179.0	225.0	.1	-13.8	10.7	.0	-18.96	-10.27	159.1	5.35
129	-22.2	17.5	194.0	145.5	175.7	218.4	-.0	-17.9	11.9	.0	-20.86	-11.21	159.5	5.34
130	-20.6	17.5	188.7	141.5	178.1	223.1	.1	-14.4	11.0	.0	-19.52	-10.57	159.9	5.34
131	-16.9	17.5	180.5	135.4	183.8	233.8	.5	-5.2	9.1	.0	-16.51	-9.09	160.3	5.33
132	-21.4	17.5	206.1	154.6	176.9	221.3	-.1	-18.4	11.3	.0	-20.02	-10.83	160.6	5.33
133	-18.1	17.5	206.0	156.0	181.9	231.4	-.1	-12.2	9.5	.0	-17.19	-9.44	161.0	5.32
134	-14.4	17.5	139.3	104.5	187.9	239.9	1.5	6.2	8.1	.0	-14.86	-8.30	161.3	5.32
135	-16.4	17.5	161.1	120.8	184.6	234.5	.9	-.9	9.0	.0	-16.33	-9.03	161.6	5.31
136	-23.9	17.5	228.4	171.3	173.2	215.0	-.5	-27.6	12.4	.0	-21.83	-11.77	161.9	5.31
137	-19.7	17.5	156.3	117.2	179.5	224.1	.6	-6.5	10.7	.0	-19.21	-10.48	162.3	5.30
138	-17.5	17.5	217.7	163.3	182.9	233.9	-.3	-13.3	9.0	.0	-16.50	-9.14	162.7	5.29
139	-21.1	17.5	234.2	175.6	177.4	223.6	-.6	-23.0	10.8	.0	-19.38	-10.58	163.0	5.29
140	-15.8	17.5	119.5	89.6	185.6	234.5	1.7	7.1	8.9	.0	-16.33	-9.07	163.4	5.28
141	-10.3	17.5	173.2	129.9	195.5	254.7	1.5	8.9	5.6	.0	-10.97	-6.41	163.7	5.28
142	-13.1	25.5	226.9	170.2	190.2	248.0	-.1	-5.1	5.5	.0	-12.72	-6.26	163.9	5.27
143	-15.0	25.5	180.9	135.7	186.9	239.6	.7	-.9	6.6	.0	-14.93	-7.16	164.1	5.27
144	-16.9	25.5	248.7	186.5	183.8	236.8	-.7	-18.0	6.9	.0	-15.70	-7.48	164.3	5.27
145	-18.1	25.5	250.6	187.9	181.9	233.0	-.6	-18.0	7.5	.0	-16.75	-7.91	164.5	5.26
146	-16.7	25.5	255.0	191.3	184.1	237.7	-.8	-16.6	6.8	.0	-15.46	-7.39	164.8	5.26
147	-15.6	25.5	256.4	192.3	185.9	241.2	-.8	-14.4	6.3	.0	-14.52	-7.01	165.0	5.26
148	-11.7	25.5	243.4	182.5	192.8	253.3	-.5	-5.1	4.7	.0	-11.32	-5.71	165.3	5.25
149	-9.2	23.0	220.6	165.4	197.7	260.7	.2	3.2	4.0	.0	-9.44	-5.14	165.4	5.25
150	-7.5	23.0	236.6	177.4	201.4	267.4	-.3	3.5	3.1	.0	-7.76	-4.41	165.6	5.25
151	-7.8	23.0	254.0	190.5	200.7	267.1	-.8	.5	3.2	.0	-7.84	-4.45	165.7	5.25
152	-11.4	23.0	264.2	198.1	193.3	255.4	-1.1	-8.1	4.7	.0	-10.79	-5.73	165.8	5.24
153	-8.9	23.0	255.4	191.5	198.3	263.4	-.9	-1.9	3.7	.0	-8.76	-4.85	165.9	5.24
154	-7.8	23.0	277.2	207.9	200.7	268.3	-1.6	-3.3	3.0	.0	-7.55	-4.32	166.1	5.24
155	-6.1	15.0	280.6	210.5	204.7	274.6	-2.0	-1.4	2.7	.0	-6.00	-4.10	166.2	5.24
156	-6.1	15.0	267.5	200.6	204.7	273.9	-1.5	.8	2.8	.0	-6.16	-4.19	166.3	5.24
157	-3.6	15.0	154.3	115.7	211.1	277.7	2.9	21.9	2.2	.0	-5.24	-3.69	166.4	5.23
158	-2.8	15.0	172.2	129.1	213.3	281.4	2.4	20.7	1.6	.0	-4.35	-3.20	166.4	5.23
159	.0	15.0	145.6	109.2	221.8	290.9	3.9	28.3	.2	.0	-2.12	-1.97	166.5	5.23
160	-.3	15.0	276.7	207.5	220.8	295.9	-2.8	8.8	-.4	.0	-.96	-1.24	166.5	5.23
161	-5.3	15.0	232.7	174.5	206.6	275.1	-.1	7.7	2.6	.0	-5.88	-4.04	166.5	5.23
162	-6.4	7.5	206.6	154.9	203.9	270.1	.6	9.3	4.4	.0	-7.10	-5.55	166.6	5.23
163	-.8	7.5	222.5	166.9	219.2	291.3	.2	16.3	.2	.0	-2.42	-1.95	166.7	5.23
164	-1.4	7.5	280.6	210.5	217.4	291.9	-2.8	6.3	.1	.0	-1.88	-1.84	166.7	5.23
165	-9.2	7.5	311.6	233.7	197.7	265.5	-3.0	-13.0	5.4	.0	-8.22	-6.35	166.7	5.23
166	-11.9	7.5	319.8	239.9	192.4	257.1	-3.0	-20.5	7.2	.0	-10.36	-7.85	166.9*	5.23
167	-6.9	7.5	228.8	171.6	202.8	269.6	-.4	4.1	4.5	.0	-7.21	-5.64	167.2	5.22
168	-2.5	7.5	255.4	191.5	214.1	286.5	-1.3	8.7	1.1	.0	-3.16	-2.77	167.3	5.22
169	.8	7.5	282.1	211.6	230.4	309.4	-2.9	10.7	-1.6	.0	.00	.00	167.4	5.22
170	4.7	7.6	266.1	199.6	243.8	309.4	16.5	62.7	-1.6	-80.0	.00	.00	167.4	5.22
171	.6	.9	118.5	88.9	223.8	291.9	5.3	33.0	.1	.0	-1.88	-1.87	167.4	5.22
172	.6	.9	235.1	176.3	223.8	297.5	-.8	15.8	-.9	.0	-.59	-.62	167.4	5.22
173	-3.6	.9	259.3	194.5	211.1	282.8	-1.5	5.7	2.4	.0	-4.03	-3.93	167.3	5.22
174	-2.2	.9	320.8	240.6	215.0	290.8	-4.5	-.6	.4	.0	-2.15	-2.14	167.4	5.22
175	-.3	.9	142.2	106.6	220.8	289.7	3.9	27.9	.7	.0	-2.40	-2.37	167.4	5.22
176	-.8	.9	316.4	237.3	219.2	295.8	-4.6	2.5	-.6	.0	-.99	-1.01	167.5	5.22
177	-5.3	22.9	335.8	251.9	206.6	280.0	-4.3	-8.0	1.5	.0	-4.70	-3.69	167.4	5.22

178	-6.1	22.9	349.0	262.3	204.7	277.7	-4.6	-11.4	1.8	.0	-3.24	-3.33	167.5	5.22
179	-3.9	22.9	315.0	236.3	210.2	284.1	-3.8	-2.6	1.0	.0	-3.70	-2.65	167.6	5.22
180	-1.4	22.9	174.7	131.0	217.4	286.8	2.5	22.5	.7	.0	-3.09	-2.37	167.6	5.22
181	-3.3	22.9	299.0	224.3	211.9	285.6	-3.2	.8	.8	.0	-3.36	-2.49	167.6	5.21
182	-5.8	22.9	343.0	257.3	205.4	278.4	-4.4	-9.8	1.7	.0	-5.07	-3.25	167.6	5.21
183	-5.8	20.4	327.5	245.6	205.4	277.9	-3.9	-8.1	1.9	.0	-5.19	-3.41	167.7	5.21
184	-.3	20.4	164.5	123.4	220.8	290.7	2.8	24.7	.2	.0	-2.16	-1.96	167.8	5.21
185	4.4	20.4	240.4	180.3	242.7	309.4	14.8	58.7	-1.6	-66.0	.00	.00	167.8	5.21
186	1.9	14.8	302.7	227.0	234.1	309.4	2.1	25.3	-1.6	-27.0	.00	.00	167.8	5.21
187	1.7	12.5	327.0	245.3	233.4	309.4	1.1	22.7	-1.6	-29.0	.00	.00	167.8	5.21
188	.8	10.0	280.0	210.0	230.4	309.4	-2.9	10.7	-1.6	1.0	.00	.00	167.8	5.21
189	.8	10.1	276.0	207.0	[illegible]	309.4	-2.9	10.7	-1.6	2.0	.00	.00	167.8	5.21
190	3.6	10.3	80.0	60.0	[illegible]	309.4	10.5	48.0	-1.6	-9.0	.00	.00	167.8	5.21
191	2.8	9.6	281.0	210.8	[illegible]	309.4	6.4	37.3	-1.6	-41.0	.00	.00	167.8	5.21
192	.0	6.1	150.0	112.5	221.8	291.0	3.8	27.9	.3	.0	-2.10	-2.02	167.8	5.21
193	-.3	6.1	196.0	147.0	220.8	292.0	1.4	20.7	.1	.0	-1.66	-1.63	167.8	5.21
194	.0	6.1	132.0	99.0	221.8	290.4	4.4	29.9	.4	.0	-2.25	-2.13	167.8	5.21
195	-.6	6.1	210.0	157.5	219.9	291.6	.7	18.1	.2	.0	-1.46	-1.91	167.8	5.21
196	2.8	6.1	288.0	216.0	237.2	309.4	6.4	37.3	-1.6	-43.0	.00	.00	167.8	5.21
197	.0	15.4	229.0	171.8	221.8	294.8	-.3	16.2	-.3	.0	-1.21	-1.43	167.8	5.21
198	1.7	15.4	157.0	117.8	227.5	298.2	3.3	28.5	-.7	.0	-.44	-.91	167.8	5.21
199	1.7	15.4	214.0	160.5	233.4	309.4	1.1	22.7	-1.6	-1.0	.00	.00	167.8	5.21
200	3.9	15.3	206.0	154.5	241.0	309.4	12.1	52.0	-1.6	-47.0	.00	.00	167.8	5.21
201	3.6	11.4	200.0	150.0	240.0	309.4	10.5	48.0	-1.6	-39.0	.00	.00	167.8	5.21
202	4.2	8.1	195.0	146.3	242.0	309.4	13.7	56.0	-1.6	-51.0	.00	.00	167.8	5.21
203	3.9	3.9	188.0	141.0	241.0	309.4	12.1	52.0	-1.6	-42.0	.00	.00	167.8	5.21
204	4.7	.3	301.0	225.8	243.8	309.4	16.5	62.7	-1.6	-88.0	.00	.00	167.8	5.21
205	5.3	.0	242.0	113.7	245.9	309.4	19.9	70.7	-1.6	-155.0	.00	.00	167.8	5.21
206	4.7	.0	161.0	72.4	243.8	309.4	16.5	62.7	-1.6	-102.0	.00	.00	162.4	5.02
207	2.2	.0	72.1	32.4	235.1	309.4	3.5	29.3	-1.7	1.0	.00	.00	158.9	4.89
208	4.4	.0	227.0	102.1	242.7	309.4	14.8	58.7	-1.7	-131.0	.00	.00	158.9	4.86
209	3.9	.0	139.0	62.5	241.0	309.4	12.1	52.0	-1.7	-72.0	.00	.00	154.4	4.70
210	4.2	.0	119.0	53.5	242.0	309.4	13.7	56.0	-1.7	-67.0	.00	.00	151.9	4.60
211	6.9	.0	332.0	149.4	251.6	309.4	29.7	92.0	-1.8	-246.0	.00	.00	149.5	4.50
212	5.6	.0	226.0	101.7	247.0	309.4	21.7	74.7	-1.9	-158.0	.00	.00	141.0	4.23
213	7.8	.0	335.0	150.7	254.9	309.4	35.7	104.0	-2.0	-269.0	.00	.00	135.6	4.05
214	8.9	.0	261.0	117.4	258.9	309.4	43.5	118.7	-2.1	-255.0	.00	.00	126.2	3.76
215	7.2	.0	175.0	78.7	252.7	309.4	31.7	96.0	-2.3	-167.0	.00	.00	117.4	3.49
216	5.8	.0	115.0	51.7	247.7	309.4	22.9	77.3	-2.4	-101.0	.00	.00	111.6	3.30

THE FOLLOWING TABLE PRESENTS THE RECORDED ICE THICKNES INFORMATION FOR THE STATION

DAY	ICE THICKNESS	SNOW DEPTH
1.	39.0	.0
8.	47.0	5.0
17.	56.0	8.0
22.	64.0	2.5
30.	72.0	8.0

36.	80.0	8.0
44.	94.0	8.0
50.	97.0	8.0
57.	104.0	5.0
72.	109.0	10.0
78.	122.0	10.0
85.	125.0	8.0
92.	135.0	10.0
100.	140.0	10.0
106.	142.0	8.0
113.	140.0	8.0
120.	152.0	18.0
127.	156.0	18.0
135.	150.0	18.0
142.	150.0	28.0
149.	161.0	23.0
155.	175.0	15.0
162.	164.0	8.0
169.	178.0	8.0
177.	178.0	23.0
183.	165.0	5.0
190.	175.0	5.0
197.	169.0	13.0
204.	147.0	2.5
211.	117.0	2.5

I HOPE YOU ENJOYED THE SEA-ICE GAME
THIS EXERCISE WAS BROUGHT TO YOU IN PART BY:
CARLETON UNIVERSITY AND
THE NATIONAL RESEARCH COUNCIL OF CANADA

BIBLIOGRAPHY

Anderson, D. 1966. Heat of freezing and melting of sea ice. C.R.R.E.L. Res. Rept. 202.

Assur, A. 1958. Composition of sea ice and its tensile strength. N.A.S.-N.R.C. Conference on Arctic Sea Ice, N.A.S.-N.R.C. Publ. No. 598, 106-138.

Banke, E.G. and S.D. Smith 1973. Wind stress on Arctic sea ice. J. Geophys. Res., 78(33): 7871-7883.

Banke, E.G., Smith, S.D., and R.J. Anderson 1976. Recent measurements of wind stress on arctic ice. J. Fish. Res. Board Can., 33:2307-2317.

Barber, F.G. 1977. A note on the oceanography of Eclipse Sound. Unpublished Manuscript, Marine Sciences Directorate, Ottawa. 44 p.

Barkstrom, B.R. 1972. Some effects of multiple scattering on the distribution of solar radiation in snow and ice. J. Glaciol., 11(63): 357-368.

Barkstrom, B.R. and C.W. Querfield 1975. Considering the effect on anisotropic scattering and finite depth on the distribution of solar radiation in snow. J. Glaciol., 14(70): 107-124.

Bennington, K.O. 1967. Desalination features in natural sea ice. J. Glaciol., 6(48): 845-857.

Bilello, M.A. 1961. Formation, growth and decay of sea ice in the Canadian arctic archipelago. Arctic, 14(1): 2-25.

Bilello, M.A. 1978. Sea ice temperature curves for Slidre Fjord, Canada. Paper presented at the Can. Assoc. Geog. 1978 Annual Meeting, University of Western Ontario, London: 12 p.

Bohren, C.F. and B.R. Barkstrom 1974. Theory of the optical properties of snow. J. Geophys. Res., 79(30): 4527-4535.

Brown, J.H. 1969. Energy exchange at a sea ice boundary. Solar Energy, 12: 469:490.

3 3

OF/DE

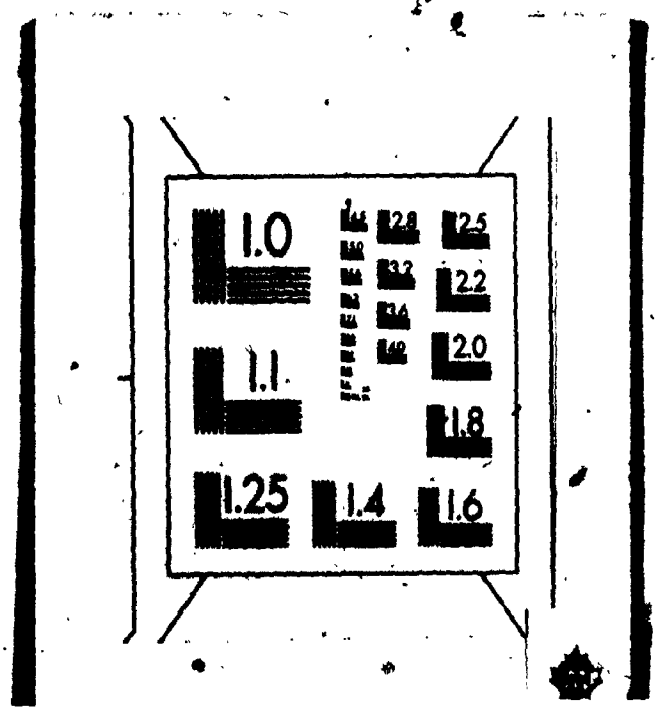

Budyko, M.I. 1974. Climate and life, Academic Press, New York (International Geophysical Series, No. 18), 508 p.

Businger, J.A., Wyngaard, J.C., Izumi, Y., and E.F. Bradley 1971. Flux-profile relationships in atmospheric surface layer. J. Atmos. Sci., 28: 181-189.

Businger, J.A. 1973. Turbulent transfer in the atmospheric surface layer in Workshop on Micrometeorology, (D.A. Haugen Ed.), American Meteorological Society, Bostom, 67-100.

Campbell, W.J., Wayenberg, J., Ramseyer, J.B., Ramseier, R.O., Vant, M.R., Weaver, R., Redmond, A., Arsenault, L., Gloersen, P., Zwally, H.J., Wilheit, T.T., Chang, T.C., Hall, D., Gray, L., Meeks, D.C., Bryan, M.L., Barath, F.T., Elachi, C., Leberl, F., and T. Farr 1978. Microwave remote sensing of sea ice in the AIDJEX main experiment. Boundary Layer Meteorology, 13: 309-337.

Cox, G.F.N. and W.F. Weeks 1974. Salinity variations in sea ice. J. Glaciol., 13(67): 109-120.

Cox, G.F.N. and W.F. Weeks 1975. Brine drainage and initial salt entrapment in sodium chloride ice. C.R.R.E.L. Res. Rept., 345: 85 p.

Doherty, B.T. and D.R. Kester 1974. Freezing point of sea water. J. Marine Res., 32(2): 285-300.

Doronin, Y.P. 1970. Thermal interaction of the atmosphere and the hydrosphere in the arctic, Israel Program for Scientific Translation, Jerusalem, 244 p.

Dorsey, N.E. 1949. Properties of ordinary water-substance in all its phases: water-vapour and all the ices, Hafner Publishing (American Chemical Society, Monograph Series, No. 81), New York. 673 p.

Eide, L.I. and S. Martin 1975. The formation of brine drainage features in young sea ice. J. Glaciol., 14(70): 137-154.

Fleagle, R.G. and J.A. Businger 1963. An introduction to atmospheric physics, Academic Press, New York, 346 p.

Fletcher, J.O. 1965. The heat budget of the Arctic Basin and its relation to climate, The Rand Corporation, R-444-PR.

Gerson, D.J. and R.J. Perchal 1973. Sea ice growth in potential arctic mine field areas. Rept. # N00-TN-7700-11-73. National Oceanographic Office, Washington, D.C.

Giddings, J.C. and E. LaChapelle 1961. Diffusion theory applied to radiant energy distribution and albedo of snow. J. Geophys. Res., 66(1): 181-189.

Gloersen, P., Ramseier, R.O., Campbell, W.J., Chang, T.C., and T.T. Wilheit 1975. Variation of ice morphology of selected mesoscale test areas during the Bering Sea experiment. USSR/USA Bering Sea Experiment, Proc. Final Symposium of the Results of the Joint Soviet-American Expedition, Leningrad 12-17 May 1974, 196-218.

Goddard, W.B. 1974. A climate simulation model applied to Arctic pack ice. AIDJEX Bulletin, (25): 55-73.

Hanson, K.J. 1960. Radiation measurements on the Antarctic snowfield, a preliminary report. J. Geophys. Res., 65: 935-947.

Harbaugh, J.W. and G. Bonham-Carter 1970. Computer simulation in geology, Wiley, New York. 575 p.

Harrison, J.D. 1965. Measurement of brine droplet migration in ice. J. Appl. Phys., 36(12): 3811-3815.

Hoekstra, P., Osterkamp, T.E. and W.F. Weeks 1965. The migration of liquid inclusions in single ice crystals. J. Geophys. Res., 70(20): 5035-5041.

Holtzmark, B. 1955. Insulating effects of a snow cover on the growth of young sea ice. Arctic, 8(1): 60-65.

Idso, S.B. and R.D. Jackson 1969. Thermal radiation from the atmosphere. J. Geophys. Res., 74(23): 5397-5403.

Kellogg, W.M. 1974. Climatic feedback mechanisms involving the polar regions, in Climate of the Arctic, (G. Weller, S.A. Bowling Eds.), Geophysical Institute, University of Alaska, 111-116.

Kingery, W.D. and W.H. Goodnow. Brine migration in salt ice in Ice and snow: properties, processes and applications (W.H. Kingery Ed.), Proceedings of a Conference held at M.I.T. Feb. 12-16, 1962., 237-247.

Kraus, H. 1972. Energy exchange at the air-ice interface. International Symposium on the role of snow and ice in hydrology, Banff, Alberta, Vol. 1., 1972, 128-164.

Kvajic, G, Pounder, E.R. and V. Brajovik 1971. Instability of a smooth-planar solid-liquid interface on an ice crystal growing from a melt. Can. J. Physics, 49: 2642-2645.

Lake, R.A. 1969. The applicability of metallurgical solidification equations to seawater. Unpublished manuscript, 7 p.

Lake, R.A. and E.L. Lewis 1970. Salt rejection by sea ice during growth. J. Geophys. Res., 75(3): 583-597.

Lake, R.A. and E.L. Lewis 1971. The microclimate beneath growing sea ice. Proc. I.A.H.R. Conf., (T. Karlsson, Ed.), Reykjavick, May 10-13, 1971, N.R.C., 241-244.

Langleben, M.P. 1966. On the factors affecting the rate of ablation of sea ice. Can. J. Earth Sci., 3: 431-439.

Langleben, M.P. 1972. A study of the roughness parameters of sea ice from wind profiles. J. Geophys. Res., 77: 5935-5944.

Langleben, M.P. and E.R. Pounder 1972. On the air drag of an arctic ice floe (abstract). Eos Trans. A.G.U., 15: 1015.

Leahey, D.M. 1966. Heat exchange and sea ice growth in Arctic Canada. Manuscript Report No. 1, Marine Sciences Centre, McGill University, 48 p.

Leavitt, E., Bell, D., Clarke, M., Andersen, R., and C. Paulson 1977. Computation of air stress and sensible heat fluxes from surface layer profile data, AIDJEX, 1975. AIDJEX Bulletin (36): 157-174.

Lewis, E.L. 1967. Heat flow through winter ice in Physics of snow and ice. (H. Oura, Ed.) International Conference on Low Temp. Sci., Hokkaido University, 569-577.

Lewis, E.L. 1976. Oil in sea ice. Pacific Marine Science Report 76-12, Institute of Ocean Sciences (Patricia Bay).

Lewis, E.L. and Walker, E.R. 1970. Water structure under a growing ice sheet. J. Geophys. Res., 75(33): 6836-6845.

List, R.J. 1949. Smithsonian meteorological tables, Sixth Revised Edition, Smithsonian Miscellaneous Collections, 114: 527 p.

McIntosh, D.H. and A.S. Thom 1972. Essentials of Meteorology, Wykeham Publications Ltd., London, 238 p.

Malmgren, F. 1927. On the properties of sea ice. Scientific Results, Norweigan North Polar Expedition with the "Maud", 1918-1925, 1(5).

Martin, S. 1973. Evolution of under-ice melt ponds or, double diffusion at the freezing point. J. Fluid Mechanics, 64: 507.

Maykut, G.A. 1978. Energy exchange over young sea ice in the central arctic. J. Geophys. Res., 83(C7): 3646-3658.

Maykut, G.A. and N. Untersteiner 1969. Numerical prediction of the thermodynamic response of arctic sea ice to environmental changes, Rand Memorandum RM-6093-PR, Nov. 1969, 173 p.

McPhee, M.G. 1975. The effect of ice motion on the mixed layer under arctic pack ice. AIDJEX Bulletin, (30): 1-27.

McPhee, M.G. and J.D. Smith 1975. Measurements of turbulent boundary layer under pack ice. AIDJEX Bulletin, (29): 49-92.

Mellor, M.A. 1977. Engineering properties of snow. J. Glaciol., 19(81): 15-66.

Michel, B. and R.O. Ramseier 1969. Classification of river and lake ice based on its genesis, structure and texture. Report S-15, Universite Laval, Department du Genie Civil (Section Mecanique des Glaces), 40 p.

Milne, A. 1976. Oil, ice and climate change; the Beaufort Sea and the search for oil, Department of Fisheries and Oceans, Ottawa, 103 p.

Montieth, J.L. 1973. Principles of environmental physics, Edward Arnold Ltd., London, 241 p.

Myrup, L.O. 1969. A numerical model of the urban heat island. J. Appl. Met., 8(6): 908-918.

Nakaya, N. 1956. Properties of single ice crystals of ice revealed by internal melting. C.R.R.E.L. Research Paper 13, 80 p.

Niedrauer, T.N. 1977. Brine drainage and convection in young sea ice. Scientific Report, Office of Naval Research, Contract N00014-76-C-0234 NR 307-252, 6 p.

NORCOR Engineering and Research Limited 1975. The interaction of crude oil with arctic sea ice. Beaufort Sea Technical Report 27, 150 p.

O'Neill, A.D. and D.M. Gray 1972. Solar radiation penetration through snow. International Symposium on the role of snow and ice in hydrology, Banff, Alberta, Vol. 1., 1972, 227-241.

Paulson, C.A. 1970. The mathematical representation of wind speed and temperature profiles in the unstable atmospheric surface layer. J. Appl. Met., 9: 11-20.

Pease, C.H. 1975. A model for the seasonal ablation and accretion of antarctic sea ice. AIDJEX Bulletin, (29): 151-172.

Polar Continental Shelf Project. Pond Inlet Ice Observations-Monthly Reports.

Pounder, E.R. 1965. The physics of ice, Pergammon Press, New York, 151 p.

Sauliev, V.K. 1957. A method of numerical solution for the diffusion equation (in Russian). Dokl. Akad. Nauk SSSR(N5), 115: 1077-1079.

Schwerdtfeger, P. 1963. The thermal properties of sea ice. J. Glaciol., 4(36): 789-808.

Schwerdtfeger, P. 1964. The effect of finite heat content and thermal diffusion on the growth of a sea-ice cover. J. Glaciol., 5(39): 315-324.

Seber, G.A.F., Linear regression analysis, John Wiley and Sons, Toronto, 1977, 464 p.

Seifert, W.J. and M.P. Langleben 1972. Air drag coefficient and roughness length of a cover of sea ice. J. Geophys. Res., 77: 2708-2713.

Sellers, W.D. 1965. Physical climatology, University of Chicago Press, Chicago, 272 p.

Semtner Jr., A.J. 1976. A model for the thermodynamic growth of sea ice in numerical investigations of climate. J. Phys. Oceanography, 6: 379-389.

Shulyakovski, L.G. 1963. Manual of forecasting ice formations for rivers and lakes. Manual of Hydrological Forecasting, No. 4, GIMIZ, © 1966 Israel Program for Scientific Translations.

Smith, S.D., Banke, E.G., and O.M. Johannsen 1970. Wind stress and turbulence over ice in the Gulf of St. Lawrence. J. Geophys. Res., 75: 2803-2212.

Sokal, R.P. and F.J. Rohlf 1969. Biometry: the principles and practices of statistics in biological research, W.H. Freeman and Co., San Francisco, 775 p.

Stefan, J. 1891. Uber die theorie der Eisbilding, inbesondere uben die Eisbilding im Polarmeere. Annalen der Physik und Chemie, Neue Folge, Bd. 42, Ht. 2, 269-286.

Thorndike, A.S., Rothrock, D.A., Maykut, G.A. and R. Colony 1975. The thickness distribution of sea ice. J. Geophys. Res., 80: 4501-4513.

Thorpe, M.R., Banke, E.G., and S.D. Smith 1973. Eddy correlation measurements of evaporation and sensible heat flux over arctic sea ice. J. Geophys. Res., 78(18): 3573-3584.

Tsurikov, V.L. 1967. Changes in the salinity of sea ice due to the migration of brine pockets. Oceanography, 7(6): 694-701.

Untersteiner, N. 1961. On the mass and heat budget of the arctic sea ice. Arch. Meteorol. Geophys. Bioklimatol., A, 12, 151-182.

Untersteiner, N. 1967. Natural desalination and equilibrium salinity profiles in Physics of snow and ice, (H. Oura Ed.), International Conference on low temp. sci., Hokkaido University, 569-577.

Van Dusen, M.S. 1929. Intl. Crit. Tables, 5: 216.

Vowinckel, E., and S. Orvig 1970. The climate of the north polar region in Climates of the polar regions, (S. Orvig Ed.), World Survey of Climatology, Vol. 14, Elsevier Pub. Co., New York, 129-252.

Walker, E.R. 1975. Oil, ice and climate in the Beaufort Sea. Technical Report No. 35, Beaufort Sea Project, Institute of Ocean Sciences (Patricia Bay), 40 p.

Wallace, J.M. and P.V. Hobbs 1977. Atmospheric science: an introductory survey, Academic Press Inc., New York, 467 p.

Weber, J.E. 1977. Heat and salt transfer associated with formation of sea-ice. Tellus, 29: 151-160.

Weeks, W.F. and A. Assur 1967. Mechanical properties of sea ice. C.R.R.E.L. Cold Regions Sciences and Engineering II-C3, 80 p.

Weller, G. 1968. Heat energy transfer through a four layer system: air, snow, sea ice, sea water. J. Geophys. Res., 73(4): 1209-1220.

Weller, G. 1972. Radiation flux investigation. AIDJEX Bulletin, (14): 28-30.

Weller, G. and B. Holmgren 1974. The microclimates of arctic tundra. J. Appl. Met., 13: 354-862.

Yen, Y.C. 1969. Recent studies on snow properties in Advances in hydroscience, Vol. 4., (V.T. Chow Ed.), Academic Press, 173-215.

Conway, F.J. 1976. A summer climate study for Barrow Strait, N.W.T., M.A. Thesis, Unpublished, Department of Meteorology, McGill University, Montreal.

Lally, G.D. 1973. Ice Formation in the Gulf of St. Lawrence, Publication in Meteorology, No. 110, McGill University, 107 p.

END

15-12-80

FIN

ARC 375